Precision Phenomenology at Colliders and Computational Methods

Gudrun Heinrich

KIT, Institute for Theoretical Physics (ITP)

Sommersemester 2021

version of July 14, 2021

Contents

1 Motivation: Collider Physics after the Higgs Discovery 4

2 A theoretical particle physicists' toolbox 5
2.1 Factorisation 5
2.2 Cross sections 5
2.3 Basics of QCD 5
2.3.1 Colour algebra 5
2.3.2 QCD Lagrangian 5
2.3.3 QCD Feynman rules 5

3 Example: top quark production 5

4 Higher orders in perturbation theory 5
4.1 Running coupling and scale dependence 5
4.2 Loops and divergences 20
4.2.1 Dimensional regularisation 20
4.2.2 One-loop integrals 23
4.3 Cancellation of infrared singularities 31
4.3.1 Structure of NLO calculations 31
4.3.2 Soft gluon emission 36
4.3.3 Collinear singularities 38
4.4 Example: $e^+e^- \to q\bar{q}$ at NLO 40
4.5 Parton evolution 41
4.5.1 Deeply inelastic scattering 41

4.5.2 Proton structure in the parton model 43
4.5.3 Proton structure in perturbative QCD 47
4.5.4 Parton evolution and the DGLAP equations 51

5 Higgs production **55**
5.1 Higgs boson production in gluon fusion 55
5.1.1 Phenomenology 55
5.1.2 Total cross section for $gg \to H$ at leading order 66
5.1.3 Heavy top limit (HTL) 68
5.2 Higgs boson pair production 69
5.2.1 Higher order corrections 71
5.2.2 $gg \to HH$ in the Standard Model 73
5.2.3 Anomalous couplings 76
5.3 Asymptotic expansions 82

Literature

- G. Dissertori, I. Knowles, M. Schmelling,
  Quantum Chromodynamics: High energy experiments and theory
  International Series of Monographs on Physics No. 115,
  Oxford University Press, Feb. 2003. Reprinted in 2005.

- R.K. Ellis, W.J. Stirling and B.R. Webber, *QCD and collider physics*,
  Cambridge University Press, Camb. Monogr. Part. Phys. Nucl. Phys. Cosmol. **8** (1996) 1.

- J. Campbell, J. Huston and F. Krauss,
  The Black Book of Quantum Chromodynamics: A Primer for the LHC Era Oxford University Press, December 2017.

- S. Dawson, C. Englert, T. Plehn,
  Higgs Physics: It ain't over till it's over, https://arxiv.org/abs/1808.01324;

- L. J. Dixon, *A brief introduction to modern amplitude methods*,
  https://arxiv.org/abs/1310.5353.

- G. Heinrich, *Collider Physics at the Precision Frontier*,
  https://arxiv.org/abs/2009.00516.

- V. A. Smirnov, *Analytic tools for Feynman integrals*, Springer Tracts Mod. Phys. **250** (2012) 1. doi:10.1007/978-3-642-34886-0.

1 Motivation: Collider Physics after the Higgs Discovery

2 A theoretical particle physicists' toolbox

2.1 Factorisation

2.2 Cross sections

2.3 Basics of QCD

2.3.1 Colour algebra

2.3.2 QCD Lagrangian

2.3.3 QCD Feynman rules

3 Example: top quark production

4 Higher orders in perturbation theory

4.1 Running coupling and scale dependence

In this section we would like to explain how it arises that theoretical predictions depend in general on at least one unphysical scale, the so-called *renormalisation scale* μ. In the case of hadronic initial state particles, there is also a *factorisation scale* μ_f involved. There can be even more unphysical scales, like fragmentation scales in the modelling of the fragmentation of final state particles into hadrons, parton shower matching scales, resummation scales, etc.

Let us first motivate how the dependence on a renormalisation scale arises. We mentioned already that the strong coupling, defined as $\alpha_s = g_s^2/(4\pi)$, is not really a constant. To leading order in the perturbative expansion, it obeys the relation

$$\alpha_s(Q^2) = \frac{1}{b_0 \log\left(Q^2/\Lambda^2_{QCD}\right)} \,, \tag{1}$$

where Λ_{QCD} is an energy scale below which non-perturbative effects start to dominate (the scale of bound states formation (hadrons)), and Q^2 is a larger energy scale, for example the centre-of-mass energy s of a scattering process. The coefficient b_0 is given by

$$b_0 = \frac{1}{4\pi}\left(\frac{11}{3}\,C_A - \frac{4}{3}T_R\,N_f\right) \,. \tag{2}$$

Note that $b_0 > 0$ for $N_f < 11/2\, C_A$.
Where does the running of the coupling come from? It is closely linked to renormalisation, which introduces the *renormalisation scale* μ.
Before we enter into the technicalities, let us look at a physical observable, for example the R-ratio which we encountered already,

$$R(s) = \frac{\sigma(e^+e^- \to \text{ hadrons})}{\sigma(e^+e^- \to \mu^+\mu^-)} \,. \tag{3}$$

We assume that the energy s exchanged in the scattering process is much larger than Λ_{QCD}.
At leading order in perturbation theory, we have to calculate tree-level diagrams for $e^+e^- \to f\bar{f}$, which however only represent a crude approximation. To get a more precise result, we should include quantum corrections, for example diagrams where virtual gluons are exchanged, such as the ones in Figs. 1a and 1b, where Fig. 1a shows corrections of order α_s and Fig. 1b shows example diagrams for $\mathcal{O}(\alpha_s^2)$ corrections. The perturbative expansion for R can be written as

$$\begin{aligned} R(s) &= K_{QCD}(s)\, R_0 \,, \quad R_0 = N_c \sum_f Q_f^2\, \theta(s - 4m_f^2) \,, \\ K_{QCD}(s) &= 1 + \frac{\alpha_s(\mu^2)}{\pi} + \sum_{n\geq 2} C_n \left(\frac{s}{\mu^2}\right) \left(\frac{\alpha_s(\mu^2)}{\pi}\right)^n \,. \end{aligned} \tag{4}$$

The higher the order in α_s the harder is the calculation. Meanwhile we know the C_n up to order α_s^4 [1, 2].

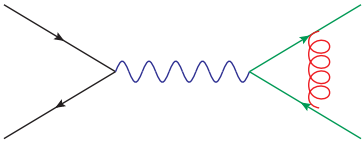

(a) 1-loop diagram contributing to $e^+e^- \to f\bar{f}$.

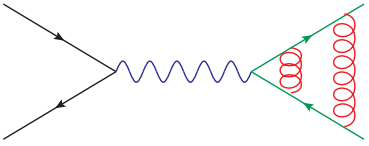

(b) 2-loop diagram example contributing to $e^+e^- \to f\bar{f}$.

However, if we try to calculate the loop diagrams, we will realize that some of the integrals over the loop momentum k are ill-defined. They diverge for $k \to \infty$. This is called an *ultraviolet divergence*. How to deal with them will be explained shortly. For the moment we just introduce an arbitrary cutoff

scale Λ_{UV} for the upper integration boundary. If we carried through the calculation, we would see that the dependence on the cutoff in diagram 1a cancels, which is a consequence of the Ward Identity in QED. However, if we go one order higher in α_s, calculating diagrams like the one in Fig. 1b, the cutoff-dependence does not cancel anymore. We obtain

$$K_{QCD}(s) = 1 + \frac{\alpha_s}{\pi} + \left(\frac{\alpha_s}{\pi}\right)^2 \left[c + b_0 \pi \, \log \frac{\Lambda_{UV}^2}{s}\right] + \mathcal{O}(\alpha_s^3) \, . \tag{5}$$

It looks like our result is infinite, as we should take the limit $\Lambda_{UV} \to \infty$. However, we did not claim that α_s is the coupling we measure. In fact, it is the "bare" coupling, also denoted as α_s^0, which appears in Eq. (5), and we can absorb the infinity in the bare coupling to arrive at the renormalised coupling, which is the one we measure.
In our case, this looks as follows. Define

$$\alpha_s(\mu) = \alpha_s^0 + b_0 \log \frac{\Lambda_{UV}^2}{\mu^2} \alpha_s^2 \, , \tag{6}$$

then replace α_s^0 by $\alpha_s(\mu)$ and drop consistently all terms of order α_s^3. This leads to

$$K_{QCD}^{\text{ren}}(\alpha_s(\mu), \mu^2/s) = 1 + \frac{\alpha_s(\mu)}{\pi} + \left(\frac{\alpha_s(\mu)}{\pi}\right)^2 \left[c + b_0 \pi \, \log \frac{\mu^2}{s}\right] + \mathcal{O}(\alpha_s^3) \, . \tag{7}$$

K_{QCD}^{ren} is finite, but now it depends on the scale μ, both explicitly and through $\alpha_s(\mu)$. However, the hadronic R-ratio is a physical quantity and therefore cannot depend on the arbitrary scale μ. The dependence of K_{QCD} on μ is an artefact of the truncation of the perturbative series after the order α_s^2.

Renormalisation group and asymptotic freedom

Since the hadronic R-ratio $R^{\text{ren}} = R_0 \, K_{QCD}^{\text{ren}}$ cannot depend μ, we know

$$\mu^2 \frac{\mathrm{d}}{\mathrm{d}\mu^2} R^{\text{ren}}(\alpha_s(\mu), \mu^2/Q^2) = \; 0 \; = \left(\mu^2 \frac{\partial}{\partial \mu^2} + \mu^2 \frac{\partial \alpha_s}{\partial \mu^2} \frac{\partial}{\partial \alpha_s}\right) R^{\text{ren}}(\alpha_s(\mu), \mu^2/Q^2) \, . \tag{8}$$

Equation (8) is called *renormalisation group equation (RGE)*. Introducing the abbreviations

$$t = \ln \frac{Q^2}{\mu^2} \, , \qquad \beta(\alpha_s) = \mu^2 \frac{\partial \alpha_s}{\partial \mu^2} \, , \tag{9}$$

the RGE becomes

$$\left(-\frac{\partial}{\partial\, t}+\beta(\alpha_s)\frac{\partial}{\partial\alpha_s}\right)\, R=0\,. \tag{10}$$

This first order partial differential equation can be solved by implicitly defining a function $\alpha_s(Q^2)$, the *running coupling*, by

$$t=\int_{\alpha_s}^{\alpha_s(Q^2)}\frac{\mathrm{d}x}{\beta(x)}\,,\quad \text{with}\quad \alpha_s\equiv\alpha_s(\mu^2)\,. \tag{11}$$

Differentiating Eq. (11) with respect to the variable t leads to

$$1=\frac{1}{\beta(\alpha_s(Q^2))}\,\frac{\partial\alpha_s(Q^2)}{\partial\, t}\,,\quad \text{which implies}\quad \beta(\alpha_s(Q^2))=\frac{\partial\alpha_s(Q^2)}{\partial\, t}\,.$$

The derivative of Eq. (11) with respect to α_s gives

$$0=\frac{1}{\beta(\alpha_s(Q^2))}\,\frac{\partial\alpha_s(Q^2)}{\partial\alpha_s}-\frac{1}{\beta(\alpha_s)}\,\frac{\partial\alpha_s}{\partial\alpha_s}\Rightarrow\frac{\partial\alpha_s(Q^2)}{\partial\alpha_s}=\frac{\beta(\alpha_s(Q^2))}{\beta(\alpha_s)}\,. \tag{12}$$

It is now easy to prove that the value of R for $\mu^2=Q^2$, $R(1,\alpha_s(Q^2))$, solves Eq. (10):

$$-\frac{\partial}{\partial\, t}R(1,\alpha_s(Q^2))=-\frac{\partial\, R}{\partial\alpha_s(Q^2)}\,\frac{\partial\alpha_s(Q^2)}{\partial\, t}=-\beta(\alpha_s(Q^2))\,\frac{\partial\, R}{\partial\alpha_s(Q^2)} \tag{13}$$

and

$$\beta(\alpha_s)\,\frac{\partial}{\partial\alpha_s}\,R(1,\alpha_s(Q^2))=\beta(\alpha_s)\,\frac{\partial\alpha_s(Q^2)}{\partial\alpha_s}\,\frac{\partial\, R}{\partial\alpha_s(Q^2)}=\beta(\alpha_s(Q^2))\,\frac{\partial\, R}{\partial\,\alpha_s(Q^2)}\,. \tag{14}$$

This means that the scale dependence in R enters only through $\alpha_s(Q^2)$, and that we can predict the scale dependence of R by solving Eq. (11), or equivalently,

$$\frac{\partial\alpha_s\big(Q^2\big)}{\partial\, t}=\beta\left(\alpha_s\big(Q^2\big)\right)\,. \tag{15}$$

We can solve Eq. (15) perturbatively using an expansion of the β-function

$$\beta(\alpha_s)=-b_0\alpha_s^2\left[1+\sum_{n=1}^{\infty}b_n\,\alpha_s^n\right], \tag{16}$$

where $b_0 = \frac{\beta_0}{4\pi}$ and $b_0 b_1 = \frac{\beta_1}{(4\pi)^2}$, etc. Explicitly, up to NNLO:

$$\mu^2 \frac{\mathrm{d}\alpha_s(\mu)}{\mathrm{d}\mu^2} = -\alpha_s(\mu) \left[\beta_0 \left(\frac{\alpha_s(\mu)}{2\pi} \right) + \beta_1 \left(\frac{\alpha_s(\mu)}{2\pi} \right)^2 + \beta_2 \left(\frac{\alpha_s(\mu)}{2\pi} \right)^3 + \mathcal{O}(\alpha_s^4) \right] .$$

The first five coefficients are known [3], where the fifth one has been calculated only recently [4–8]. The first 3 coefficients ($\overline{\mathrm{MS}}$-scheme) are

$$\begin{aligned} \beta_0 &= \frac{11\, C_A - 4 T_R N_F}{6} , \\ \beta_1 &= \frac{17\, C_A^2 - 10 C_A T_R N_F - 6 C_F T_R N_F}{6} , \\ \beta_2 &= \frac{1}{432} \big(2857 C_A^3 + 108 C_F^2 T_R N_F - 1230 C_F C_A T_R N_F - 2830 C_A^2 T_R N_F \\ &\quad + 264 C_F T_R^2 N_F^2 + 316 C_A T_R^2 N_F^2 \big) . \end{aligned} \tag{17}$$

Introducing Λ as integration constant with $L = \log(\mu^2/\Lambda^2)$ yields the following solution up to order NNLO:

$$\alpha_s(\mu) = \frac{4\pi}{\beta_0 L} \left(1 - \frac{\beta_1}{\beta_0^2} \frac{\log L}{L} + \frac{1}{\beta_0^2 L^2} \left(\frac{\beta_1^2}{\beta_0^2} \left(\log^2 L - \log L - 1 \right) + \frac{\beta_2}{\beta_0} \right) \right) . \tag{18}$$

Truncating the series Eq. (16) at leading order leads to the simple solution Eq. (1), or, without introducing Λ,

$$\begin{aligned} Q^2 \frac{\partial \alpha_s}{\partial Q^2} = \frac{\partial \alpha_s}{\partial t} = -b_0 \alpha_s^2 \;&\Rightarrow\; -\frac{1}{\alpha_s(Q^2)} + \frac{1}{\alpha_s(\mu^2)} = -b_0\, t \\ &\Rightarrow\; \alpha_s(Q^2) = \frac{\alpha_s(\mu^2)}{1 + b_0\, t\, \alpha_s(\mu^2)} . \end{aligned} \tag{19}$$

Eq. (19) implies that

$$\alpha_s(Q^2) \overset{Q^2 \to \infty}{\longrightarrow} \frac{1}{b_0 t} \overset{Q^2 \to \infty}{\longrightarrow} 0 . \tag{20}$$

This behaviour is called *asymptotic freedom*: the larger Q^2, the smaller the coupling, so at very high energies (small distances), the quarks and gluons can be treated as if they were free particles. The behaviour of α_s as a function of Q^2 is illustrated in Fig. 2 including recent measurements. Note that the

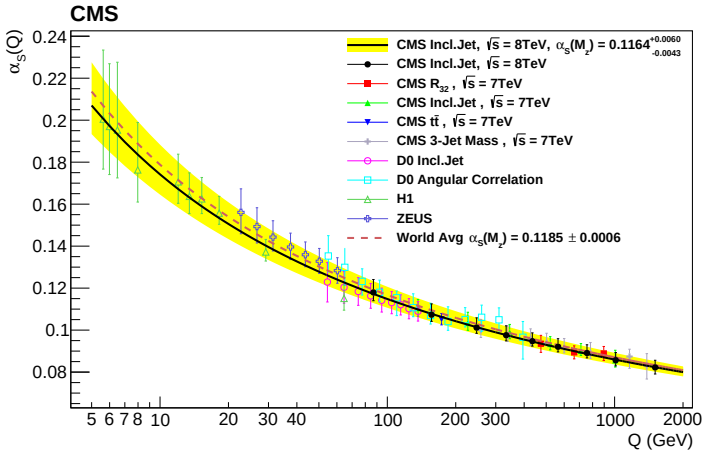

Figure 2: The running coupling $\alpha_s(Q^2)$. *Figure from arXiv:1609.05331.*

sign of b_0 is positive for QCD, while it is negative for QED. It can be proven that, in 4 space-time dimensions, only non-Abelian gauge theories can be asymptotically free. For the discovery of asymptotic freedom in QCD [9, 10], Gross, Politzer and Wilczek got the Nobel Prize in 2004.
Note that in the derivation of the RGE above, we have assumed that the observable R does not depend on other mass scales like quark masses. However, the renormalisation group equations can be easily extended to include mass renormalisation, which will lead to running quark masses:

$$\left(\mu^2\frac{\partial}{\partial\mu^2} + \beta(\alpha_s)\frac{\partial}{\partial\alpha_s} - \gamma_m(\alpha_s)m\frac{\partial}{\partial m}\right) R\left(\frac{Q^2}{\mu^2}, \alpha_s, \frac{m}{Q}\right) = 0\,, \tag{21}$$

where γ_m is called the *mass anomalous dimension* and the minus sign before γ_m is a convention. In a perturbative expansion we can write the mass anomalous dimension as $\gamma_m(\alpha_s) = c_0\,\alpha_s\,(1 + \sum_n c_n\alpha_s^n)$. The coefficients are known up to c_4 [11–14].

Scale uncertainties

From the perturbative solution of the RGE we can derive how a physical quantity $O^{(N)}(\mu)$, expanded in α_s as $O^{(N)}(\mu) = \sum_{n=0}^{N} C_n(\mu)\alpha_s^{n+k}(\mu^2)$ and truncated at order N in perturbation theory (k is the power of α_s at leading

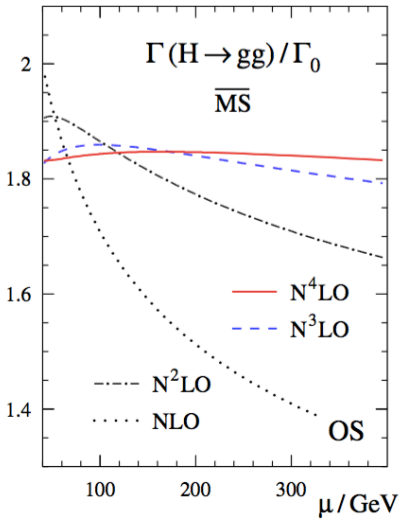

Figure 3: Example $H \to gg$ for the reduction of the scale dependence at higher orders. *Figure from Ref. [2], see also [8].*

order), changes with the renormalisation scale μ:

$$\frac{\mathrm{d}}{\mathrm{d}\log(\mu^2)} O^{(N)}(\mu) \sim \mathcal{O}\left(\alpha_s(\mu^2)^{N+1}\right) \ . \tag{22}$$

Therefore it is clear that, the more higher order coefficients c_n we can calculate, the less our result will depend on the unphysical scale μ^2. Therefore the dependence of the scale is used to estimate the uncertainty of a result calculated to a certain order in perturbation theory. Usually the scale is varied by a factor of two up and down. An example for the reduction of the scale dependence at higher orders is shown in Fig. 3.

An expansion up to NNLO of an observable O normalised to the LO cross section σ_0 can be written as

$$\frac{1}{\sigma_0}\frac{\mathrm{d}\sigma}{dO} = \left(\frac{\alpha_s}{2\pi}\right)\frac{\mathrm{d}C_1}{\mathrm{d}O} + \left(\frac{\alpha_s}{2\pi}\right)^2\frac{\mathrm{d}C_2}{\mathrm{d}O} + \left(\frac{\alpha_s}{2\pi}\right)^3\frac{\mathrm{d}C_3}{\mathrm{d}O} + \mathcal{O}(\alpha_s^4)\,. \tag{23}$$

In terms of the running coupling $\alpha_s(\mu)$, the NNLO expression becomes

$$\begin{aligned}
&\frac{1}{\sigma_0}\frac{\mathrm{d}\sigma}{\mathrm{d}O}(s,\mu^2,O) = \\
&\left(\frac{\alpha_s(\mu)}{2\pi}\right)\frac{\mathrm{d}C_1}{\mathrm{d}O} + \left(\frac{\alpha_s(\mu)}{2\pi}\right)^2\left(\frac{\mathrm{d}C_2}{\mathrm{d}O} + \frac{\mathrm{d}C_1}{\mathrm{d}O}\beta_0\log\frac{\mu^2}{s}\right) \\
&+ \left(\frac{\alpha_s(\mu)}{2\pi}\right)^3\left(\frac{\mathrm{d}C_3}{\mathrm{d}O} + 2\frac{\mathrm{d}C_2}{\mathrm{d}O}\beta_0\log\frac{\mu^2}{s} + \frac{\mathrm{d}C_1}{\mathrm{d}O}\left(\beta_0^2\,\log^2\frac{\mu^2}{s} + \beta_1\,\log\frac{\mu^2}{s}\right)\right) \\
&+ \mathcal{O}(\alpha_s^4)\,. \qquad (24)
\end{aligned}$$

As an example we consider an observable called *thrust*, shown in Fig. 4. Thrust is an example of so-called *event-shape* observables, which describes how "pencil-like" an event looks like. Events shapes can be defined based on hadronic tracks in the detector, avoiding jet definitions, and are particularly useful in e^+e^- annihilation, where the total energy of the partonic event is known. Thrust T is defined by

$$T = \max_{\vec{n}}\frac{\sum_{i=1}^m |\vec{p}_i\cdot\vec{n}|}{\sum_{i=1}^m |\vec{p}_i|}\,, \qquad (25)$$

where $\vec{n}$ is a three-vector (the direction of the thrust axis) such that T is maximal. The particle three-momenta $\vec{p}_i$ are defined in the e^+e^- centre-of-mass frame.

Fig. 4 shows several features: 1. the scale dependence is reduced as the perturbative order increases, 2. the NNLO curve is closest to the data, 3. the data are still not well described by NNLO. The reasons for the latter are well understood: The perturbative prediction for the thrust distribution becomes singular as $T \to 1$, there is also a logarithmic divergence $\sim \ln(1-T)$. The latter is characteristic for events shape distributions. In perturbation theory at nth order logarithms of the form $\alpha_s^n \ln^m(1/(1-T))$ with $m \leq 2n$ appear. These spoil the convergence of the perturbative series and should be "resummed" if we want to make reliable prediction near the phase space region where $T \to 1$. Furthermore, the so-called *power corrections*, the terms of $\mathcal{O}\left(\frac{\Lambda}{Q}\right)^p$ in Eq. (**??**), play a role for this observable.

In hadronic collisions there is another scale, the factorisation scale μ_f, which needs to be taken into account when assessing the uncertainty of the theoretical prediction. Varying both μ_r and μ_f simultaneously in the same directions

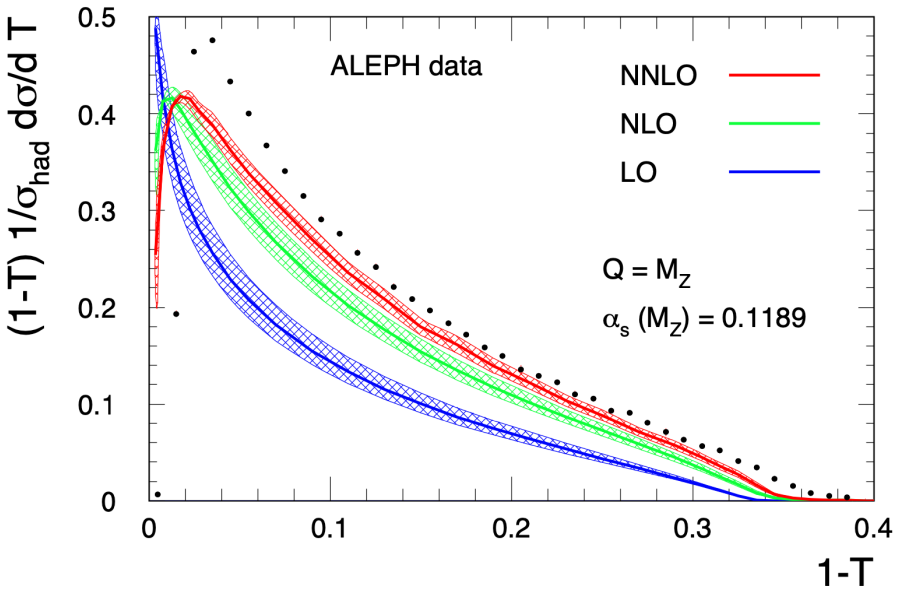

Figure 4: One minus thrust distribution at different orders in perturbation theory, including scale uncertainty bands. *Figure from Ref. [15].*

can lead to accidental cancellations and hence underestimation of the perturbative uncertainties. Therefore, in the presence of both μ_r and μ_f, often so-called *7-point scale variations* are performed, which means $\mu_{r,f} = c_{r,f}\mu_0$, where $c_r, c_f \in \{2, 1, 0.5\}$ and where the extreme variations $(c_r, c_f) = (2, 0.5)$ and $(c_r, c_f) = (0.5, 2)$ have been omitted.
Still, the question remains what to choose for the central scale μ_0. A convenient choice is a scale where the higher order corrections are small, i.e. a scale showing good "perturbative stability". In Fig. 3, a good choice would be $\mu_0 \approx 150\,\text{GeV}$.
Let us now see a few examples where such scale variations do not capture the true uncertainties. First some prelimiary remarks, along the lines of Ref. [16]. If there is only one scale μ_r involved, the the scale dependence of an observable is given through $\alpha_s(\mu_r)$, and we can use the beta-function, resp. Eq. (18), to move from a result at a scale μ_0 to a result at a different scale. For an observable O, known to order α_s^N,

$$O = \sum_{n=0}^{N} C_n(\mu_r)\alpha_s^{n+k}(\mu_r);\,,$$

where k is the power of α_s at leading order, we therefore have (this time not normalised to the LO cross section)

$$O = C_0\alpha_s^k(\mu_r) + \left(C_1 + b_0 C_0 \ln\left(\frac{\mu_r^2}{\mu_0^2}\right)\right)\alpha_s^{k+1}(\mu_r) + \mathcal{O}(\alpha_s^{k+2})\,. \tag{26}$$

Variations of μ_r will change the C_0-part of the $\mathcal{O}(\alpha_s^{k+2})$ term, however the magnitude of C_1 can only be known by direct calculation.
To illustrate the improvement in scale uncertainty that may occur at NNLO, let us consider the corrections up to (N)NLO for an observable as for example a jet cross section as a function of transverse energy, where $k = 2$. The renormalisation scale dependence is entirely predictable,

$$\begin{aligned}\frac{d\sigma}{dE_T} &= \alpha_s^2(\mu_r)C_0 \\ &\quad + \alpha_s^3(\mu_r)\left(C_1 + 2b_0 L C_0\right) \\ &\quad + \alpha_s^4(\mu_r)\left(C_2 + 3b_0 L C_1 + (3b_0^2 L^2 + 2b_1 L)C_0\right)\end{aligned} \tag{27}$$

with $L = \ln(\mu_r/E_T)$. C_0 and C_1 are the known LO and NLO coefficients. Now assume that C_2 is an unknown NNLO term (note however that C_2 is

known meanwhile [17,18]). Fig. 5 shows that the scale dependence is systematically reduced by increasing the number of terms in the perturbative exp nsion. At NLO, there is always a turning point where the prediction is insensitive to small changes in μ_r. If this occurs at a scale far from the typically chosen values of μ_r, the NLO K-factor (defined as $K = 1 + \alpha_s(\mu_r)C_1/C_0$) will be large. At NNLO the scale dependence is clearly significantly reduced. However, a more quantitative statement requires knowledge of C_2.

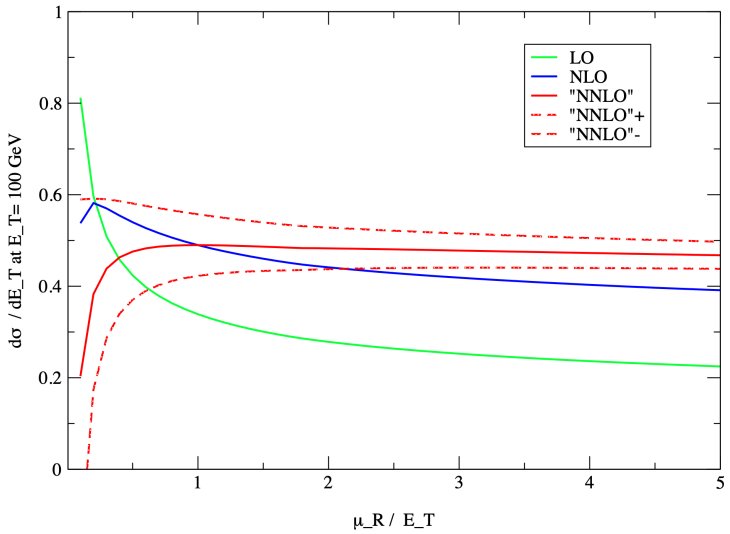

Figure 5: Single jet inclusive distribution at $E_T = 100$ GeV and $0.1 < |\eta| < 0.7$ at $\sqrt{s} = 1800$ GeV at LO (green), NLO (blue) and NNLO (red). The solid and dashed red lines show the NNLO prediction if $C_2 = 0$, $C_2 = \pm C_1^2/C_0$ respectively. Figure from Ref. [16].

For some processes, C_1 (and C_2) turned out to be pretty large, and the scale uncertainty bands obtained form 7-point scale variations do not (fully) overlap between the different orders. One such example is Higgs production in gluon fusion, known to order N^3LO. Fig. 6 shows a very nice stabilisation of the scale dependence, however the higher order corrections are very large. The standard scale uncertainty bands are shown in Fig. 7. Among the reasons for the large K-factors, in particular the NLO K-factor, are large colour factors and new partonic channels opening up.
In Fig. 8 the μ_f and μ_r dependence is shown separately. Usually one can see

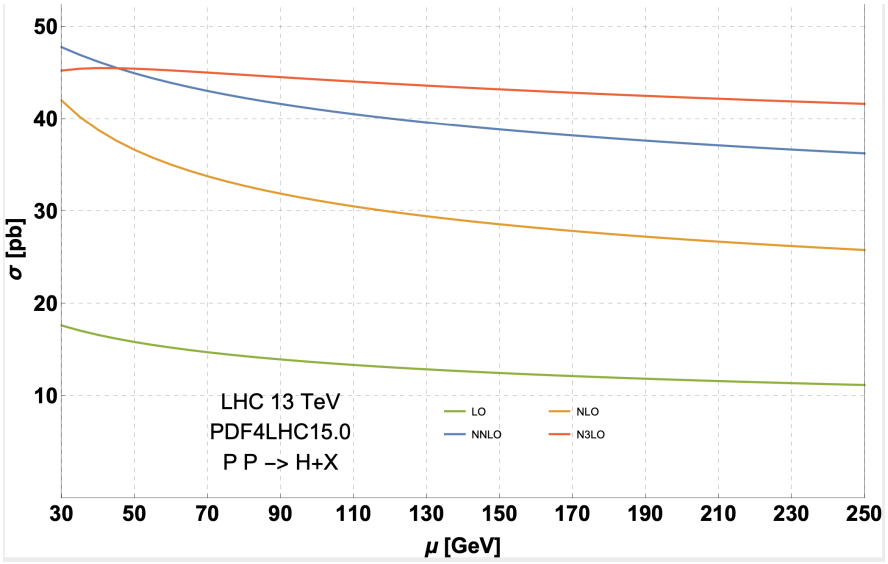

Figure 6: Higgs production in gluon fusion, stabilisation of the scale dependence. Figure from Ref. [19].

that the perturbative series stabilises at latest between NNLO and N3LO. However, for charged current Drell-Yan production and a central scale of $Q = 100\,\text{GeV}$, shown in Fig. 9, the NNLO and N3LO uncertainty bands do not overlap.
Looking at the μ_f dependence separately, one can see that the NNLO band is accidentally small, see Fig. 10.
Furthermore, the behaviour of the scale uncertainty bands can depend sensitively on the definition of the central scale, see Fig. 11. The different central scale choices are

- the individual jet transverse momentum p_T. This however can lead to the scale being set to values that are not representative of the scale of the underlying hard scattering process.

- The leading-jet transverse momentum $p_{T,1}$, This scale uses the transverse momentum of the hardest jet in the event, which is a better proxy for the scale of the hard interaction compared to the $\mu = p_T$ choice.

- The scalar sum of the transverse momenta of all reconstructed jets H_T, $H_T = \sum_{i \in \text{jets}} p_{T,i}$.

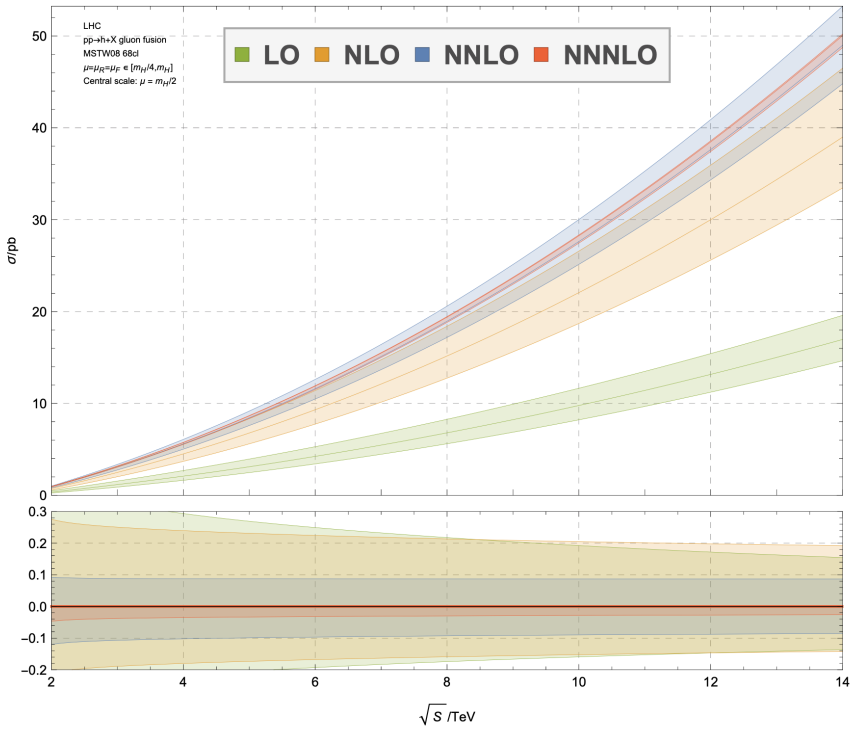

Figure 7: Scale uncertainty bands for Higgs production in gluon fusion. Figure from Ref. [20].

- The scalar sum of the transverse momenta of all partons $\hat{H}_T$: the transverse momentum sum is not based on the reconstructed jets, but instead obtained as the transverse momentum sum of all partons in the event: $\hat{H}_T = \sum_{i \in \text{partons}} p_{T,i}$. This scale choice also has the advantage of being insensitive to the jet reconstruction applied in the analysis and is an infrared-safe event shape variable.

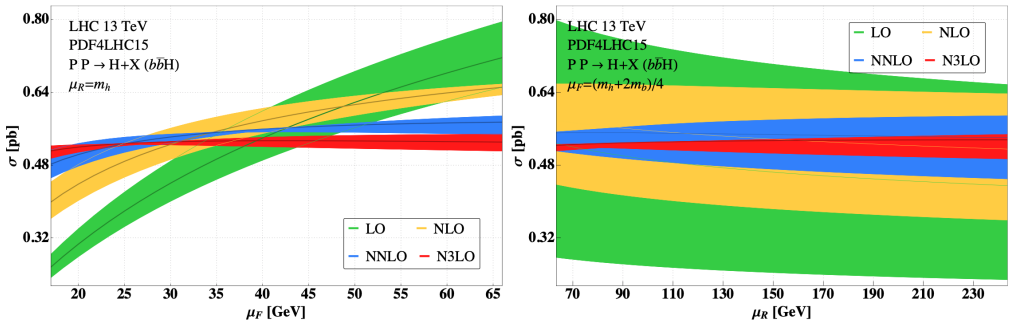

Figure 8: Higgs production in bottom quark fusion. Figure from Ref. [21].

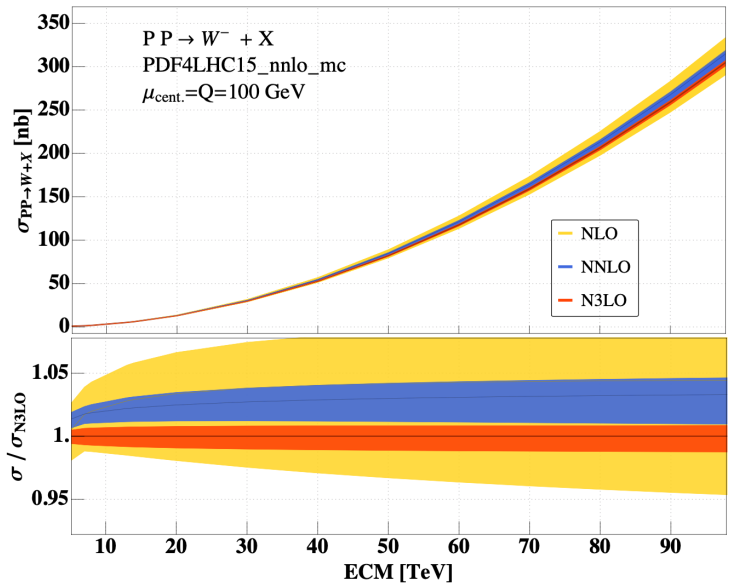

Figure 9: Charged current Drell-Yan production, $pp \to W^-$. Figure from Ref. [22].

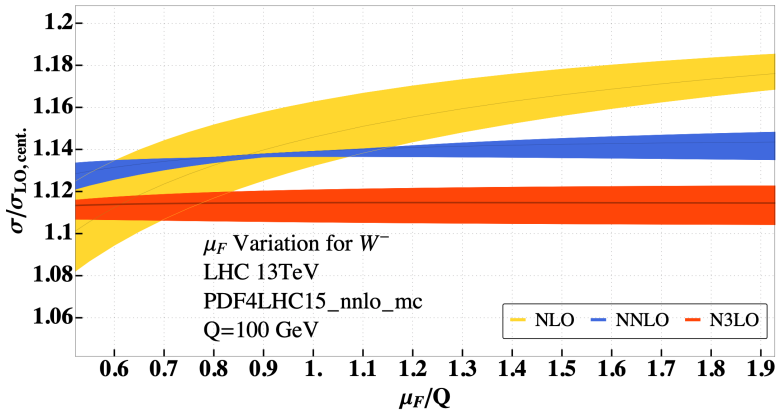

Figure 10: Charged current Drell-Yan production, μ_f-dependence. Figure from Ref. [22].

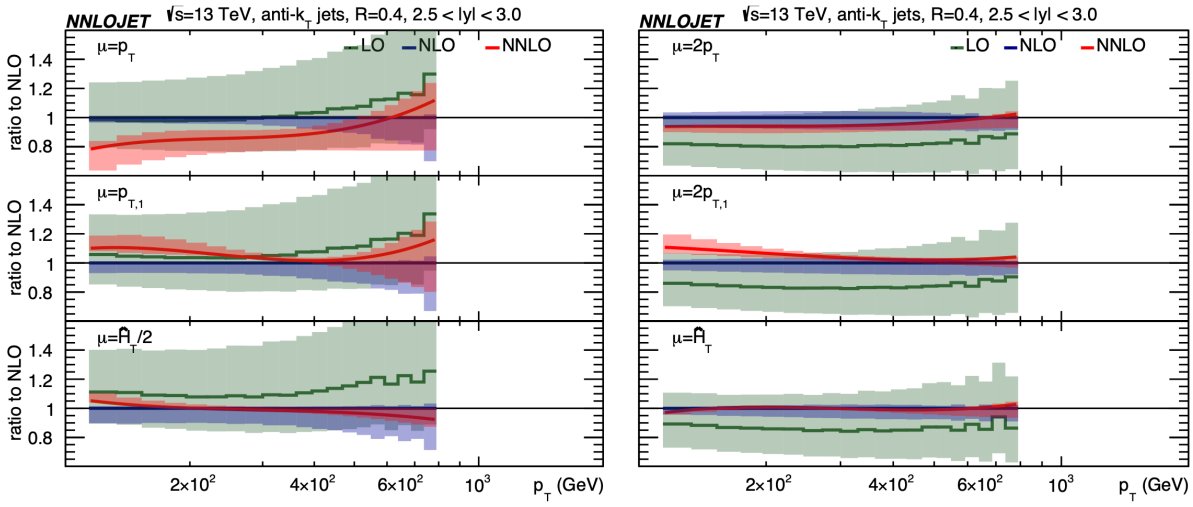

Figure 11: Inclusive jet p_T spectrum integrated over rapidity at LO (green), NLO (blue) and NNLO (red) normalised to the NLO prediction as a function of the central scale choice for cone size $R = 0.4$. Figure from Ref. [23].

4.2 Loops and divergences

4.2.1 Dimensional regularisation

Tree level results in QCD are mostly not accurate enough to match the current experimental precision and suffer from large scale uncertainties. When calculating higher orders, we encounter singularities: ultraviolet (UV) singularities, and infrared (IR) singularities due to soft or collinear massless particles. Therefore the introduction of a *regulator* is necessary.
Let us first have a look at UV singularities: The expression for the one-loop two-point function shown below naively would be

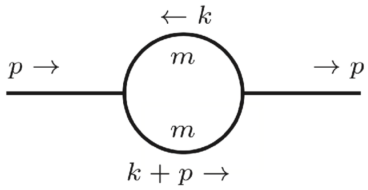

Figure 12: One-loop two-point function ("bubble").

$$I_2 = \int_{-\infty}^{\infty} \frac{d^4k}{(2\pi)^4} \frac{1}{[k^2 - m^2 + i\delta][(k+p)^2 - m^2 + i\delta]} \,. \tag{28}$$

If we are only interested in the behaviour of the integral for $|k| \to \infty$ we can neglect the masses, transform to polar coordinates and obtain

$$I_2 \sim \int \mathrm{d}\Omega_3 \int_0^{\infty} \mathrm{d}|k| \frac{|k|^3}{|k|^4} \,. \tag{29}$$

This integral is clearly not well-defined. If we introduce an upper cutoff Λ (and a lower limit $|k|_{\min}$ because we neglected the masses and p^2, which would serve as an IR regulator), it is regulated:

$$I_2 \sim \int_{|k|_{\min}}^{\Lambda} \mathrm{d}|k| \frac{1}{|k|} \sim \log\left(\frac{\Lambda}{|k|_{\min}}\right) \,. \tag{30}$$

The integral has a logarithmic UV divergence for $\Lambda \to \infty$. The problem with cut-off regularisation with a regulator Λ is that it is neither a Lorentz invariant nor a gauge invariant way to regulate integrals over loop momenta.

A regularisation method which preserves the symmetries is *dimensional regularisation.*
Dimensional regularisation has been introduced in 1972 by 't Hooft and Veltman [24] (and by Bollini and Giambiagi [25]) as a method to regularise UV divergences in a gauge invariant way, thus completing the proof of renormalisability.
The idea is to work in $D = 4 - 2\epsilon$ space-time dimensions. Divergences for $D \to 4$ will appear as poles in $1/\epsilon$. This means that the Lorentz algebra objects (momenta, polarisation vectors, metric tensor) live in a D-dimensional space. The γ-algebra also has to be extended to D dimensions. How to treat internal and external Lorentz vectors and the γ-algebra is not unique. There are several *regularisation schemes* within dimensional regularisation. For example, when doing a calculation in supersymmetry, you may not want to use a scheme where massless bosons have $D - 2$ polarisation states while massless fermions have 2 polarisation states. Of course the different schemes must lead to the same result for physical quantities.
An important feature of dimensional regularisation is that it regulates IR singularities, i.e. divergences occurring when massless particles become soft and/or collinear, as well. Ultraviolet divergences occur for loop momenta $k \to \infty$, so in general the UV behaviour becomes better for $\epsilon > 0$, while the IR behaviour becomes better for $\epsilon < 0$. Certainly we cannot have $D < 4$ and $D > 4$ at the same time. What is formally done is to first assume the IR divergences are regulated in some other way, e.g. by assuming all external legs are off-shell or by introducing a small mass for all massless particles. In this case all poles in $1/\epsilon$ will be of UV nature and renormalisation can be performed. Then we can analytically continue to the whole complex D-plane, in particular to $\mathrm{Re}(D) > 4$. If we now remove the auxiliary IR regulator, the IR divergences will show up as $1/\epsilon$ poles. (This is however not done in practice, where all poles just show up as $1/\epsilon$ poles, and after UV renormalisation, the remaining poles must be of IR nature.)

Naive degree of divergence

The naive degree of UV divergence ω of an integral can be determined by power counting: if we work in D dimensions at L loops, and consider an integral with P propagators and n_l factors of the loop momentum belonging to loop $l \in \{1, \ldots, L\}$ in the numerator, we have $\omega = D\,L - 2P + 2\sum_l \lfloor n_l/2 \rfloor$, where $\lfloor n_l/2 \rfloor$ is the nearest integer less or equal to $n_l/2$. We have logarith-

mic, linear, quadratic,... overall divergences for $\omega = 0, 1, 2, \ldots$ and no UV divergence for $\omega < 0$. This means that in 4 dimensions at one loop, we have UV divergences in all two-point functions, three-point functions with rank ≥ 2 and four-point functions with rank ≥ 4.
These considerations do not take into account UV subdivergences of multi-loop integrals, or a reduction of the degree of divergence due to gauge cancellations. Therefore ω is called *naive* or *superficial* degree of divergence.

In dimensional regularisation, the only change to the Feynman rules to be made is to multiply the couplings in the Lagrangian by a factor μ^ϵ: $g \to g\mu^\epsilon$, where μ is an arbitrary mass scale. This ensures that each term in the Lagrangian has the correct mass dimension. The momentum integration involves $\int \frac{d^D k}{(2\pi)^D}$ for each loop.

D-dimensional treatment of γ_5

Extending the Clifford algebra to D dimensions implies

$$\{\gamma^\mu, \gamma^\nu\} = 2\, g^{\mu\nu} \quad \text{with} \quad g^\mu_\mu = D \;, \tag{31}$$

leading for example to $\gamma_\mu \not{p} \gamma^\mu = (2 - D)\not{p}$. However, it is not obvious how to continue the Dirac matrix γ_5 to D dimensions. In 4 dimensions it is defined as

$$\gamma_5 = i\, \gamma_0 \gamma_1 \gamma_2 \gamma_3 \tag{32}$$

which is an intrinsically 4-dimensional definition. In 4 dimensions, γ_5 has the algebraic properties $\gamma_5^2 = 1$, $\{\gamma_\mu, \gamma_5\} = 0$, $\mathrm{Tr}\,(\gamma_\mu \gamma_\nu \gamma_\rho \gamma_\sigma \gamma_5) = 4i\epsilon_{\mu\nu\rho\sigma}$. However, in D dimensions, the latter two conditions cannot be maintained simultaneously unless we give up cyclicity of the trace whenever an odd number of γ_5 matrices is present in the trace *(see Exercise 7)*. Remember $\epsilon_{\mu\nu\rho\sigma} = 1$ if $(\mu\nu\rho\sigma)$ is an even permutation of (0123), -1 if $(\mu\nu\rho\sigma)$ is an odd permutation of (0123) and 0 otherwise.
Therefore we need a prescription how to deal with γ_5 in D dimensions. The most commonly used prescription [24, 26–28] for γ_5 is to define

$$\gamma_5 = \frac{i}{4!}\, \epsilon_{\mu_1\mu_2\mu_3\mu_4} \gamma^{\mu_1} \gamma^{\mu_2} \gamma^{\mu_3} \gamma^{\mu_4} \;, \tag{33}$$

where the Lorentz indices of the "ordinary" γ-matrices will be contracted in D dimensions. Doing so, Ward identities relying on $\{\gamma_5, \gamma_\mu\} = 0$ break down

due to an extra $(D-4)$-dimensional contribution. These need to be repaired by so-called "finite renormalisation" terms [27]. For practical calculations it can be convenient to split the other Dirac matrices into a 4-dimensional and a $(D-4)$-dimensional part, $\gamma_\mu = \bar{\gamma}_\mu + \tilde{\gamma}_\mu$, where $\bar{\gamma}_\mu$ is 4-dimensional and $\tilde{\gamma}_\mu$ is $(D-4)$-dimensional. The definition (33) implies

$$\{\gamma^\mu, \gamma_5\} = \begin{cases} 0 & \mu \in \{0,1,2,3\} \\ 2\tilde{\gamma}^\mu \gamma_5 & \text{otherwise.} \end{cases}$$

The second line above can also be read as $[\gamma_5, \tilde{\gamma}^\mu] = 0$, which can be interpreted as γ_5 acting trivially in the non-physical dimensions. There are other prescriptions for γ_5, which maintain $\{\gamma_\mu^{(D)}, \gamma_5\} = 0$, but then have to give up the cyclicity of the trace [29].

4.2.2 One-loop integrals

Integration in D dimensions

We first consider a scalar one-loop diagram with N external legs and N propagators, as given in (34). The case with loop momenta in the numerator ("tensor integrals") will be treated later. If k is the loop momentum, the momenta of the propagators are $q_i = k + r_i$, where $r_i = \sum_{j=1}^{i} p_j$. If we define all momenta as incoming, momentum conservation implies $\sum_{j=1}^{N} p_j = 0$ and hence $r_N = 0$.

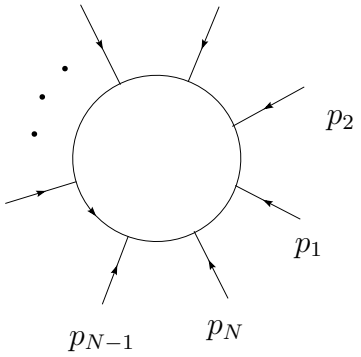

Figure 13: Generic one-loop integral

$$I_N^D \;=\; \int_{-\infty}^{\infty} \frac{d^Dk}{i\pi^{\frac{D}{2}}} \frac{1}{\prod_{i=1}^N (q_i^2 - m_i^2 + i\delta)} \,. \tag{34}$$

We use the integration measure $d^Dk/i\pi^{\frac{D}{2}} \equiv d\kappa$ to avoid ubiquitous factors of $i\pi^{\frac{D}{2}}$ which will arise upon momentum integration.

Feynman parameters

To combine products of denominators of the type $d_i^{n_i} = [(k+r_i)^2 - m_i^2 + i\delta]^{n_i}$ into one single denominator, we can use the identity

$$\frac{1}{d_1^{n_1} d_2^{n_2} \ldots d_N^{n_N}} = \frac{\Gamma(\sum_{i=1}^N n_i)}{\prod_{i=1}^N \Gamma(n_i)} \int_0^\infty \prod_{i=1}^N dz_i \, z_i^{n_i-1} \frac{\delta(1 - \sum_{j=1}^N z_j)}{[z_1 d_1 + z_2 d_2 + \ldots + z_N d_N]^{\sum_{i=1}^N n_i}} \tag{35}$$

The integration parameters z_i are called *Feynman parameters*. For generic one-loop diagrams we have $n_i = 1 \; \forall i$. Propagator powers n_i different from one become important when we derive relations between integrals.

Schwinger parametrisation

An alternative to Feynman parametrisation is the so-called "Schwinger parametrisation", based on

$$\frac{1}{\prod_{i=1}^N d_i^{n_i}} = \frac{1}{\prod_{i=1}^N \Gamma(n_i)} \int_0^\infty \left(\prod_{j=1}^N \mathrm{d}\alpha_j \, \alpha_j^{n_j-1} \right) \exp\left(- \sum_{i=1}^N \alpha_i d_i \right) . \tag{36}$$

which can be derived from the definition of the Γ-function

$$\Gamma(t) = \int_0^\infty dx \, x^{t-1} \exp(-x), \quad Re(t) > 0 \,. \tag{37}$$

The Gaussian integration formula

$$\int_{-\infty}^{\infty} d^D r_E \exp(-\alpha \, r_E^2) = \left(\frac{\pi}{\alpha} \right)^{\frac{D}{2}} \;, \; \alpha > 0 \tag{38}$$

can be used to integrate over the momenta (after Wick rotation) in the Schwinger parametrisation.

Simple example: one-loop two-point function

For $N = 2$, (2-point integral), the Feynman parametrisation is given by

$$\begin{aligned} I_2 &= \int_{-\infty}^{\infty} \mathrm{d}\kappa \, \frac{1}{[k^2 - m^2 + i\delta][(k+p)^2 - m^2 + i\delta]} \\ &= \Gamma(2) \int_0^{\infty} dz_1 dz_2 \int_{-\infty}^{\infty} \mathrm{d}\kappa \, \frac{\delta(1 - z_1 - z_2)}{[z_1 \, (k^2 - m^2) + z_2 \, ((k+p)^2 - m^2) + i\delta]^2} \\ &= \int_0^1 dx \int_{-\infty}^{\infty} \mathrm{d}\kappa \, \frac{1}{[k^2 + 2xk \cdot p + xp^2 - m^2 + i\delta]^2} \, , \end{aligned} \tag{39}$$

where we have substituted $z_1 = (1-x)\, u, z_2 = x$ before the last line. As the momentum integral is shift invariant, we can substitute $l = k + xp$ to eliminate the term linear in the loop momentum, to arrive at

$$I_2 = \int_0^1 dx \int_{-\infty}^{\infty} \frac{\mathrm{d}^D l}{i\pi^{\frac{D}{2}}} \, \frac{1}{[l^2 + p^2 x(1-x) - m^2 + i\delta]^2} \, . \tag{40}$$

For integrals with more external legs the linear term can be eliminated by an analogous shift of the loop momentum. Therefore, the generic form of a one-loop integral after Feynman parametrisation and after having performed the shift to achieve a quadratic form in the loop momentum is given by

$$I_N^D = \Gamma(N) \int_0^{\infty} \prod_{i=1}^{N} dz_i \, \delta(1 - \sum_{j=1}^{N} z_j) \int_{-\infty}^{\infty} \frac{\mathrm{d}^D l}{i\pi^{\frac{D}{2}}} \, \left[l^2 - R^2 + i\delta\right]^{-N} \tag{41}$$

where for $N = 2$ and both propagators massive we have just derived
$R = -p^2 x(1-x) + m^2$.
For the general case, the denominator would be of the form
$\left[k^2 + 2k \cdot Q + \sum_{i=1}^{N} z_i \, (r_i^2 - m_i^2) + i\delta\right]^{-N}$ with $Q^\mu = \sum_{i=1}^{N} z_i \, r_i^\mu$ and the shift $l = k + Q$ would eliminate the linear term in the loop momentum. One finds

$$\begin{aligned} R^2 &= -\frac{1}{2} \sum_{i,j=1}^{N} z_i \, z_j \, \mathcal{S}_{ij} \qquad \text{with} \\ \mathcal{S}_{ij} &= (r_i - r_j)^2 - m_i^2 - m_j^2 \, , \quad \sum_{i=1}^{N} z_i = 1 \, . \end{aligned} \tag{42}$$

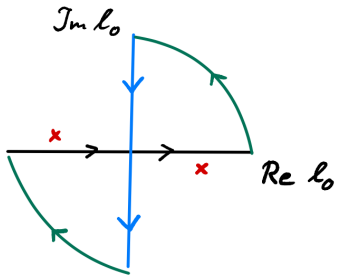

Figure 14: Integration contour after Wick rotation.

The matrix $\mathcal{S}_{ij}$, sometimes also called *modified Cayley matrix*, is the quantity encoding all the kinematic dependence of the integral. It plays a major role in the algebraic reduction of tensor integrals or integrals with higher N to simpler objects, as well as in the analysis of the kinematic singularities of the integrand.

Momentum integration for scalar one-loop N-point integrals

Now we perform the momentum integration for an integral of the form Eq. (41). Remember that we are in Minkowski space, where $l^2 = l_0^2 - \vec{l}^2$, so temporal and spatial components are not on equal footing. The poles of the denominator in Eq. (41) are located at $l_0^2 = R^2 + \vec{l}^2 - i\delta \Rightarrow l_0^{\pm} \simeq \pm\sqrt{R^2 + \vec{l}^2} \mp i\,\delta$. Thus the $i\delta$ term shifts the poles away from the real axis in the l_0-plane.
For the integration over the loop momentum, we better work in Euclidean space where $l_E^2 = \sum_{i=1}^{D} l_i^2$. Hence we make the transformation $l_0 \to i\,l_4$, such that $l^2 \to -l_E^2 = -(l_4^2 + \vec{l}^2)$, which implies that the integration contour in the complex l_0-plane is rotated by 90° such that the contour in the complex l_4-plane looks as shown below. This is called *Wick rotation*. We see that the $i\delta$ prescription is exactly such that the contour does not enclose any poles. Therefore the integral over the closed contour is zero, and we can use the identity

$$\int_{-\infty}^{\infty} dl_0 f(l_0) = i \int_{-\infty}^{\infty} dl_4 f(l_4) \tag{43}$$

Our integral now reads

$$I_N^D = (-1)^N \Gamma(N) \int_0^\infty \prod_{i=1}^N dz_i \, \delta(1 - \sum_{l=1}^N z_l) \int_{-\infty}^\infty \frac{d^D l_E}{\pi^{\frac{D}{2}}} \left[l_E^2 + R^2 - i\delta \right]^{-N} \quad (44)$$

Now we can introduce polar coordinates in D dimensions to evaluate the momentum integral.

$$\int_{-\infty}^\infty d^D l_E = \int_0^\infty dr \, r^{D-1} \int d\Omega_{D-1} \, , \; r = \sqrt{l_E^2} = \left(\sum_{i=1}^D l_i^2 \right)^{\frac{1}{2}} \quad (45)$$

$$\int d\Omega_{D-1} = V(D) = \frac{2\pi^{\frac{D}{2}}}{\Gamma(\frac{D}{2})} \quad (46)$$

where $V(D)$ is the volume of a unit sphere in D dimensions, which we encountered already in the context of D-dimensional phase space integrals. Thus we have

$$I_N^D = 2(-1)^N \frac{\Gamma(N)}{\Gamma(\frac{D}{2})} \int_0^\infty \prod_{i=1}^N dz_i \, \delta(1 - \sum_{l=1}^N z_l) \int_0^\infty dr \, r^{D-1} \, \frac{1}{[r^2 + R^2 - i\delta]^N}$$

Substituting $r^2 = x$:

$$\int_0^\infty dr \, r^{D-1} \, \frac{1}{[r^2 + R^2 - i\delta]^N} = \frac{1}{2} \int_0^\infty dx \, x^{D/2-1} \, \frac{1}{[x + R^2 - i\delta]^N} \quad (47)$$

Now the substitution $x = zR^2$ can be done to arrive at

$$\frac{1}{2} \int_0^\infty dx \, x^{D/2-1} \, \frac{1}{[x + R^2 - i\delta]^N} = \frac{1}{2} \left[\, R^2 - i\delta \, \right]^{\frac{D}{2}-N} \int_0^\infty dz \, z^{D/2-1} \, [1+z]^{-N} \, . \quad (48)$$

Note that we still carry along the $-i\delta$ term because it can be useful to indicate the direction of the analytic continuation when performing the integrals over the Feynman parameters. As it only indicates an infinitesimal shift, we can always rescale δ by a positive quantity. The z-integral can be identified as the Euler Beta-function $B(a,b)$, defined as

$$B(a,b) = \int_0^\infty dz \, \frac{z^{a-1}}{(1+z)^{a+b}} = \int_0^1 dy \, y^{a-1} (1-y)^{b-1} = \frac{\Gamma(a)\Gamma(b)}{\Gamma(a+b)} \, , \quad (49)$$

to finally arrive at

$$I_N^D \;=\; (-1)^N \Gamma(N-\frac{D}{2}) \int_0^\infty \prod_{i=1}^N dz_i\, \delta(1-\sum_{l=1}^N z_l)\, \left[\, R^2 - i\delta \,\right]^{\frac{D}{2}-N} \;. \quad (50)$$

The integration over the Feynman parameters remains to be done, but for one-loop applications, the integrals we need to know explicitly have maximally $N = 4$ external legs. Integrals with $N > 4$ can be expressed in terms of boxes, triangles, bubbles and tadpoles (in the case of massive propagators). The analytic expressions for these "master integrals" are well-known. The most complicated analytic functions which can appear at one loop are dilogarithms.

The generic form of the derivation above makes clear that we do not have to go through the procedure of Wick rotation explicitly each time. All we need (for scalar integrals) is to use the following general formula for D-dimensional momentum integration (in Minkowski space, and after having performed the shift to have a quadratic form in the denominator):

$$\int \frac{d^D l}{i\pi^{\frac{D}{2}}} \frac{(l^2)^r}{[l^2 - R^2 + i\delta]^N} = (-1)^{N+r} \frac{\Gamma(r+\frac{D}{2})\Gamma(N-r-\frac{D}{2})}{\Gamma(\frac{D}{2})\Gamma(N)} \left[R^2 - i\delta\right]^{r-N+\frac{D}{2}} \quad (51)$$

Example one-loop two-point function

Applying the above procedure to our two-point function, we obtain

$$I_2 \;=\; \Gamma(2-\frac{D}{2}) \int_0^1 dx\, [-p^2\, x\, (1-x) + m^2 - i\delta\,]^{\frac{D}{2}-2} \;. \quad (52)$$

For $m^2 = 0$, the result can be expressed in terms of Γ-functions:

$$I_2 = \left(-p^2\right)^{\frac{D}{2}-2} \Gamma(2-D/2)\, B(D/2-1, D/2-1) \;, \quad (53)$$

where the $B(a,b)$ is defined in Eq. (49). The two-point function has an UV pole which is contained in

$$\Gamma(2-D/2) = \Gamma(\epsilon) = \frac{1}{\epsilon} - \gamma_E + \mathcal{O}(\epsilon) \;, \quad (54)$$

where γ_E is "Euler's constant", $\gamma_E = \lim_{n\to\infty}\left(\sum_{j=1}^{n}\frac{1}{j} - \ln n\right) = 0.5772156649\ldots$.
Including the factor $g^2\mu^{2\epsilon}$ which usually comes with the loop, and multiplying by $\frac{i\pi^{\frac{D}{2}}}{(2\pi)^D}$ for the normalisation conventions, we obtain

$$g^2\mu^{2\epsilon}\frac{i\pi^{\frac{D}{2}}}{(2\pi)^D}\,I_2 = (4\pi)^\epsilon\; i\,\frac{g^2}{(4\pi)^2}\,\Gamma(\epsilon)\left(-p^2/\mu^2\right)^{-\epsilon}\,B(1-\epsilon,1-\epsilon)\;. \tag{55}$$

Remarks:

- As the combination $\Delta = \frac{1}{\epsilon} - \gamma_E + \ln(4\pi)$ always occurs in combination with a pole, in the so-called $\overline{\text{MS}}$ subtraction scheme ("modified Minimal Subtraction"), the whole combination Δ is subtracted in the renormalisation procedure.

- Scaleless integrals (i.e. integrals containing no dimensionful scale like masses or external momenta) are zero in dimensional regularisation, we use

$$\int_{-\infty}^{\infty}\frac{d^Dk}{k^{2\rho}} = 0\;. \tag{56}$$

Tensor integrals

If we have loop momenta in the numerator, the integration procedure is essentially the same, except for combinatorics and additional Feynman parameters in the numerator. The substitution $k = l - Q$ introduces terms of the form $(l-Q)^{\mu_1}\ldots(l-Q)^{\mu_r}$ into the numerator of eq. (41). As the denominator is symmetric under $l \to -l$, only the terms with even numbers of l^μ in the numerator will give a non-vanishing contribution upon l-integration. We can use a *form factor representation* of a tensor integral, where the Lorentz structure has been extracted, each Lorentz tensor multiplying a scalar quantity, the *form factor*.
Historically, tensor integrals occurring in one-loop amplitudes were reduced to scalar integrals using so-called *Passarino-Veltman* reduction [30]. It is based on the fact that at one loop, scalar products of loop momenta with external momenta can always be expressed as combinations of propagators. The problem with Passarino-Veltman reduction is that it introduces powers of inverse Gram determinants $1/(\det G)^r$ for the reduction of a rank r tensor

integral. This can lead to numerical instabilities upon phase space integration in kinematic regions where $\det G \to 0$.

Example for *Passarino-Veltman reduction:*
Consider the form factor representation of a rank one three-point integral

$$\begin{aligned} I_3^{D,\mu} &= \int_{-\infty}^{\infty} d\kappa \, \frac{k^\mu}{[k^2+i\delta][(k+p_1)^2+i\delta][(k+p_1+p_2)^2+i\delta]} = A_1\, r_1^\mu + A_2\, r_2^\mu \\ r_1 &= p_1 \ , \ r_2 = p_1 + p_2 \ . \end{aligned}$$

Contracting with r_1 and r_2 and using the identities

$$k \cdot r_i = \frac{1}{2}\left[(k+r_i)^2 - k^2 - r_i^2\right] \ , \ i \in \{1,2\}$$

we obtain, after cancellation of numerators

$$\left(\begin{array}{cc} 2\, r_1 \cdot r_1 & 2\, r_1 \cdot r_2 \\ 2\, r_2 \cdot r_1 & 2\, r_2 \cdot r_2 \end{array} \right) \left(\begin{array}{c} A_1 \\ A_2 \end{array} \right) = \left(\begin{array}{c} R_1 \\ R_2 \end{array} \right) \tag{57}$$

$$\begin{aligned} R_1 &= I_2^D(r_2) - I_2^D(r_2 - r_1) - r_1^2 I_3(r_1, r_2) \\ R_2 &= I_2^D(r_1) - I_2^D(r_2 - r_1) - r_2^2 I_3(r_1, r_2) \ . \end{aligned}$$

Solving for the form factors A_1 and A_2 we see that the solution involves the inverse of the Gram matrix $G_{ij} = 2\, r_i \cdot r_j$.

Libraries where the scalar integrals and tensor one-loop form factors can be obtained numerically:

- `LoopTools` [31, 32]
- `OneLoop` [33]
- `golem95` [34–36]
- `Collier` [37]
- `Package-X` [38]

Scalar integrals only: `QCDLoop` [39, 40].

The calculation of one-loop amplitudes with many external legs is most efficiently done using "unitarity-cut-inspired" methods, for a review see e.g. Ref. [41]. One of the advantages is that it allows (numerical) reduction at *integrand level* (rather than integral level), which helps to avoid the generation of spurious terms which can blow up intermediate expressions.

4.3 Cancellation of infrared singularities

4.3.1 Structure of NLO calculations

Next-to-leading order calculations consist of several parts, which can be classified as virtual corrections (containing usually one loop), real corrections (radiation of extra particles relative to the leading order) and subtraction terms to deal with singularities. In the following we will assume that the virtual corrections already include UV renormalisation, such that the subtraction terms only concern the subtraction of the infrared (IR) singularities. IR singularities occur when a massless particle becomes soft (low energy) or when two massless particles become collinear to each other.
We will consider "NLO" as next-to-leading order in an expansion in the strong coupling constant α_s. The general structure is very similar for electroweak corrections. The real and virtual contributions to the simple example $\gamma^* \to q\bar{q}$ are shown in Fig. 15.

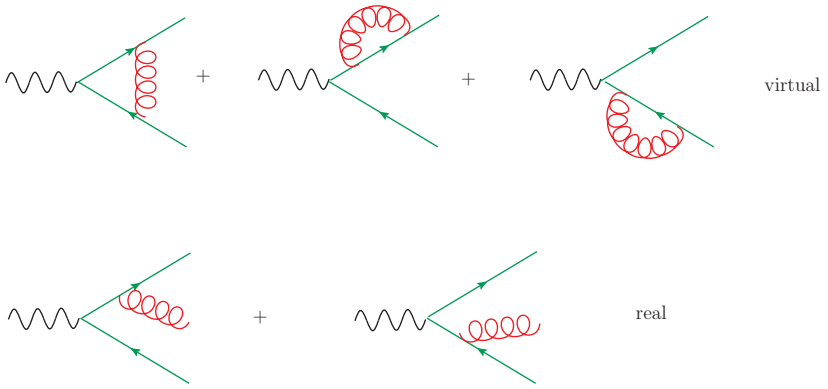

Figure 15: The real and virtual NLO contributions to $\gamma^* \to q\bar{q}$.

If $\mathcal{M}_0$ is the leading order (LO) amplitude (also called *Born* amplitude) and $\mathcal{M}_{\text{virt}}, \mathcal{M}_{\text{real}}$ are the virtual and real NLO amplitudes as shown in Fig. 15, the corresponding cross section is given by

$$\sigma^{NLO} = \underbrace{\int \mathrm{d}\phi_2 \, |\mathcal{M}_0|^2}_{\sigma^{LO}} + \int_R \mathrm{d}\phi_3 \, |\mathcal{M}_{\text{real}}|^2 + \int_V \mathrm{d}\phi_2 \, 2Re\left(\mathcal{M}_{\text{virt}} \mathcal{M}_0^*\right) \ . \tag{58}$$

The sum of the integrals $\int_R$ and $\int_V$ above is finite. However, this is not true for the individual contributions. The real part contains divergences due to

soft and collinear radiation of massless particles. While $\mathcal{M}_{\rm real}$ itself is a tree level amplitude and thus finite, the divergences show up upon integration over the phase space $\mathrm{d}\Phi_3$. In $\int_V$, the phase space is the same as for the Born amplitude, but the loop integrals in $\mathcal{M}_{\rm virt}$ contain IR singularities.
Let us anticipate the answer, which we will (partly) calculate later. We find:

$$\sigma_R = \sigma^{\rm Born}\tilde{H}(\epsilon)\, C_F \frac{\alpha_s}{2\pi}\left(\frac{2}{\epsilon^2}+\frac{3}{\epsilon}+\frac{19}{2}\right) , \tag{59}$$
$$\sigma_V = \sigma^{\rm Born}H(\epsilon)\, C_F \frac{\alpha_s}{2\pi}\left(-\frac{2}{\epsilon^2}-\frac{3}{\epsilon}-8\right) ,$$

where $H(\epsilon) = \left(\frac{4\pi\mu^2}{-Q^2}\right)^\epsilon \frac{\Gamma(1+\epsilon)\Gamma^2(1-\epsilon)}{\Gamma(1-2\epsilon)}$ and $\tilde{H}(\epsilon) = H(\epsilon) + \mathcal{O}(\epsilon^3)$. The exact ϵ-dependence of $H(\epsilon) = 1 + \mathcal{O}(\epsilon)$ is irrelevant after summing up real and virtual contributions, because the poles in ϵ all cancel!
This must be the case according to the **KLN theorem** (Kinoshita-Lee-Nauenberg) [42, 43]. It says that

IR singularities must cancel when summing the transition rate over all degenerate (initial and final) states.

In our example, we do not have initial state singularities. However, in the final state we can have a massless quark accompanied by a soft gluon, or a collinear quark-gluon pair. Such a state cannot be distinguished from just a quark state, and therefore is "degenerate". Only when summing over all the final state multiplicities contributing to the cross section at a given order in α_s, the divergences cancel. Another way of stating this is by looking at the squared amplitude at order α_s and considering all cuts, see Fig. 16 (contributions which are zero for massless quarks are not shown). The KLN theorem states that *the sum of all cuts leading to physical final states is free of IR poles.*
The cancellations between $\int_R$ and $\int_V$ in Eq. (58) are non-trivial, because the phase space integrals contain a different number of particles in the final state. Methods trying to exploit the KLN-cancellations at integrand level, mostly based on *loop-tree-duality* [44,45], also exist. They rely on numerical integrals over 4-dimensional momenta, arranging the loop momentum integration such that it can be combined with the phase space integration over the real radiation, in a way that enforces the cancellations of the IR singularities locally. However these methods are numerically very challenging.

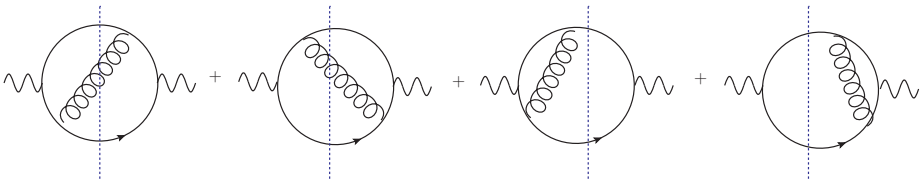

Figure 16: The sum over cuts of the amplitude squared shown above is finite according to the KLN theorem.

Infrared singularities in one-loop integrals

For loop integrals, after momentum integration, singularities can arise if the polynomial forming the integrand vanishes for some values of the Feynman parameters and kinemtic invariants (and has a negative power). At one loop the analysis is relatively simple because the integrand is a quadratic form in the Feynman parameters, see Eq. (42).
Quite in general, necessary (but not sufficient) conditions for divergences in Feynman parametrised loop integrals (with L loops) are given by the *Landau equations* [46, 47]:

$$\begin{aligned} z_i \left(q_i^2(\{k_l, p\}) - m_i^2\right) = 0 \quad \forall\, i \in \{1, \ldots, N\}\ , \\ \frac{\partial}{\partial k_l^\mu} \sum_{i \in \text{loop}\, l} z_i \left(q_i^2(\{k_l, p\}) - m_i^2\right) = 0 \quad \forall\, l \in \{1, \ldots, L\}\ . \end{aligned} \tag{60}$$

The Landau equations have two classes of solutions:

(a) Solutions where particles in the loop go on-shell, corresponding in general to physical (or anomalous) thresholds. If eq. (60) has a solution $z_i > 0$ for every $i \in \{1, \ldots, N\}$, i.e. all particles in the loop are *simultaneously on-shell*, then the singularity is called *leading Landau singularity*. If a solution exists where some $z_i = 0$ while the other z_j are positive, the Landau condition corresponds to a sub-leading Landau singularity.

(b) Soft and/or collinear singularities appearing as poles in $1/\epsilon$ are always stemming from some $z_i = 0$.

At one loop, we can analyze the singularities in terms of the kinematic matrix S of Eq. (42) (or a minor of the latter for sub-divergences)

$$S_{ij} = (r_i - r_j)^2 - m_i^2 - m_j^2 \equiv (q_i - q_j)^2 - m_i^2 - m_j^2\ . \tag{61}$$

Thus at one loop, the second Landau equation reads $\sum_{i=1}^{N} z_i\, q_i^\mu = 0$. Contracting the second Landau equation with q_j^μ corresponds to $\sum_{i=1}^{N} z_i\, q_i \cdot q_j = 0 \Rightarrow Q \cdot \vec{z} = 0$, with $Q_{ij} = q_i \cdot q_j$, and therefore to $\det Q = 0$ for $z_i \neq 0$.
At one loop it follows that a necessary condition for a soft or collinear singularity is that for at least one value of the index i we have

$$S_{i+1\,i+1} = S_{i+1\,i+2} = S_{i+1\,i} = 0 \;: \qquad \text{soft singularity}\,, \tag{62}$$

$$S_{i\,i} = S_{i+1\,i+1} = S_{i\,i+1} = 0 \;: \qquad \text{collinear singularity}\,. \tag{63}$$

(The indices in eq. (63) should be interpreted mod N, where N is the number of external legs.) We have $S_{i\,i+1} = p_{i+1}^2 - m_i^2 - m_{i+1}^2$, so this expression is zero if one of the masses is zero and p_{i+1}^2 equals the other mass squared, or p_{i+1}^2 is light-like and both masses are zero. Therefore, in order to have a soft divergence, we must have either a massless particle connecting two on-shell massive particles or a massless particle connecting two light-like particles. For a collinear divergence, we must have at least two adjacent propagators massless, and the external line between these two propagatrs must be light-like. In other words, the structure of the Cayley matrices for integrals having a soft or collinear divergence is

$$S_{\text{soft}} = \begin{pmatrix} \dots & 0 & \dots & \dots \\ 0 & 0 & 0 & \dots \\ \dots & 0 & \dots & \dots \\ \dots & \dots & \dots & \dots \end{pmatrix}, \quad S_{\text{collinear}} = \begin{pmatrix} \dots & \dots & \dots & \dots \\ \dots & 0 & 0 & \dots \\ \dots & 0 & 0 & \dots \\ \dots & \dots & \dots & \dots \end{pmatrix}. \tag{64}$$

If both of these structures are present, we have a soft and collinear divergence.

Infrared safety

If we want to calculate a prediction for a certain observable, based on an n-particle final state, we need to multiply the amplitude by a *measurement function* $J(p_1 \dots p_n)$. The measurement function can contain for example a jet definition, or the definition of thrust, or it defines the transverse momentum distribution of a final state particle. Schematically, the structure of the NLO cross section then is the following. In the real radiation part, we have $n+1$ particles in the final state. Therefore the measurement function in the real radiation part must depend on $n+1$ particles. Let us consider the case where we have an IR pole if the variable x, denoting for example the energy

of an extra gluon with momentum p_{n+1} in the real radiation part, goes to zero. If we define

$$\begin{aligned}
\mathcal{B}_n &= \int \mathrm{d}\phi_n \, |\mathcal{M}_0|^2 = \int \mathrm{d}\phi_n B_n \\
\mathcal{V}_n &= \int \mathrm{d}\phi_n \, 2Re\,(\mathcal{M}_{\mathrm{virt}}\mathcal{M}_0^*) = \int \mathrm{d}\phi_n \frac{V_n}{\epsilon} \\
\mathcal{R}_n &= \int \mathrm{d}\phi_{n+1} \, |\mathcal{M}_{\mathrm{real}}|^2 = \int \mathrm{d}\phi_n \int_0^1 \mathrm{d}x \, x^{-1-\epsilon} \, R_n(x)
\end{aligned} \tag{65}$$

and a measurement function $J(p_1 \ldots p_n, p_{n+1})$ we have

$$\sigma^{NLO} = \int \mathrm{d}\phi_n \left\{ \left(B_n + \frac{V_n}{\epsilon} \right) J(p_1 \ldots p_n, 0) + \int_0^1 \mathrm{d}x \, x^{-1-\epsilon} \, R_n(x) \, J(p_1 \ldots p_{n+1}) \right\} . \tag{66}$$

In the inclusive case (calculation of the total cross section) we have $J \equiv 1$. The integration over x leads to the explicit $1/\epsilon$ poles which must cancel with the virtual part:

$$\int_0^1 \mathrm{d}x \, x^{-1-\epsilon} \, R_n(x) = -\frac{R_n(0)}{\epsilon} + \int_0^1 \mathrm{d}x \, x^{-\epsilon} \frac{R_n(x) - R_n(0)}{x} \tag{67}$$

The cancellation of the poles between $\frac{V_n}{\epsilon}$ and $\frac{R_n(0)}{\epsilon}$ in the non-inclusive case will only work if

$$\lim_{p_{n+1} \to 0} J(p_1 \ldots p_n, p_{n+1}) = J(p_1 \ldots p_n, 0) \, . \tag{68}$$

This is a non-trivial condition for the definition of an observable, for example a jet algorithm, and is called *infrared safety*. The formulation above is taylored to the soft limit where all components of p_{n+1} go to zero, however an analogous condition must hold if two momenta become collinear.
As mentioned above, the measurement function is also important if we define differential cross sections $\mathrm{d}\sigma/\mathrm{d}X$ (also called distributions), for example the transverse momentum distribution $\mathrm{d}\sigma/\mathrm{d}p_T$ of one of the final state particles. In this case we have $J(p_1 \ldots p_n) = \delta(X - \chi_n(p_i))$, where $\chi_n(p_i)$ is the definition of the observable, based on n partons. Again, infrared safety requires $\chi_{n+1}(p_i) \to \chi_n$ if one of the p_i becomes soft or two of the momenta become collinear to each other.

4.3.2 Soft gluon emission

Soft gluon emission is very important in QCD. In contrast to the collinear case, soft gluons are insensitive to the spin of the partons. The only feature they are sensitive to is the colour charge.
To see this, consider the amplitude for the second line in Fig. 15, with momentum k and colour index a for the gluon, and momenta and colour indices p, i $(\bar{p}, j)$ for the quark (antiquark). The amplitude for massless quarks is given by

$$\mathcal{M}_{ij}^{a,\mu} = t_{ij}^a \, g_s \, \mu^\epsilon \bar{u}(p) \not{\epsilon}(k) \frac{\not{p} + \not{k}}{(p+k)^2} \Gamma^\mu v(\bar{p}) - t_{ij}^a \, g_s \, \mu^\epsilon \bar{u}(p) \Gamma^\mu \frac{\not{\bar{p}} + \not{k}}{(\bar{p}+k)^2} \not{\epsilon}(k) v(\bar{p}) \, , \tag{69}$$

where Γ^μ describes a general interaction vertex with the photon, in our case $\Gamma^\mu = \gamma^\mu$. Now we take the soft limit, which means that all components of k are much smaller than p and $\bar{p}$, thus neglecting factors of $\not{k}$ in the numerator and k^2 in the denominator. Using the Dirac equation leads to

$$\begin{aligned} \mathcal{M}_{ij,soft}^{a,\mu} &= g_s \, \mu^\epsilon \, t_{ij}^a \, \bar{u}(p) \, \Gamma^\mu \, v(\bar{p}) \left(\frac{2\epsilon(k) \cdot p}{2p \cdot k} - \frac{2\epsilon(k) \cdot \bar{p}}{2\bar{p} \cdot k} \right) \\ &= g_s \, \mu^\epsilon \, J_{ij}^{a,\nu}(k) \epsilon_\nu(k) \, \mathcal{M}_{Born}^\mu \quad , \quad \mathcal{M}_{Born}^\mu = \bar{u}(p) \Gamma^\mu v(\bar{p}) \, . \end{aligned} \tag{70}$$

We see that the amplitude factorises completely into the product of the Born amplitude and the *soft gluon current*

$$J_{ij}^{a,\nu}(k) = \sum_{r=p,\bar{p}} \tilde{T}_{ij}^a \, \frac{r^\nu}{r \cdot k} \, , \tag{71}$$

In our example $\tilde{T}_{ij}^a = t_{ij}^a$ for $r = p$ and $\tilde{T}_{ij}^a = -t_{ij}^a$ for $r = \bar{p}$. This type of factorisation actually holds for an arbitrary number of soft gluon emissions, and can be obtained using the "soft Feynman rules" shown in Fig. 17.

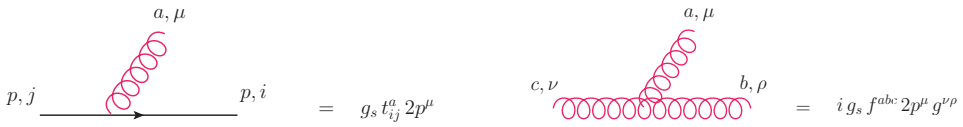

Figure 17: The Feynman rules for gluon emission in the soft limit.

Following the standards set by Refs. [48, 49], the soft gluon current is more conveniently expressed in terms of colour charge operators $\mathbf{T}_i$, where i now labels the *parton* i emitting a gluon (not its colour index). The action of $\boldsymbol{T}_i$ onto the colour space is defined by

$$\langle a_1, \ldots, a_i, \ldots, a_m, a \,|\boldsymbol{T}_i| b_1, \ldots, b_i, \ldots, b_m \rangle = \delta_{a_1 b_1} .... T^a_{a_i b_i} \ldots \delta_{a_m b_m} \quad , \tag{72}$$

where $T^a_{kl} \equiv t^a_{kl}$ ($SU(3)$ generator in the fundamental representation) if the emitting particle i is a quark. In the case of an emitting antiquark $T^a_{kl} \equiv \bar{t}^a_{kl} = -t^a_{lk}$. If the emitting particle i is a gluon, $T^a_{bc} \equiv -if_{abc}$ ($SU(3)$ generator in the adjoint representation).
Then we can write down the universal behaviour of the matrix element $\mathcal{M}(k, p_1, \ldots, p_m)$ in the limit where the momentum k of the gluon becomes soft. Denoting by a and $\varepsilon^\mu(k)$ the colour and the polarisation vector of the soft gluon, the matrix element fulfils the following factorisation formula:

$$\mathcal{M}^a(k, p_1, \ldots, p_m) \simeq g_s \, \mu^\epsilon \varepsilon^\mu(k) \, J^a_\mu(k) \, \mathcal{M}(p_1, \ldots, p_m) \, , \tag{73}$$

where $\mathcal{M}^a(p_1, \ldots, p_m)$ is obtained from the original matrix element by removing the soft gluon k. The factor $\boldsymbol{J}_\mu(k)$ is the soft-gluon current

$$\boldsymbol{J}^\mu(k) = \sum_{i=1}^{m} \boldsymbol{T}_i \, \frac{p_i^\mu}{p_i \cdot k} \, , \tag{74}$$

which depends on the momenta and colour charges of the hard partons in the matrix element on the right-hand side of Eq. (73). The symbol '$\simeq$' means that on the right-hand side we have neglected contributions that are less singular than $1/|k|$ in the soft limit $k \to 0$.
Squaring Eq. (73) and summing over the gluon polarisations leads to the *universal soft-gluon factorisation formula* at $\mathcal{O}(\alpha_s)$ for the squared amplitude [48]

$$|\mathcal{M}(k, p_1, \ldots, p_m)|^2 \simeq -g_s^2 \, \mu^{2\epsilon} \, 2 \sum_{i,j=1}^{m} S_{ij}(k) \, |\mathcal{M}_{(i,j)}(p_1, \ldots, p_m)|^2 \quad , \tag{75}$$

where the factor

$$S_{ij}(p_s) = \frac{p_i \cdot p_j}{2 \, (p_i \cdot \, p_s) \, (p_j \cdot \, p_s)} = \frac{s_{ij}}{s_{is} \, s_{js}} \tag{76}$$

is called *Eikonal factor*. It can be generalised to the emission of n soft gluons and plays an important role in resummation.
The colour correlations produced by the emission of a soft gluon are taken into account by the square of the colour-correlated amplitude $|\mathcal{M}_{(i,j)}|^2$, given by

$$\begin{aligned} &|\mathcal{M}_{(i,j)}(p_1,\ldots,p_m)|^2 \\ &\equiv \langle\, \mathcal{M}(p_1,\ldots,p_m)\,|\,\boldsymbol{T}_i\cdot\boldsymbol{T}_j\,|\,\mathcal{M}(p_1,\ldots,p_m)\rangle \\ &= \left(\mathcal{M}_{c_1..b_i...b_j...c_m}(p_1,\ldots,p_m)\right)^*\; T^a_{b_i d_i}\,T^a_{b_j d_j}\;\mathcal{M}_{c_1..d_i...d_j...c_m}(p_1,\ldots,p_m)\;. \end{aligned} \tag{77}$$

The angular brackets in the second line denote a basis in colour space.

4.3.3 Collinear singularities

Let us come back to the amplitude for the real radiation given in Eq. (69). In a frame where $p = E_p(1,\vec{0}^{(D-2)},1)$ and $k = k_0(1,\vec{0}^{(D-3)}\sin\theta,\cos\theta)$, the denominator $(p+k)^2$ is given by

$$(p+k)^2 = 2k_0E_p\,(1-\cos\theta) \quad \to 0 \text{ for } \quad \left\{ \begin{array}{ll} k_0\to 0 & \text{(soft)} \\ \theta\to 0 & \text{(collinear)} \end{array}\right. \tag{78}$$

Note that if the quark line was massive, $p^2 = m^2$, we would have

$$(p+k)^2 - m^2 = 2k_0E_p\,(1-\beta\cos\theta)\,,\ \beta = \sqrt{1-m^2/E_p^2}$$

and thus the collinear singularity would be absent. This is why it is sometines also called *mass singularity*, since the propagator only can become collinear divergent if the partons are all massless, while the soft singularity is present irrespective of the quark mass.
The important point to remember is that in the collinear limit, we also have a form of factorisation, shown schematically in Fig. 18.
The universal factorisation behaviour can be described as

$$|\mathcal{M}_{m+1}|^2\,\mathrm{d}\Phi_{m+1} \to |\mathcal{M}_m|^2\mathrm{d}\Phi_m\,\frac{\alpha_s}{2\pi}\,\frac{\mathrm{d}k_\perp^2}{k_\perp^2}\,\frac{\mathrm{d}\phi}{2\pi}\,\mathrm{d}z\,P_{a\to bc}(z)\;. \tag{79}$$

The function $P_{a\to bc}(z)$ is the so-called *Altarelli-Parisi splitting function* describing the splitting of parton a into partons b and c, and z is the momentum fraction of the original parton a taken away by parton b after emission of c. For example, consider collinear gluon emission off a quark:

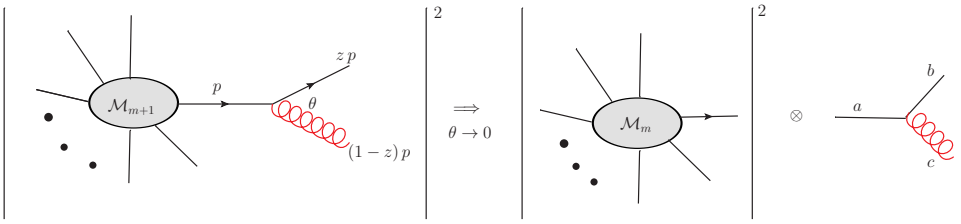

Figure 18: Factorisation in the collinear limit.

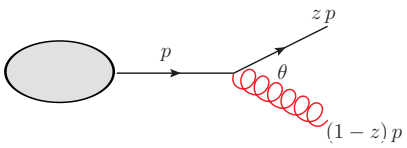

Figure 19: Gluon emission leading to $P_{q\to qg}(z)$.

The corresponding Altarelli-Parisi splitting function for $z < 1$ is given by

$$P_{q\to qg}(z) = C_F\,\frac{1+z^2}{1-z}\,, \tag{80}$$

and is often just denoted as $P_{qq}(z)$. The other possible splitting functions have the following form:

$$P_{q\to gq}(z) = C_F\,\frac{1+(1-z)^2}{z}\,, \tag{81}$$

$$P_{g\to q\bar{q}}(z) = T_R\,\left(z^2+(1-z)^2\right)\,,\; P_{g\to gg}(z) \;= C_A\left(z\,(1-z)+\frac{z}{1-z}+\frac{1-z}{z}\right)\,.$$

We will come back to them later when we discuss parton distribution functions.

To see how the factorisation formula Eq. (79) comes about, a convenient parametrisation of the gluon momentum k is the so-called *Sudakov parametrisation*:

$$\begin{aligned} k^\mu &= (1-z)\,p^\mu + \beta\,n^\mu + k_\perp^\mu\,, \\ k^+ &= k\cdot n = (1-z)\,p\cdot n\,,\; k^- = k\cdot p = \frac{k_\perp^2}{2(1-z)}\,, \end{aligned} \tag{82}$$

where n^μ is a light-like vector with $p \cdot n \neq 0$ and $k_\perp \cdot n = 0$, and β can be determined by the requirement that k must be light-like:

$$k^2 = 0 = 2(1-z)\,\beta\, p\cdot n - k_\perp^2 \Rightarrow \beta = \frac{k_\perp^2}{2\,p\cdot n\,(1-z)}\ , \tag{83}$$

and therefore $(p-k)^2 = -k_\perp^2/(1-z)$. The part of the phase space due to the gluon emission then reads (in 4 dimensions, for D dimensions see below)

$$\mathrm{d}\Phi_k \equiv \frac{\mathrm{d}^4k}{(2\pi)^3}\delta(k^2) = \frac{1}{8\pi^2}\frac{\mathrm{d}\phi}{2\pi}\frac{\mathrm{d}k^+}{2k^+}\,\mathrm{d}k_\perp^2 = \frac{1}{16\pi^2}\frac{\mathrm{d}z}{(1-z)}\,\mathrm{d}k_\perp^2\ . \tag{84}$$

In this parametrisation, the soft gluon limit is $z \to 1$, the collinear singularity occurs for $k_\perp^2 \to 0$.

4.4 Example: $e^+e^- \to q\bar{q}$ at NLO

Now let us see explicitly in the $e^+e^- \to q\bar{q}$ example how the singularities manifest themselves as $1/\epsilon$ poles when we integrate over the D-dimensional phase space.
Using

$$\begin{aligned}\mathrm{d}\Phi_{1\to3} \;=\; & (2\pi)^{3-2\,D}\,2^{-1-D}(Q^2)^{D-3}\,\mathrm{d}\Omega_{D-2}\,\mathrm{d}\Omega_{D-3}\,\mathrm{d}y_1\,\mathrm{d}y_2\,\mathrm{d}y_3 \\ & (y_1\,y_2\,y_3)^{D/2-2}\;\Theta(y_1)\,\Theta(y_2)\,\Theta(y_3)\,\delta(1-y_1-y_2-y_3)\end{aligned} \tag{85}$$

we are in the position to calculate the full real radiation contribution. The matrix element (for one quark flavour with charge Q_f) in the variables defined above Eq. (**??**), where p_3 in our case is the gluon, is given by

$$|\mathcal{M}|^2_{\mathrm{real}} = C_F e^2 Q_f^2 g_s^2\,8\,(1-\epsilon)\,\left\{\frac{2}{y_2y_3} + \frac{-2+(1-\epsilon)y_3}{y_2} + \frac{-2+(1-\epsilon)y_2}{y_3} - 2\epsilon\right\}\ . \tag{86}$$

In our variables, soft singularities mean gluon momentum $p_3 \to 0$ and therefore both y_2 and $y_3 \to 0$. $p_3 \parallel p_1$ means $y_2 \to 0$ and $p_3 \parallel p_2$ means $y_3 \to 0$. Combined with the factors $(y_2\,y_3)^{D/2-2}$ from the phase space it is clear that the first term in the bracket of Eq. (86) will lead to a $1/\epsilon^2$ pole, coming from the region in phase space where soft and collinear limits coincide. To eliminate the δ-distribution, we make the substitutions

$$y_1 = 1-z_1, y_2 = z_1z_2, y_3 = z_1(1-z_2)\ \ ,\ \ \det J = z_1$$

to arrive at

$$\int \mathrm{d}\Phi_3 |\mathcal{M}|^2_{\text{real}} = \alpha\, C_F \frac{\alpha_s}{\pi}\, Q_f^2\, \tilde{H}(\epsilon)\, (Q^2)^{1-2\epsilon} \int_0^1 \mathrm{d}z_1 \int_0^1 \mathrm{d}z_2\, z_1^{-2\epsilon} \Big(z_2(1-z_1)(1-z_2)\Big)^{-\epsilon} \left\{ \frac{2}{z_1 z_2 (1-z_2)} + \frac{-2+(1-\epsilon)z_1(1-z_2)}{z_2} + \frac{-2+(1-\epsilon)z_1 z_2}{1-z_2} - 2\epsilon z_1 \right\} . \tag{87}$$

The integrals can be expressed in terms of Euler Beta-functions and lead to the result quoted in Eq. (59).

4.5 Parton evolution

4.5.1 Deeply inelastic scattering

In the previous section we have only considered leptons in the initial state (e^+e^- annihilation). Now we consider the case where we have an electron-proton collider, like for example HERA (at DESY Hamburg), which operated until 2007 and offered unique opportunities to study the proton structure. We consider the scattering of leptons off the proton, as depicted in Fig. 20, in a kinematic regime where the squared momentum transfer Q^2 is large compared to the proton mass squared ($M \sim 1\,\text{GeV}$), so we consider deeply inelastic scattering. The relations between the involved momenta and kine-

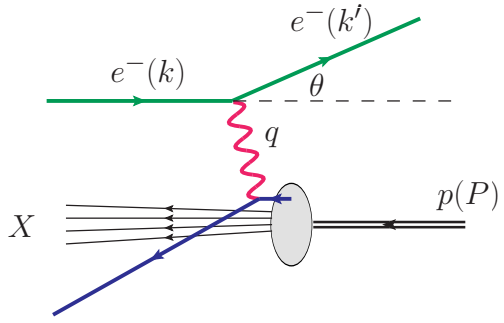

Figure 20: Deeply inelastic scattering, partonic picture. Figure from Ref. [50].

matic variables are

$$\begin{aligned} s &= (P+k)^2 \ \text{ [cms energy]}^2 \\ q^\mu &= k^\mu - k'^\mu \ \text{ [momentum transfer]} \\ Q^2 &= -q^2 = 2MExy \\ x &= \frac{Q^2}{2P\cdot q} \ \text{ [scaling variable]} \\ \nu &= \frac{P\cdot q}{M} = E - E' \ \text{ [energy loss]} \\ y &= \frac{P\cdot q}{P\cdot k} = 1 - \frac{E'}{E} \ \text{ [relative energy loss]} \, . \end{aligned} \tag{88}$$

The cross section for $e(k) + p(P) \to e(k') + X$ can be written as

$$\int \mathrm{d}\sigma = \sum_X \frac{1}{4ME} \int \mathrm{d}\Phi \, \frac{1}{4} \sum_{\text{spins}} |\mathcal{M}|^2 \, . \tag{89}$$

We can factorise the phase space and the squared matrix element into a leptonic and a hadronic part:

$$\mathrm{d}\Phi = \frac{\mathrm{d}^3k'}{(2\pi)^3 2E'} \, \mathrm{d}\Phi_X \ , \ \frac{1}{4} \sum_{\text{spins}} |\mathcal{M}|^2 = \frac{e^4}{Q^4} L^{\mu\nu} H_{\mu\nu} \, . \tag{90}$$

Then the hadronic part of the cross section can be described by the dimensionless Lorentz tensor $W_{\mu\nu} = \frac{1}{8\pi} \sum_X \int \mathrm{d}\Phi_X H_{\mu\nu}$. As it depends only on two momenta P^μ and q^μ, the most general gauge and Lorentz invariant expression must be of the form

$$\begin{aligned} W_{\mu\nu}(P,q) = &\left(-g_{\mu\nu} + \frac{q_\mu q_\nu}{q^2} \right) W_1(x, Q^2) \\ &+ \left(P_\mu - q_\mu \frac{P\cdot q}{q^2} \right) \left(P_\nu - q_\nu \frac{P\cdot q}{q^2} \right) \frac{W_2(x,Q^2)}{P\cdot q} \ , \end{aligned} \tag{91}$$

where the structure functions $W_i(x, Q^2)$ are dimensionless functions of the scaling variable x and the momentum transfer Q^2.
For the leptonic part we use the relations $E' = (1-y)E$, $\cos\theta = 1 - \frac{xyM}{(1-y)E}$ to change variables to the so-called *scaling variable* x and the relative energy loss y

$$\frac{\mathrm{d}^3k'}{(2\pi)^3 2E'} = \frac{\mathrm{d}\phi}{2\pi} \frac{E'}{8\pi^2} \, \mathrm{d}E' \, \mathrm{d}\cos\theta = \frac{\mathrm{d}\phi}{2\pi} \, \frac{yME}{8\pi^2} \, \mathrm{d}y \, \mathrm{d}x \, ,$$

and compute the trace $L^{\mu\nu} = \frac{1}{2}Tr[\not{k}\gamma^\mu \not{k}'\gamma^\nu] = k^\mu k'^\nu + k^\nu k'^\mu - g^{\mu\nu} k \cdot k'$. Then the differential cross section in x and y is obtained from Eq. (89) as

$$\frac{\mathrm{d}^2\sigma}{\mathrm{d}x\,\mathrm{d}y} = \frac{4\pi\alpha^2}{y\,Q^2}\left[y^2 W_1(x,Q^2) + \left(\frac{1-y}{x} - xy\frac{M^2}{Q^2}\right) W_2(x,Q^2)\right] .$$

In the *scaling limit*, defined by $Q^2 \to \infty$ with x fixed, we use $W_1 \to -F_1, W_2 \to F_2$, neglect the term $\sim M^2/Q^2$ and obtain

$$\frac{\mathrm{d}^2\sigma}{\mathrm{d}x\,\mathrm{d}y} = \frac{4\pi\alpha^2}{y\,Q^2}\left[\big(1+(1-y)^2\big)F_1 + \frac{1-y}{x}\big(F_2 - 2xF_1\big)\right] . \tag{92}$$

The functions F_1 and F_2 are called "structure functions", where the combination $F_L = F_2 - 2xF_1$ is also called the longitudinal structure function because it is related to the absorption of a longitudinally polarised virtual photon. They were first measured by the SLAC-MIT experiment (USA) in 1970, and have been measured very accurately at the HERA collider. The interesting feature is that, in the scaling limit, $2xF_1 \to F_2$ and F_2 becomes independent of Q^2, $F_2(x,Q^2) \to F_2(x)$, a feature which is often called *Bjorken scaling*. The *Callan-Gross* relation $F_2(x) = 2x\,F_1(x)$ which reflects that this scaling can be derived from the assumption that the photon scatters at point-like spin-1/2 particles. The observation of Bjorken scaling was very important to establish the quark model. How the scaling looks in experiment is shown in Fig. 21, where we observe that the scaling violations increase at small x. We will see in the following that scaling is violated at higher orders.

4.5.2 Proton structure in the parton model

Now let us assume the proton consists of free quarks and the lepton exchanges a hard virtual photon with one of those quarks as shown in Fig. 20. The struck quark carries a momentum p^μ, which is a fraction of the proton momentum, $p^\mu = \xi P^\mu$, so we consider the process $e(k) + q(p) \to e(k') + q(p')$. The corresponding cross section is

$$\hat{\sigma} = \frac{1}{2\hat{s}} \int \mathrm{d}\Phi_2 \, \frac{1}{4} \sum_{\text{spins}} |\mathcal{M}|^2 . \tag{93}$$

with $\hat{s} = (p+k)^2$. The "hat" indicates that we consider the partonic cross section. The squared matrix element is proportional to the product of the

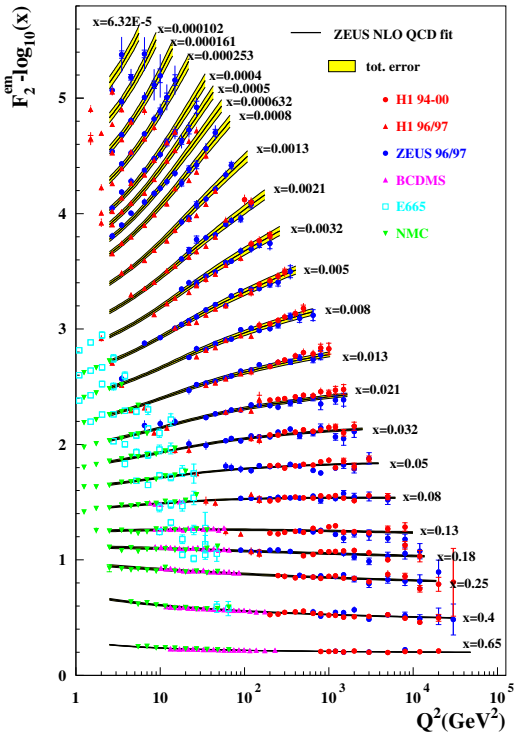

Figure 21: The structure function F_2 for different values of Q^2. Figure from Ref. [51].

lepton tensor $L^{\mu\nu}$ and a quark tensor $Q_{\mu\nu} = \frac{1}{2}Tr[\not{p}\gamma^\mu \not{p}'\gamma^\nu] = p^\mu p'^\nu + p^\nu p'^\mu - g^{\mu\nu} p\cdot p'$, leading to $L^{\mu\nu}Q_{\mu\nu} = 2(\hat{s}^2 + \hat{u}^2)$, where $\hat{u} = (p-k')^2 = -2p\cdot k'$. As $y = Q^2/\hat{s}$ we can derive, using $\hat{u}^2 = (1-y)^2\hat{s}^2$,

$$\frac{1}{4}\sum_{\text{spins}} |\mathcal{M}|^2 = \frac{e_q^2 e^4}{Q^4} L^{\mu\nu}Q_{\mu\nu} = 2e_q^2 e^4 \frac{\hat{s}^2}{Q^4}\big(1+(1-y)^2\big)\,. \tag{94}$$

Using $p'^2 = 2p\cdot q - Q^2 = Q^2(\xi/x - 1)$, the two-particle phase space (in 4 dim.) can be written as (*see Exercise 11*)

$$\mathrm{d}\Phi_2 = \frac{\mathrm{d}^3k'}{(2\pi)^3 2E'}\,\frac{\mathrm{d}^4p'}{(2\pi)^3}\,\delta\big(p'^2\big)\,(2\pi)^4\,\delta^{(4)}(k+p-k'-p') = \frac{\mathrm{d}\phi}{(4\pi)^2}\,\mathrm{d}y\,\mathrm{d}x\,\delta(\xi - x)\,. \tag{95}$$

The differential cross section in x and y for one quark flavour is then given by

$$\frac{\mathrm{d}^2\hat{\sigma}}{\mathrm{d}x\,\mathrm{d}y} = \frac{4\pi\alpha^2}{yQ^2}\left[1+(1-y)^2\right]\frac{1}{2}e_q^2\delta(\xi-x)\;. \tag{96}$$

Comparing Eqs. (92) and (96), we find the parton model predictions

$$\hat{F}_1(x) \propto e_q^2\delta(\xi-x)\,, \qquad F_2 - 2xF_1 = 0\;. \tag{97}$$

The above relations are called *Callan-Gross* relations. Thus the structure functions probe the quark constituents of the proton with $\xi = x$. However, this prediction cannot be the end of the story because experimentally, we observe that F_2 does depend on Q^2, as can be seen from Fig. 21, even though the dependence is not strong.
To see how the Q^2 dependence comes in, let us define the following:

$f_i(\xi)\mathrm{d}\xi$ is the probability to find a parton $(q, \bar{q}, g)$ with flavour i in the proton, carrying a momentum fraction of the proton between ξ and $\xi + \delta\xi$.

The function $f_i(\xi)$ is called *parton distribution function (PDF).*

Using the relations $\mathrm{d}y = \mathrm{d}Q^2/\hat{s}$ and $\delta(\xi - x) = \frac{1}{\xi}\delta\left(1-\frac{x}{\xi}\right)$, we can write the full cross section as a combination of the PDF and the differential cross section (96),

$$\frac{\mathrm{d}^2\sigma}{\mathrm{d}x\,\mathrm{d}Q^2} = \int_x^1 \frac{\mathrm{d}\xi}{\xi}\sum_i f_i(\xi)\frac{\mathrm{d}^2\hat{\sigma}}{\mathrm{d}x\,\mathrm{d}Q^2}\left(\frac{x}{\xi}, Q^2\right)\;. \tag{98}$$

This means that the cross section is a convolution of a long-distance component, the parton distribution function $f_i(\xi)$ for a parton of type i, and a short-distance component, the partonic hard scattering cross section $\hat{\sigma}$. This form is highly non-trivial, because it means that we can separate *short-distance* effects, which are calculable in perturbation theory, from *long-distance* effects, which belong to the domain of non-perturbative QCD and have to be modelled and fitted from data (or calculated by lattice QCD if possible). This *factorisation*, shown schematically in Fig. 22, can be proven rigorously in DIS using operator product expansion, and less rigorously in hadron-hadron collisions. It also holds once higher orders in α_s are taken into account (in

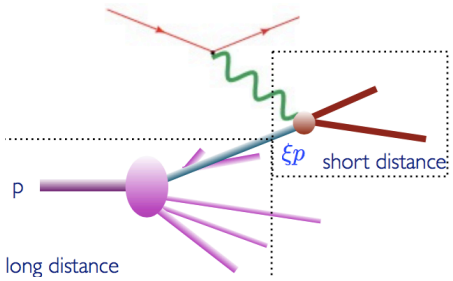

Figure 22: Deeply inelastic scattering, partonic picture of factorisation. Figure by F. Maltoni.

a form which we will discuss below). Factorisation only holds for large Q^2, it has corrections which are suppressed by powers of order $(\Lambda/Q)^p$ (called "power corrections").
According to eqs. (92) and (98), we find in the naïve parton model

$$F_2(x) = 2xF_1(x) = \sum_i \int_0^1 \mathrm{d}\xi\, f_i(\xi)\, x\, e_{q_i}^2\, \delta(x-\xi) = x \sum_i e_{q_i}^2\, f_i(x)\,. \qquad (99)$$

For a proton probed at a scale Q, we expect it consists mostly of uud. Writing $f_i(x) = u(x), d(x)$ etc. for $i = u, d, \ldots$ we have in the naïve parton model

$$F_2^{\text{proton}}(x) = x\Big[\frac{4}{9}\big(u(x)+\bar{u}(x)\big) + \frac{1}{9}\big(d(x)+\bar{d}(x)\big)\Big]\,. \qquad (100)$$

If we define the so-called "valence quarks" $u_v(x)u_v(x)d_v(x)$,

$$u(x) = u_v(x) + \bar{u}(x)\ ,\ d(x) = d_v(x) + \bar{d}(x)\ ,\ s(x) = \bar{s}(x)\ ,$$

we expect the "sum rules"

$$\int_0^1 \mathrm{d}x\, u_v(x) = 2\ ,\ \int_0^1 \mathrm{d}x\, d_v(x) = 1\ ,\ \int_0^1 \mathrm{d}x\, (s(x)-\bar{s}(x)) = 0\,. \qquad (101)$$

In Figs. 23 and 24 it is illustrated that the smaller x and the larger Q^2, the more the "sea quarks" and gluons in the proton are probed. In fact, it turns

out that $\sum_{i=q,\bar{q}} \int_0^1 \mathrm{d}x\, x f_{i/p}(x) \simeq 0.5$, so quarks carry only about half of the momentum of the proton. We know that the other half is carried by gluons, but clearly the naïve parton model is not sufficient to describe the gluon distribution in the proton.

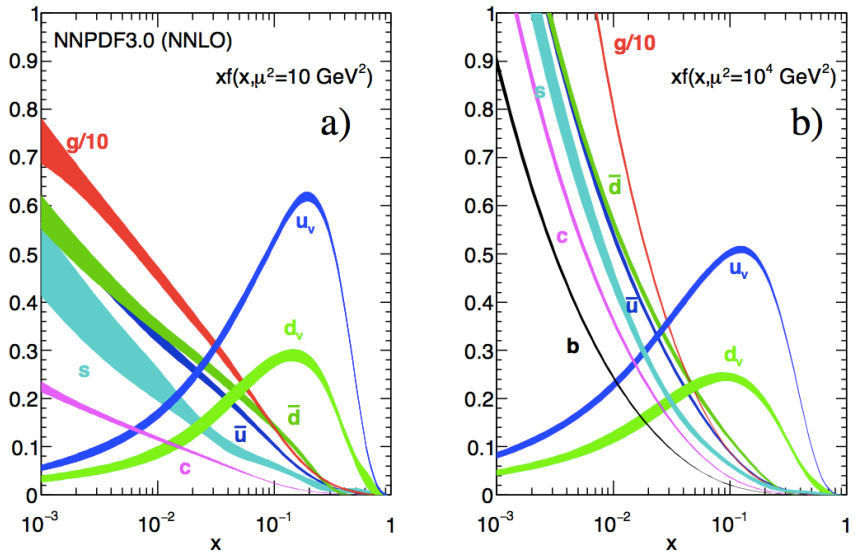

Figure 23: Parton distribution functions in the proton as a function of x. Source: Particle Data Group.

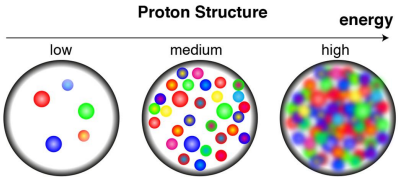

Figure 24: Proton structure depending on how well it can be resolved. Source: Utrecht University.

4.5.3 Proton structure in perturbative QCD

To see what happens in the "QCD-improved" parton model, we will encounter again IR singularities and splitting functions. Let us denote the

hard scattering cross section by σ_h. For final state radiation, we found that the IR singularities due to soft and collinear configurations cancel against IR divergences in the virtual correction for infrared safe quantities.
If there is a coloured parton in the *initial* state, the splitting may occur *before* the hard scattering, such that the momentum of the parton that enters the hard process is reduced to xp^μ.

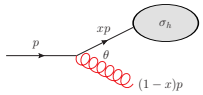

$$\mathrm{d}\sigma_{h+g}(p) \simeq \sigma_h(xp)\; 2C_F \frac{\alpha_s}{\pi}\frac{\mathrm{d}E}{E}\frac{\mathrm{d}\theta}{\theta} \to \sigma_h(xp)\, C_F \frac{\alpha_s}{\pi}\,\mathrm{d}x\,(1-x)^{-1-\epsilon}\,\mathrm{d}k_\perp^2\,(k_\perp^2)^{-1-\epsilon}\,.$$

Integrating over x up to one and over $k_\perp$ we find a soft and collinear divergence. The corresponding ϵ poles multiply $\sigma_h(xp)$, while in the virtual correction the poles multiply $\sigma_h(p)$, irrespective whether the IR divergence is in the initial or final state:

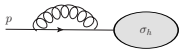

$$\mathrm{d}\sigma_{h+V} \simeq -\sigma_h(p)\, C_F \frac{\alpha_s}{\pi}\,\mathrm{d}x\,(1-x)^{-1-\epsilon}\,\mathrm{d}k_\perp^2\,(k_\perp^2)^{-1-\epsilon}\,.$$

The sum of the real and virtual corrections contains an uncanceled singularity!

$$\mathrm{d}(\sigma_{h+g}+\sigma_{h+V}) \simeq C_F\frac{\alpha_s}{\pi}\,\mathrm{d}k_\perp^2\,(k_\perp^2)^{-1-\epsilon}\mathrm{d}x\;\underbrace{(1-x)^{-1-\epsilon}[\sigma_h(xp)-\sigma_h(p)]}_{\text{finite}}\,, \quad (102)$$

Note that the soft singularity for $x \to 1$ vanishes in the sum of real and virtual parts. The uncanceled collinear singularity in the initial state however remains. Fortunately its form is universal, i.e. independent of the details of the hard scattering process, only dependent on the type of parton splittings. Therefore we can also eliminate it in a universal way: It is absorbed into "bare" parton densities, $f_i^{(0)}(x)$, such that the measured parton densities are the "renormalised" ones. This procedure is very similar to the renormalisation of UV divergences and introduces a scale μ_f, the *factorisation scale*, into the parton densities. Let us see how this works for the structure function F_2. We first consider the *partonic* structure functions $\hat{F}_{2,q}, \hat{F}_{2,g}$, where the subscript q indicates that a quark is coming out of the proton, analogous for a gluon g. Note that a gluon coming from the proton does not interact with a photon, therefore the gluonic contribution is zero at leading order, but it will appear at order α_s because the gluon can split into a $q\bar{q}$ pair and then

one of the quarks interacts with the photon. Therefore we have

$$\hat{F}_{2,q}(x) = \left.\frac{\mathrm{d}^2\hat{\sigma}}{\mathrm{d}x\,\mathrm{d}Q^2}\right|_{F_2} = e_q^2 x\left[\delta(1-x)+\frac{\alpha_\mathrm{s}}{4\pi}\left(-\left(\frac{Q^2}{\mu^2}\right)^{-\epsilon}\frac{1}{\epsilon}\,P_{q\to qg}(x)+C_2^q(x)\right)\right], \tag{103}$$

and

$$\hat{F}_{2,g}(x) = \left.\frac{\mathrm{d}^2\hat{\sigma}}{\mathrm{d}x\,\mathrm{d}Q^2}\right|_{F_2} = \sum_q e_q^2 x\left[0+\frac{\alpha_s}{4\pi}\left(-\left(\frac{Q^2}{\mu^2}\right)^{-\epsilon}\frac{1}{\epsilon}\,P_{g\to q\bar{q}}(x)+C_2^g(x)\right)\right], \tag{104}$$

where $P_{j\to ik}(x)$ is the Altarelli-Parisi splitting function (regularised at $x = 1$) which we already encountered when discussing collinear singularities. It denotes the probability that a parton j splits collinearly into partons i and k, with i carrying a momentum fraction x of the original parton j. Note that the type of parton k is fixed by i and j. Therefore i and j are sufficient to label the splitting functions. For the labelling different conventions are in use. They are summarised in Table 1. $C_2(x)$ is the remaining finite term, sometimes called coefficient function. The partonic scattering function $\hat{F}_2$ is not measurable, only the structure function is physical. Therefore we have to form the convolution of the partonic part with the parton distribution functions.

$P_{ij}(x)$	$P_{j\to ik}(x)$	$P_{i/j}(x)$
$P_{qq}(x)$	$P_{q\to qg}(x)$	$P_{q/q}(x)$
$P_{gq}(x)$	$P_{q\to gq}(x)$	$P_{g/q}(x)$
$P_{qg}(x)$	$P_{g\to q\bar{q}}(x)$	$P_{q/g}(x)$
$P_{gg}(x)$	$P_{g\to gg}(x)$	$P_{g/g}(x)$

Table 1: Translation between different conventions for the labelling of the splitting functions, see also Fig. 25.

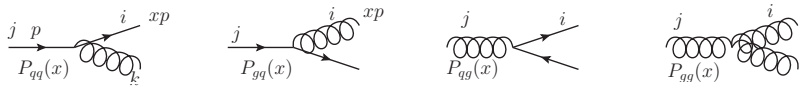

Figure 25: Splitting functions with labelling.

$$F_{2,q}(x,Q^2) = x\sum_i e_{q_i}^2 \left[f_i^{(0)}(x) + \frac{\alpha_s}{2\pi}\int_x^1 \frac{\mathrm{d}\xi}{\xi} f_i^{(0)}(\xi)\left(-\left(\frac{Q^2}{\mu^2}\right)^{-\epsilon}\frac{1}{\epsilon}\,P_{q\to qg}\left(\frac{x}{\xi}\right) + C_2^q\left(\frac{x}{\xi}\right)\right)\right]. \tag{105}$$

Now we absorb the singularity into the parton distribution function (PDF) by the definition

$$f_i(x,\mu_f^2) = f_i^{(0)}(x) + \frac{\alpha_s}{2\pi}\int_x^1 \frac{\mathrm{d}\xi}{\xi}\left\{ f_i^{(0)}(\xi)\left[-\frac{1}{\epsilon}\left(\frac{\mu_f^2}{\mu^2}\right)^{-\epsilon} P_{q\to qg}\left(\frac{x}{\xi}\right) + K_{qq}\right]\right\}, \tag{106}$$

where K_{qq} denotes finite terms depending on the regularisation scheme. Then the structure function becomes

$$\begin{aligned} F_{2,q}(x,Q^2) =& x\sum_i e_{q_i}^2 \int_x^1 \frac{\mathrm{d}\xi}{\xi} f_i(\xi,\mu_f^2)\times \\ & \left\{\delta(1-\frac{x}{\xi}) + \frac{\alpha_s(\mu_r)}{2\pi}\left[P_{q\to qg}\left(\frac{x}{\xi}\right)\ln\frac{Q^2}{\mu_f^2} + \left(C_2^q - K_{qq}\right)\right]\right\} \\ =& x\sum_i e_{q_i}^2 \int_x^1 \frac{\mathrm{d}\xi}{\xi} f_i(\xi,\mu_f^2)\,\hat{F}_{2,i}(\frac{x}{\xi},Q^2,\mu_r,\mu_f)\ . \end{aligned} \tag{107}$$

Defining a convolution in x-space by $f\otimes_x g \equiv \int_x^1 \frac{\mathrm{d}\xi}{\xi} f(\xi)\, g\left(\frac{x}{\xi}\right)$, we see that the structure function is factorised in the form of a convolution,

$$F_{2,q}(x,Q^2) = x\sum_i e_{q_i}^2\, f_i(\mu_f)\otimes_x \hat{F}_{2,i}(\mu_r,t) \ \text{ with } \ t = \ln\frac{Q^2}{\mu_f^2}\ . \tag{108}$$

The long distance physics is factored into the PDFs which depend on the *factorisation scale* μ_f. The short distance physics is factored into the hard

scattering cross section which depends on both the factorisation and the renormalisation scales. Both scales are arbitrary, unphysical scales. The term K_{ij} depends on the *factorisation scheme*. It is not unique, as finite terms can be shifted between the short and long distance parts. It is important that the same scheme is used for the real and virtual corrections (usually $\overline{\text{MS}}$).

4.5.4 Parton evolution and the DGLAP equations

With eq. (108) we again have an equation where an unphysical scale appears on the right-hand side, while the left-hand side is a physical quantity and therefore should not depend on the scale μ_f (when calculated to all orders in perturbation theory). This gives us something like a renormalisation group equation, which means that we can calculate how the PDFs evolve as the scale μ_f is changed. As the convolution in Eq. (108) is somewhat inconvenient, we go to Mellin space, where the convolution in the factorisation formula Eq. (108) above turns into simple products. The Mellin transform is defined by

$$f(N) \equiv \int_0^1 \mathrm{d}x\, x^{N-1} f(x) \; .$$

The structure function in Mellin space then becomes

$$F_{2,q}(N, Q^2) = x \sum_i e_{q_i}^2 \, f_i(N, \mu_f^2) \, \hat{F}_{2,i}(N, \mu_r, t) \; . \tag{109}$$

As a measurable quantity, the structure function must be independent of μ_f, therefore

$$\frac{\mathrm{d}F_{2,q}(N, Q^2)}{\mathrm{d}\mu_f} = 0 \; . \tag{110}$$

Note that if F_2 is calculated to order α_s^n, we have $\mu_f^2 \, \mathrm{d}F_{2,q}(N, Q^2)/\mathrm{d}\mu_f^2 = \mathcal{O}(\alpha_s^{n+1})$: as in the case of the renormalisation scale μ_r, the truncation of the perturbative series introduces a dependence on the unphysical scale in the observable, which gets weaker the more orders we calculate. x For simplicity, let us leave out the sum over i in Eq. (109) and consider only one quark flavour q. We obtain from Eq. (110)

$$\hat{F}_{2,q}(N, t) \frac{\mathrm{d}f_q(N, \mu_f^2)}{\mathrm{d}\mu_f^2} + f_q(N, \mu_f^2) \frac{\mathrm{d}\hat{F}_{2,q}(N, t)}{\mathrm{d}\mu_f^2} = 0 \; . \tag{111}$$

Dividing by $f_q\,\hat{F}_{2,q}$ and multiplying by μ_f^2 we obtain

$$\mu_f^2 \frac{\mathrm{d}\ln f_q(N,\mu_f^2)}{\mathrm{d}\mu_f^2} = -\mu_f^2 \frac{\mathrm{d}\ln \hat{F}_{2,q}(N,t)}{\mathrm{d}\mu_f^2} \equiv \gamma_{qq}(N)\;. \tag{112}$$

Using $t = \ln\left(Q^2/\mu_f^2\right)$ this can be written as

$$\frac{\mathrm{d}f_q(N,t)}{\mathrm{d}t} = \gamma_{qq}(N)\, f_q(N,t)\;, \tag{113}$$

where

$$\gamma_{qq}(N) = \int_0^1 \mathrm{d}x\, x^{N-1} P_{qq}(x) = P_{qq}(N)\;. \tag{114}$$

$\gamma_{qq}(N)$ is called the *anomalous dimension* because it measures the deviation of $\hat{F}_{2,q}$ from its naïve scaling dimension. It corresponds to the Mellin transform of the splitting functions.
Very importantly, Eq. (113) implies that the *scale dependence* of the PDFs can be calculated in perturbation theory. The PDFs themselves are non-perturbative, so they have to be extracted from experiment. However, the universality of the PDFs (for each flavour) and the calculable scale dependence means that we can measure the PDFs in one process at a certain scale and then use it in another process at a different scale.
A rigorous treatment based on operator product expansion and the renormalisation group equations extends the above result to all orders in perturbation theory, leading to

$$\boxed{\frac{\partial}{\partial t} f_{q_i}(x,t) = \int_x^1 \frac{\mathrm{d}\xi}{\xi} P_{q_i/q_j}\left(\frac{x}{\xi}, \alpha_s(t)\right) f_{q_j}(\xi,t)\;.} \tag{115}$$

The splitting functions P_{q_i/q_j} are calculated as a power series in α_s:

$$P_{q_i/q_j}(x,\alpha_s) = \frac{\alpha_s}{2\pi} P_{ij}^{(0)}(x) + \left(\frac{\alpha_s}{2\pi}\right)^2 P_{ij}^{(1)}(x) + \left(\frac{\alpha_s}{2\pi}\right)^3 P_{ij}^{(2)}(x) + \mathcal{O}(\alpha_s^4)\;. \tag{116}$$

Eq. (115) holds for distributions which are *non-singlets* under the flavour group: either a single flavour or a combination $q_{\mathrm{ns}} = f_{q_i} - f_{q_j}$ with q_i, q_j being a quark or antiquark of any flavour. The cutting edge calculations for the non-singlet splitting functions are four loops ($P_{\mathrm{ns}}^{(3)}(x)$) [52–54]. More

generally, the DGLAP equation is a $(2n_f+1)-$dimensional matrix equation in the space of quarks, antiquarks and gluons,

$$\frac{\partial}{\partial t}\begin{pmatrix} f_{q_i}(x,t) \\ f_g(x,t) \end{pmatrix} = \sum_{q_j,\bar{q}_j}\int_x^1 \frac{d\xi}{\xi}\begin{pmatrix} P_{q_i/q_j}(\frac{x}{\xi},\alpha_s(t)) & P_{q_i/g}(\frac{x}{\xi},\alpha_s(t)) \\ P_{g/q_j}(\frac{x}{\xi},\alpha_s(t)) & P_{g/g}(\frac{x}{\xi},\alpha_s(t)) \end{pmatrix}\begin{pmatrix} f_{q_j}(\xi,t) \\ f_g(\xi,t) \end{pmatrix} . \tag{117}$$

Eq. (117) and (115) are called *DGLAP equations*, named after Dokshitzer [55], Gribov, Lipatov [56] and Altarelli, Parisi [57]. They are among the most important equations in perturbative QCD.

Note that because of charge conjugation invariance and $SU(n_f)$ flavour symmetry the splitting functions $P_{q/g}$ and $P_{g/q}$ are independent of the quark flavour and the same for quarks and antiquarks.
Defining the singlet distribution

$$\Sigma(x,t) = \sum_{i=1}^{n_f}\left[\, f_{q_i}(x,t) + f_{\bar{q}_i}(x,t)\,\right] \tag{118}$$

and taking into account the considerations above, Eq. (117) simplifies to

$$\frac{\partial}{\partial t}\begin{pmatrix} \Sigma(x,t) \\ g(x,t) \end{pmatrix} = \int_x^1 \frac{d\xi}{\xi}\begin{pmatrix} P_{q/q}(\frac{x}{\xi},\alpha_s(t)) & 2n_f P_{q/g}(\frac{x}{\xi},\alpha_s(t)) \\ P_{g/q}(\frac{x}{\xi},\alpha_s(t)) & P_{g/g}(\frac{x}{\xi},\alpha_s(t)) \end{pmatrix}\begin{pmatrix} \Sigma(\xi,t) \\ g(\xi,t) \end{pmatrix} . \tag{119}$$

The splitting functions $P_{a/b}(x)$ can be interpreted as the probabilities of finding a parton of type a in a parton of type b with a fraction x of the longitudinal momentum of the parent parton and a transverse momentum squared much less than μ^2. The interpretation as probabilities implies that the splitting functions are positive definite for $x<1$, and satisfy the following sum rules which correspond to quark number conservation and momentum conservation in the splittings of quarks respectively gluons:

$$\begin{aligned} \int_0^1 dx P_{q/q}(x) &= 0 \,, \\ \int_0^1 dx\, x\,[P_{q/q}(x) + P_{g/q}(x)] &= 0 \,, \\ \int_0^1 dx\, x\,[2n_f P_{q/g}(x) + P_{g/g}(x)] &= 0 \,. \end{aligned} \tag{120}$$

The leading order splitting functions including the regulating contributions at $x = 1$ are given by

$$P_{q/q}^{(0)}(x) = C_F\Big\{\frac{1+x^2}{(1-x)_+} + \frac{3}{2}\,\delta(1-x)\Big\} \tag{121}$$

$$P_{q/g}^{(0)}(x) = T_R\Big\{x^2 + (1-x)^2\Big\} \quad T_R = \frac{1}{2} \tag{122}$$

$$P_{g/q}^{(0)}(x) = C_F\Big\{\frac{1+(1-x)^2}{x}\Big\} \tag{123}$$

$$\begin{aligned} P_{g/g}^{(0)}(x) = {} & 2N_c\Big\{\frac{x}{(1-x)_+} + \frac{1-x}{x} + x(1-x)\Big\} \\ & + \delta(1-x)[\frac{11}{6}N_c - \frac{2}{3}n_f T_R] \end{aligned} \tag{124}$$

Let us now solve the simplified DGLAP equation, Eq. (113), in Mellin space. It is a first order differential equation, solved by the ansatz

$$f_{q_i}(N,Q^2) = f_{q_i}(N,Q_0^2)\,\exp\left[\int_{t_0}^{t}\,\mathrm{d}\tilde{t}\,\gamma_{qq}\,(N,\alpha_s)\right]\,.$$

Using leading order expressions $\alpha_s(Q^2) = 1/(b_0 t)$ with $t = \ln\frac{Q^2}{\Lambda^2}$ and $\gamma_{qq} = \frac{\alpha_s}{2\pi}\,\gamma_{qq}^{(0)} + \mathcal{O}(\alpha_s^2)$, we have, introducing the abbreviation $d_{qq}^{(0)}(N) = \gamma_{qq}^{(0)}(N)/(2\pi b_0)$,

$$\begin{aligned} & f_{q_i}(N,Q^2) = f_{q_i}(N,Q_0^2)\,\exp\left[d_{qq}^{(0)}(N)\int_{t_0}^{t}\,\frac{\mathrm{d}\tilde{t}}{\tilde{t}}\right] \\ & \Rightarrow f_{q_i}(N,Q^2) = f_{q_i}(N,Q_0^2)\,\left(\frac{t}{t_0}\right)^{d_{qq}^{(0)}(N)} \simeq f_{q_i}(N,Q_0^2)\,\left(\frac{\alpha_s(Q_0^2)}{\alpha_s(Q^2)}\right)^{d_{qq}^{(0)}(N)}\,. \end{aligned} \tag{125}$$

Now we see how the scaling violations arise, and how they are related to the anomalous dimension $\gamma_{qq}(N)$. We have

$$\gamma_{qq}^{(0)}(N) = C_F\left[\frac{1}{N(N+1)} + \frac{3}{2} - 2\sum_{m=1}^{N}\frac{1}{m}\right]\,. \tag{126}$$

As $d_{qq}^{(0)}(1) = 0$, the valence quark with flavour i in the proton, given by the integral $\int_0^1 \mathrm{d}x\, f_{q_i}(x,Q^2)$, is independent of Q^2. Further, $d_{qq}^{(0)}(N) < 0$ for $N > 1$. In x-space soft gluon radiation leads to enhancements of the form

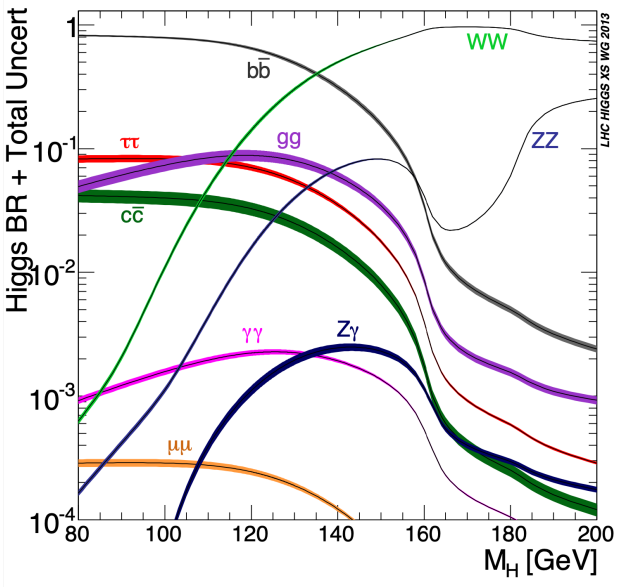

Figure 26: Higgs boson decay channels (branching ratios).

$\alpha_s \ln(\frac{1}{x})$, which compete with the trend of f_{q_i}, f_g to decrease with increasing Q^2. Therefore, as Q^2 increases, f_{q_i}, f_g decrease at large x and increase at small x. Physically this can be attributed to an increase in the phase space for gluon emission by quarks as Q^2 increases, leading to a loss of momentum. This trend can be seen in Fig. 21.

5 Higgs production

5.1 Higgs boson production in gluon fusion

5.1.1 Phenomenology

The main Higgs production channels and the corresponding cross sections already have been shown in Fig. **??**. The main decay channels and the corresponding branching rations are shown in Fig. 26. Note that the discovery channel $H \to \gamma\gamma$ has a relatively small branching ratio, however it provides a very "clean" signal, while the decay into $b\bar{b}$ is plagued by large backgrounds. Even though the exploration of the Higgs sector can still offer surprises, the couplings of the Higgs boson to other particles measured so far confirmed

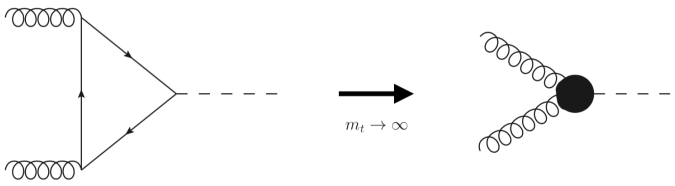

Figure 27: Heavy top limit leading to an effective vertex coupling the Higgs boson to gluons.

the Standard Model expectations, see Fig. **??**. It is impressive that the experiments meanwhile have established the coupling of the Higgs boson to all the electroweak gauge bosons [58], the top [59,60] and bottom quarks [61, 62], the tau lepton [63, 64] and are recently moving towards indication for Higgs couplings to muons [65, 66], which means entering the domain of 2nd generation fermions. In addition to these important results, it is also crucial to study Higgs boson self-couplings, which provide a way to explore the potential that drives the electroweak symmetry breaking mechanism. The trilinear Higgs boson self-coupling is still rather weakly constrained, even though the limits have improved considerably in Run II [67–70], the best limit being now at $-1.5 \leq \lambda/\lambda_{SM} \leq 6.7$ [70].

QCD corrections in the Higgs sector are special as the Higgs boson does not couple directly to gluons. Therefore, the precision calculations for loop-induced processes, such as Higgs (plus jets) production in gluon fusion, can be roughly divided into two categories: (a) calculations based on an effective Lagrangian containing effective Higgs-gluon couplings which arise in the $m_t \to \infty$ approximation, also called "heavy top limit (HTL)" (and sometimes also called HEFT), and (b) calculations in the full Standard Model. As the HTL shrinks the top quark loop mediating Higgs-gluon interactions to a point (see Fig. 27), calculations in the HTL start at tree level and involve only massless partons in the five-flavour scheme, in contrast to the full SM where the leading order Higgs-gluon interaction is loop-induced.

Therefore, calculations in the HTL can be pushed to higher orders more easily than calculations in the full SM. In fact, most calculations of highest available order for observables at hadron colliders are in the Higgs sector.

Status of higher order corrections

For the inclusive case in the threshold approximation, the N^{3}LO corrections to Higgs production in gluon fusion in the HTL, have been calculated in Refs. [20,71], see Figs. 6, 7. The threshold approximation has been overcome in Ref. [19], presenting the exact N^{3}LO inclusive cross section in the HTL. Furthermore, N^{4}LO soft and virtual corrections to inclusive Higgs production have been calculated [72, 73], as well as Higgs decay into photons to four loops [74].
N^{3}LO differential results for the Higgs boson rapidity distribution (without decay) have been calculated in Refs. [75, 76]. A very recent perturbative highlight is the calculation of the exact top-quark mass dependence in gluon fusion Higgs production at NNLO [77], which involves 3-loop diagrams with full top quark mass dependence.

Fiducial cross sections

Cross sections which correspond to directly measurable final states are also called *fiducial* cross sections. They allow to place exactly the same kinematic requirements ("cuts") in the calculation as in the experimental setup.
Very recently, fully differential predictions up to N^{3}LO in QCD for Higgs boson production via gluon fusion in the di-photon decay channel have been achieved [78], see Fig. 28. The resummed q_T-spectrum at N^{3}LL$'$+N^{3}LO, both inclusively and with fiducial cuts, has been presented in Ref. [79], featuring the highest precision achieved so far for a transverse momentum distribution at a hadron collider, see Fig. 29.

Top quark mass dependence

How good is the $m_t \to \infty$ approximation? The short answer is: it works very well for the inclusive cross section, however for Higgs boson production in gluon fusion in association with jets, it is a bad approximation at high energies, where the top quark loops can be "resolved". Formally, the assumption $\sqrt{\hat{s}} \ll m_t$, underlying the heavy top limit, is simply not valid, so the approximation should break down around the top quark pair production threshold $\sqrt{\hat{s}} = 2m_t$.
We will calculate the heavy top limit at LO in section 5.1.3, here we just show the result. In Fig. 30 the heavy to limit (red) is compared to the full result (blue) for $gg \to H$ at LO. One caqn clearly see that the two results

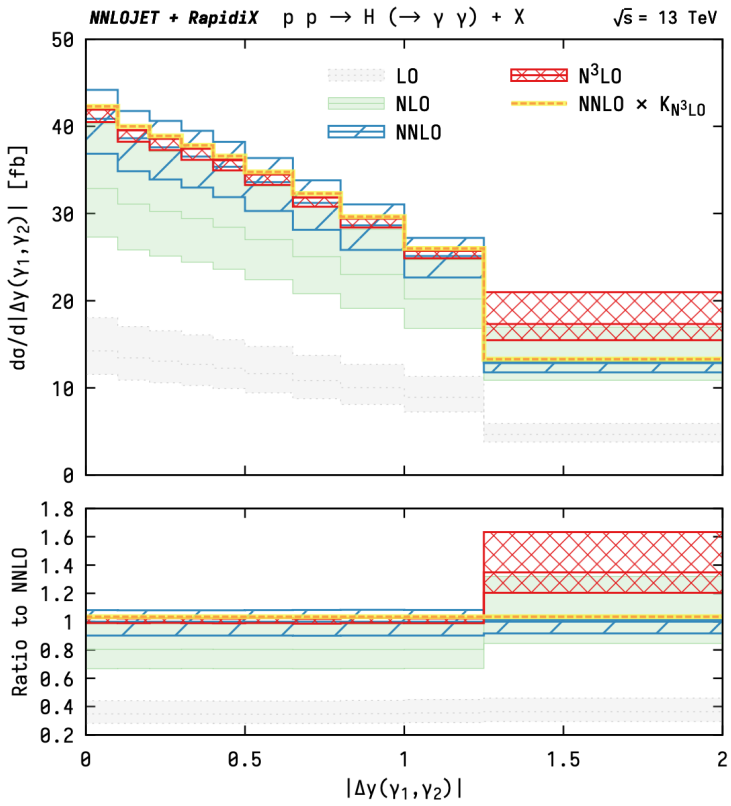

Figure 28: Differential predictions for the rapidity of the leading photon (left) and the absolute value of the rapidity difference of the two photons (right). Predictions are shown at LO (grey), NLO (green), NNLO (blue), N^{3}LO (red), and for the NNLO prediction rescaled by the inclusive K_{N3LO}-factor (orange). The shaded vertical band in the left plot corresponds to the region excluded by the fiducial cuts. Figures from Ref. [78].

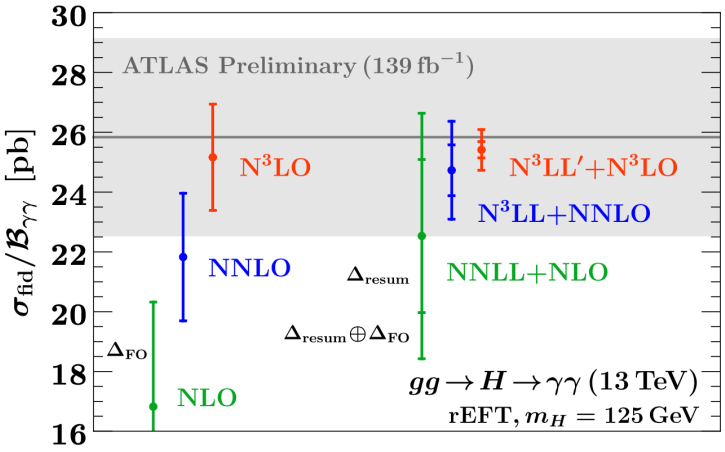

Figure 29: $gg \to H \to \gamma\gamma$ cross section (divided by the branching ratio $\mathcal{B}_{\gamma\gamma}$) at different perturbative orders. Figure from Ref. [79].

only agree well before the top quark pair production threshold $\sqrt{\hat{s}} = 2m_t$. However, it is important to note that in Hinclusive Higgs production, the following "trick" works very well: calculate NLO (or higher) corrections in the HTL and rescale with the Born cross section calculated with full mass dependence in the loops. This is called *Born-improved NLO*:

$$\sigma_{NLO}^{B-imp.} = \sigma_{NLO}^{HTL} \frac{\sigma_{LO}(m_t)}{\sigma_{LO}^{HTL}} \tag{127}$$

How well this works is shown in Fig. 30 (right). The reason is that for inclusive Higgs production, the cross section is dominated by Higgs production close to the production threshold, so $\hat{s} \approx m_H^2 < 4m_t^2$. How badly this works for Higgs+jet production is shown in Fig. 31.
To profit from available calculations of Higgs+jet at NNLO in the heavy top limit [82–86] a combination similar in spirit as given in Eq. (127) also can be done at higher orders. This has been done in Ref. [87], together with an extensive study of Higgs production at large transverse momentum, $p_T^H \geq 400\,\text{GeV}$. It contains the currently best predictions for Higgs+jet production in the boosted regime, shown in Fig. 32. The combinations of full NLO with NNLO in the HTL are defined as follows

$$\Sigma^{\text{EFT-improved (1), NNLO}}(p_\perp^{\text{cut}}) \equiv \frac{\Sigma^{\text{SM, NLO}}(p_\perp^{\text{cut}})}{\Sigma^{\text{EFT, NLO}}(p_\perp^{\text{cut}})} \Sigma^{\text{EFT, NNLO}}(p_\perp^{\text{cut}})\,, \tag{128}$$

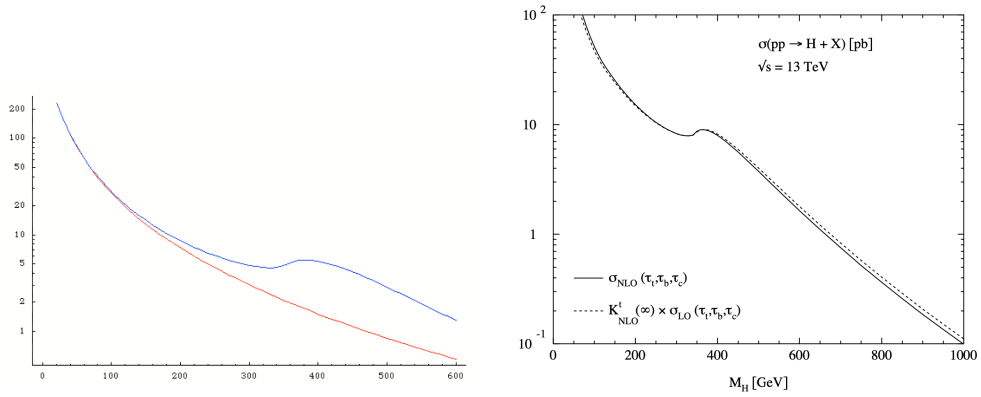

Figure 30: Left: The full LO expression for $gg \to H$ compared to the heavy top limit. Right: full NLO compared to "Born-improved" heavy top limit. *Figure on the right from [80].*

analogously for a rescaling with the full LO result,

$$\Sigma^{\text{EFT-improved (0), NNLO}}(p_\perp^{\text{cut}}) \equiv \frac{\Sigma^{\text{SM, LO}}(p_\perp^{\text{cut}})}{\Sigma^{\text{EFT, LO}}(p_\perp^{\text{cut}})}\, \Sigma^{\text{EFT, NNLO}}(p_\perp^{\text{cut}})\,. \qquad (129)$$

These combinations are shown in Fig. 33.
The Higgs boson transverse momentum is certainly a very important observable at the LHC, as the Higgs p_T-spectrum is sensitive to New Physics effects. For example, it allows to break the degeneracy along $c_t + c_g = \text{const.}$ which is present when measuring the inclusive Higgs boson production cross section [88–90].

Other production modes

Higgs plus two or more jets:

The production of a Higgs boson in association with two jets has two main production modes, vector boson fusion (VBF) and genuine QCD production. The VBF channel is the second largest Higgs production channel, and as it probes gauge boson scattering, it directly probes our understanding of perturbative unitarity as guaranteed by the SM Higgs mechanism.

Higgs production in association with a vector boson:

The production of a Higgs boson in association with a vector boson,

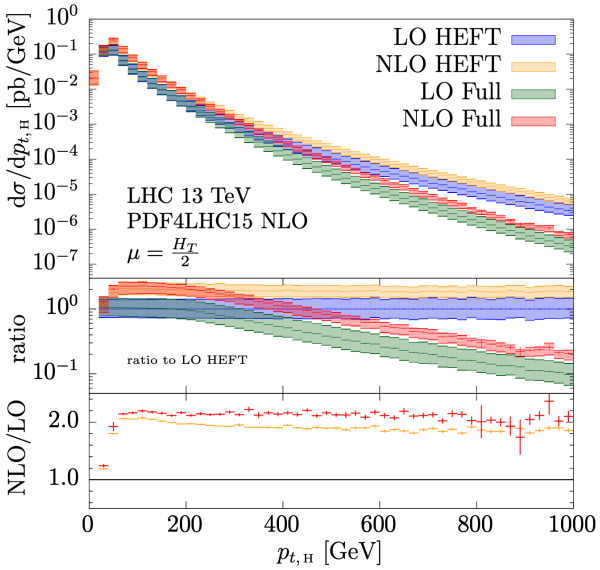

Figure 31: Higgs+jet production, full calculation compared to the heavy top limit (here called HEFT). Figure from Ref. [81].

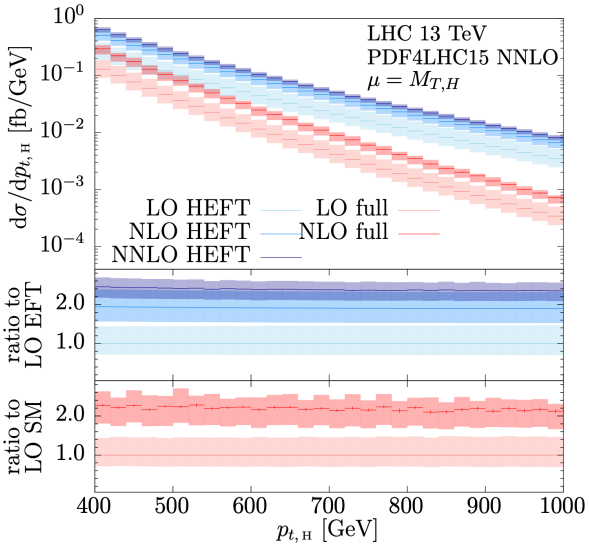

Figure 32: Full results up to NLO and results in the heavy top limit up to NNLO. Figure from Ref. [87].

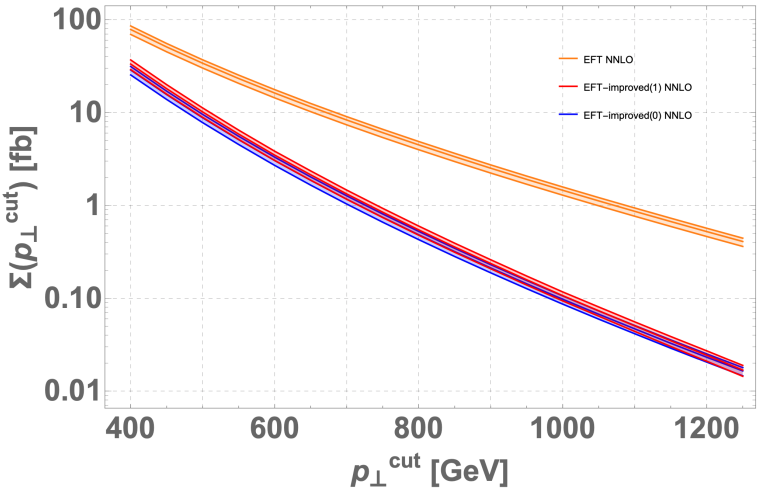

Figure 33: Cumulative cross section as a function of the $p_\perp$-cut at NNLO in the HTL, as well as rescaled by the LO (NLO) full-SM spectrum labelled by EFT-improved(0) (EFT-improved(1)). Figure from Ref. [87].

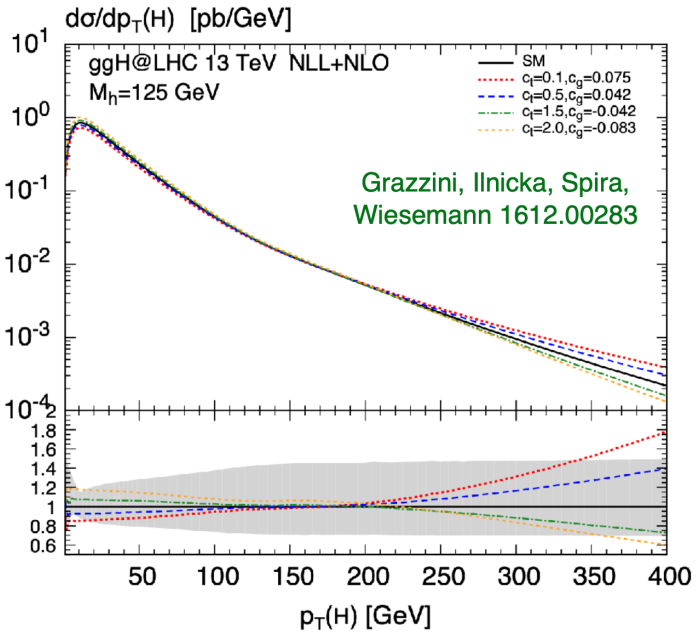

Figure 34: Effects of anomalous Higgs couplings on the transverse momentum distribution of the Higgs boson. Figure from Ref. [90].

also known as *Higgs-Strahlung*, is an important process at the LHC, as well as at lepton colliders. Even though the cross sections at the LHC are smaller than for Higgs production in gluon fusion and VBF, this process has many appealing features. For example, for ZH production combined with a leptonic Z-decay, triggering is straightforward, independent of the Higgs decay. This makes this channel especially attractive in combination with challenging Higgs decays, like invisible or hadronic Higgs decays, in particular $H \to b\bar{b}$ [91]. Furthermore, VH production provides the opportunity to probe the Higgs couplings to gauge bosons.

Top quark pair associated Higgs production, H+single top:
The process $t\bar{t}H$ is particularly interesting due to its direct sensitivity to the top-Yukawa coupling y_t. However, this process suffers from large systematic uncertainties due to the very complicated final states. Currently the combination with $H \to \gamma\gamma$ is the most promising channel [91–93], however the $H \to b\bar{b}$ channel is of increasing importance as deep learning methods gain momentum as a way to improve the signal-to-background ratio.

NLO QCD results in the Standard Model Effective Field Theory (SMEFT) have been calculated in Ref. [94], including also a study of the processes $pp \to H$, $pp \to H\,j$ and $pp \to HH$, which also involve the Higgs-top and Higgs-gluon operators. As already shown in Fig. **??**, a combined fit based on these processes can break the degeneracies in the coupling parameter space present in the individual processes.

For more details we refer to Ref. [95]. The Feynman rules for Higgs boson couplings are given in Figs. 35 to 38.

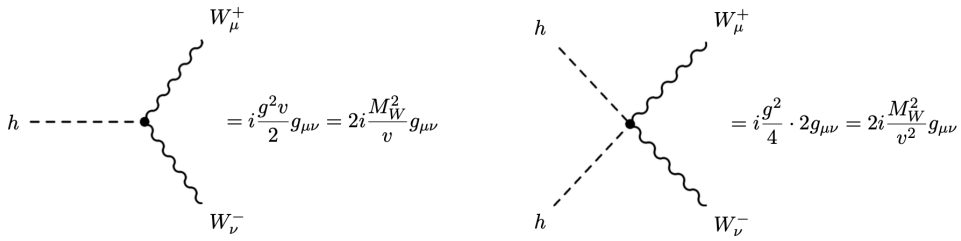

Figure 35: Feynman rules for Higgs couplings to W-bosons. Figure from Ref. [96].

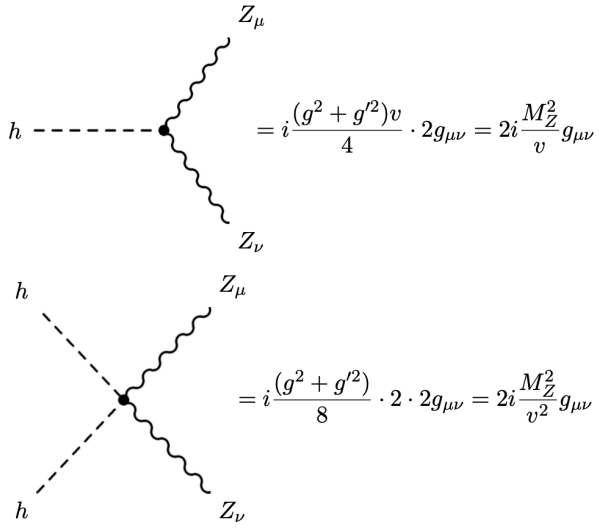

Figure 36: Feynman rules for Higgs couplings to Z-bosons. Figure from Ref. [96].

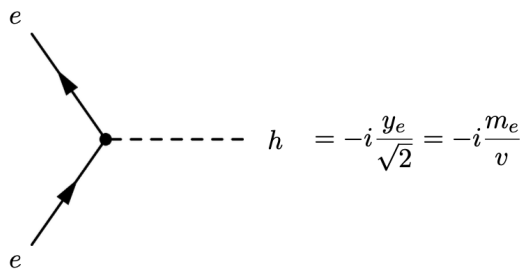

Figure 37: Feynman rules for Higgs couplings to fermions.

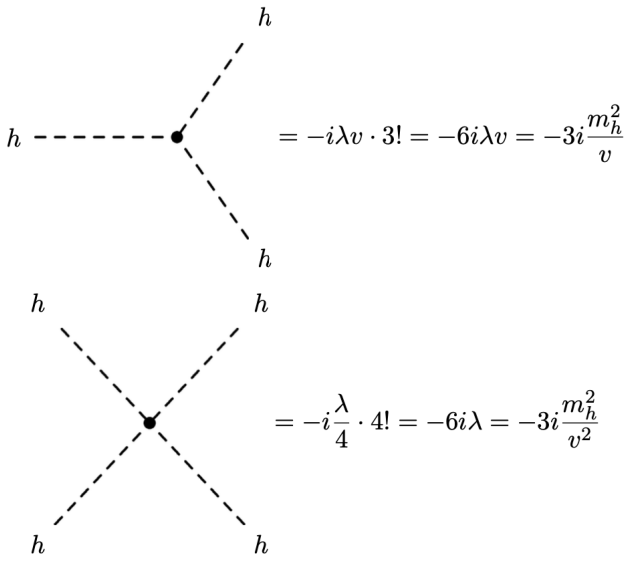

Figure 38: Feynman rules for Higgs couplings to themselves. Figure from Ref. [96].

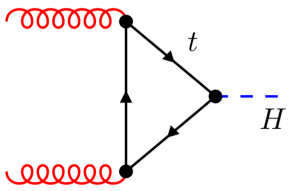

Figure 39: Higgs production in gluon fusion at leading order.

5.1.2 Total cross section for $gg \to H$ at leading order

Higgs production by gluon fusion is mediated by massive quark loops, see Fig. 39. We consider the top quark loop which provides the leading contribution.
Up to a trivial colour factor δ_{ab}, the amplitude is given by

$$\mathcal{M} = i\frac{m_t}{v}\frac{g_s^2}{(4\pi)^{D/2}}\int \frac{d^Dk}{i\,\pi^{D/2}}\frac{\mathrm{Tr}[\not\varepsilon_1(\not q_1+m_t)(\not q_2+m_t)\not\varepsilon_2(\not k+m_t)]}{(k^2-m_t^2)(q_1^2-m_t^2)(q_2^2-m_t^2)}\,, \tag{130}$$

where $q_1 = k - p_1, q_2 = k + p_2$, $p_i^2 = 0$, and the gluon polarisation vectors ε_i fulfill $p_i \cdot \varepsilon_i = 0$. Apart from m_t^2, the only non-vanishing Lorentz invariant is $2p_1 \cdot p_2 = s = m_H^2$ for on-shell Higgs boson production.
We write the amplitude as

$$\mathcal{M} = \varepsilon_1^\mu \varepsilon_2^\nu \mathcal{M}_{\mu\nu}\,. \tag{131}$$

Gauge invariance requires $p_1^\mu \mathcal{M}_{\mu\nu} = 0, p_2^\nu \mathcal{M}_{\mu\nu} = 0$, therefore we must have the following structure

$$\mathcal{M}^{\mu\nu} = i\frac{m_t}{v}\frac{g_s^2}{(4\pi)^{D/2}}F_{12}\,T^{\mu\nu} \equiv c\,F_{12}\,T^{\mu\nu}\,, \tag{132}$$

$$T^{\mu\nu} = g^{\mu\nu} - \frac{p_2^\mu p_1^\nu}{p_1\cdot p_2}\,.$$

Defining the *projector*

$$P_{\mu\nu} = \frac{1}{D-2}\,T_{\mu\nu} \tag{133}$$

we have $P_{\mu\nu}T^{\mu\nu} = 1$ and therefore $P_{\mu\nu}\mathcal{M}^{\mu\nu} = c\,F_{12}$, such that we have projected the amplitude onto the scalar *form factor* F_{12}. Using such projections

onto form factors can be beneficial quite in general, in particular for amplitudes which are *loop-induced*, i.e. where the leading order is not given by tree-level diagrams. The form factor will be a linear combination of loop integrals.
The trace in Eq. (130) evaluates to (we already drop terms which vanish due to $p \cdot \varepsilon(p) = 0$)

$$\begin{aligned} &\mathrm{Tr}[\gamma^\mu \, (\not{p}_1 + m_t)(\not{p}_2 + m_t)\gamma^\nu \, (\not{k} + m_t)] \\ &= 4m_t \left(g^{\mu\nu}(m_t^2 - m_H^2/2 - k^2) + 4k^\mu k^\nu + p_2^\mu p_1^\nu \right) \; + \; \text{vanishing} \, . \end{aligned} \tag{134}$$

It is interesting to note that this expression is proportional to m_t. If the quark circulating in the loop was massless, the trace would vanish due to helicity conservation, independent of the value of the Yukawa coupling, because the interaction with the gluon does not change the spin of the fermion. Usually diagrams with heavy particles with mass m in the loop vanish like $1/m^2$ for $m \to \infty$. However due to one factor of m from the trace and another one from the Yukava coupling, this diagram goes to a (nonzero) constant for $m \to \infty$.
In general we perform a reduction to so-called *master integrals* at this point. Master integrals are linearly independent integrals which form a "basis" such that the amplitude can be expressed as a linear combination of master integrals. In our case, in D dimensions there are just two master integrals the scalar triangle, defined as

$$\begin{aligned} &C_0(p_1^2, p_2^2, m_H^2; m_t, m_t, m_t) \equiv \\ &\int \frac{d^D k}{i\,\pi^{D/2}} \frac{1}{[k^2 - m_t^2][(k+p_1)^2 - m_t^2][(k+p_1+p_2)^2 - m_t^2]} \end{aligned} \tag{135}$$

and the scalar two-point function (which leads to a so-called "rational part", because only the pole term, multiplied by $D-4$, is contributing). If we introduce Feynman parameters, shift the loop momentum to obtain a quadratic form in the denominator, use

$$\int \frac{d^D l}{i\,\pi^{D/2}} \frac{l^\mu l^\nu}{(l^2 - R^2 + i\delta)^m} = \frac{g^{\mu\nu}}{D} \int \frac{d^D l}{i\,\pi^{D/2}} \frac{l^2}{(l^2 - R^2 + i\delta)^m} \tag{136}$$

and take the limit $D \to 4$ we arrive finally at

$$F_{12} = 2m_t \left(2 + (4m_t^2 - m_H^2)\, C_0(0, 0, m_H^2; m_t, m_t, m_t) \right) \, , \tag{137}$$

where

$$C_0(0,0,m_H^2;m_t,m_t,m_t) = \frac{1}{m_H^2}\int_0^1 \frac{dx}{x}\,\log\left(1-x(1-x)\frac{m_H^2}{m_t^2}\right) \qquad (138)$$
$$\equiv -\frac{2f(\tau)}{m_H^2}\ ,\quad \tau = \frac{4m_t^2}{m_H^2}\ ,$$

$$\text{with}\qquad f(\tau) = \begin{cases} \left(\arcsin\sqrt{\dfrac{1}{\tau}}\right)^2 & \tau \geq 1 \\ -\dfrac{1}{4}\left(\log\dfrac{1+\sqrt{1-\tau}}{1-\sqrt{1-\tau}} - i\pi\right)^2 & \tau < 1 \end{cases} . \qquad (139)$$

5.1.3 Heavy top limit (HTL)

Collecting all factors in Eq. (132) reads

$$\mathcal{M}^{\mu\nu} = i\frac{\alpha_s}{4\pi}\frac{m_H^2}{v}\,\tau\,\left[1+(1-\tau)\,f(\tau)\right]T^{\mu\nu}\ . \qquad (140)$$

This can be viewed as an effective coupling of two gluons to the Higgs boson, described by a dimension–5 operator divided by the electroweak scale v:

$$\mathcal{L} \supset\ \frac{1}{v}\,c_{ggH}\,H\,G_a^{\mu\nu}G^a_{\mu\nu} \qquad \text{with} \qquad c_{ggH} = i\frac{\alpha_s}{8\pi}\,\tau\,[1+(1-\tau)f(\tau)]\ . \qquad (141)$$

The expression in square brackets encodes the loop function. Assuming $m_H^2 \ll m_t^2$ we can expand this function in $1/\tau$, leading to

$$f(\tau) = \left[\arcsin\frac{1}{\tau^{1/2}}\right]^2 = \left[\frac{1}{\tau^{1/2}} + \frac{1}{6\tau^{3/2}} + \mathcal{O}\left(\frac{1}{\tau^{5/2}}\right)\right]^2$$
$$= \frac{1}{\tau} + \frac{1}{3\tau^2} + \mathcal{O}\left(\frac{1}{\tau^3}\right) \stackrel{\tau\to\infty}{\longrightarrow} 0\ , \qquad (142)$$

and combine it with the other τ-dependent terms in Eq.(141) to find

$$\begin{aligned}\tau\,[1+(1-\tau)f(\tau)] &= \tau\,\left[1+(1-\tau)\left(\frac{1}{\tau}+\frac{1}{3\tau^2}+\mathcal{O}\left(\frac{1}{\tau^3}\right)\right)\right] \\ &= \tau\,\left[1+\frac{1}{\tau}-1-\frac{1}{3\tau}+\mathcal{O}\left(\frac{1}{\tau^2}\right)\right] \\ &= \tau\,\left[\frac{2}{3\tau}+\mathcal{O}\left(\frac{1}{\tau^2}\right)\right] \\ &= \frac{2}{3}+\mathcal{O}\left(\frac{1}{\tau}\right)\,. \end{aligned} \tag{143}$$

This implies

$$c_{ggH} \overset{\tau\to\infty}{\longrightarrow} i\,\frac{\alpha_s}{12\pi}\,. \tag{144}$$

5.2 Higgs boson pair production

Similar to single Higgs production, the main Higgs boson pair production channels are gluon fusion, VBF, associated production with a vector boson and associated production with a top quark pair. The corresponding cross sections as functions of energy are shown in Figs. 40, 41.

Higgs boson pair production is an interesting process due to its potential to access the trilinear Higgs boson self-coupling, which is one of the few SM parameters being still largely unconstrained. The projection for the HL-LHC is to constrain it to about 50% uncertainty after $3000\,\text{fb}^{-1}$, combining different decay channels and the two experiments ATLAS and CMS [98]. At a future FCC-hh operating at $\sqrt{s} = 100\,\text{TeV}$, an accuracy of about 5% could be achieved with $30\,\text{ab}^{-1}$ [99]. As in the SM the Higgs boson self-couplings are completely determined by the Higgs VEV and its mass, any statistically significant deviation from the predicted value would be a clear sign of New Physics. Currently the most stringent 95% CL limit on the total $gg \to HH$ cross section at $\sqrt{s} = 13\,\text{TeV}$ is $\sigma^{HH}_{\text{max}} = 4.1 \times \sigma_{SM}$, constraining trilinear coupling modifications to the range $-1.5 \leq \lambda/\lambda_{\text{SM}} \leq 6.7$ [70] with the assumption that all other couplings are SM-like.

The LO diagrams are shown in Fig. 42.

The trilinear Higgs couplings can also be constrained in an indirect way, through measurements of processes which are sensitive to these couplings via electroweak corrections, as first suggested in Ref. [100]. Example diagrams

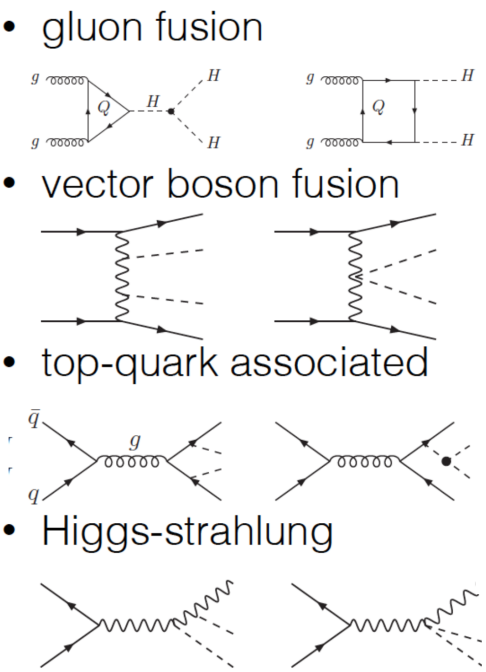

Figure 40: The main production channels for Higgs boson pair production.

are shown in Fig. 43. Such processes offer important complementary information. However the number of operators entering the loop corrections at the same level in an EFT expansion is in general larger than the leading set of operators entering Higgs boson pair production. Therefore the limits on $c_{hhh} = \lambda/\lambda_{\mathrm{SM}}$ extracted this way risk to be weakened by the larger number of parameters to fit. An experimental analysis based on single Higgs boson production processes has been performed to derive combined constraints from single and double Higgs boson production [101]. Under the assumption that all deviations from the SM expectation are stemming from a modification of the trilinear coupling, the derived bounds on c_{hhh} at 95% CL from the combined analysis are $-2.3 \leq c_{hhh} \leq 10.3$ [101]. However once the couplings to vector bosons and/or fermions are allowed to vary as well, these bounds deteriorate significantly.

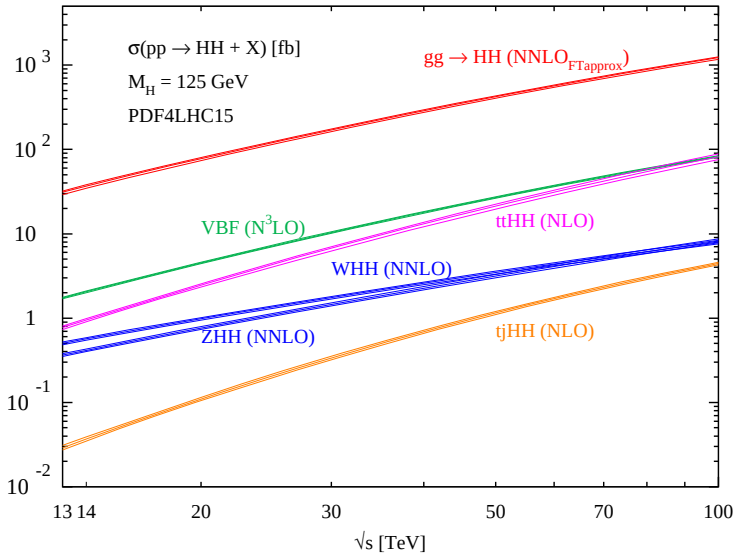

Figure 41: Cross sections for the main production channels for Higgs boson pair production. Figure from Ref. [97].

5.2.1 Higher order corrections

The process $gg \to HH$ at leading order has been calculated in Refs. [102,103]. Before the full NLO QCD corrections became available, the $m_t \to \infty$ limit ("Heavy Top Limit, HTL"), sometimes also called "Higgs Effective Field Theory (HEFT)" approximation, has been used. In this limit, the NLO corrections were first calculated in Ref. [104] using the so-called "Born-improved HTL", which involves rescaling the NLO results in the $m_t \to \infty$ limit by the LO result in the full theory. In Ref. [105] an approximation called "$\text{FT}_{\text{approx}}$", was introduced, which contains the real radiation matrix elements with full top quark mass dependence, while the virtual part is calculated in the Born-improved HTL approximation. The NLO QCD corrections with full top quark mass dependence became available more recently [106–109]. The NLO results of Refs. [106, 107] have been combined with parton shower Monte Carlo programs in Refs. [110–113], where Ref. [113] introduced the possibility of varying five Higgs couplings.
In the $m_t \to \infty$ limit, the NNLO QCD corrections have been computed in Refs. [114–118]. The calculation of Ref. [118] has been combined with results including the top quark mass dependence as far as available in Ref. [119], defining an $\text{NNLO}_{\text{FTapprox}}$ result which contains the full top quark mass de-

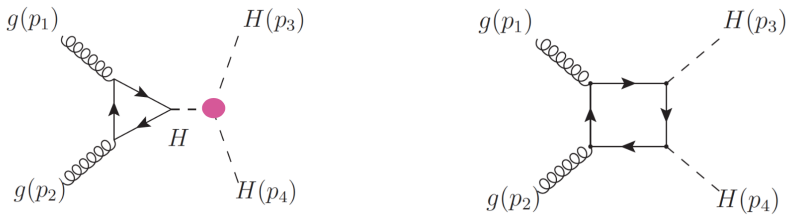

Figure 42: Leading order diagrams for Higgs boson pair production in gluon fusion. Note that the box diagram is only a representative. Two more box topologies contribute, obtained from the one shown here by $p_3 \leftrightarrow p_4$ and $p_1 \leftrightarrow p_3$, respectively.

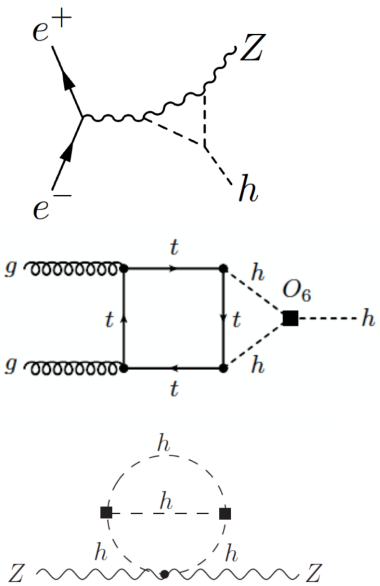

Figure 43: Example diagrams for an indirect determination of the trilinear Higgs coupling through electroweak corrections.

pendence at NLO as well as in the double real radiation part. In Ref. [120] a study of the anomalous couplings relevant to the process $gg \to HH$ within a non-linear EFT expansion, at approximate NNLO in QCD has been performed. N^{3}LO corrections are also available [121, 122], where in Ref. [122] the N^{3}LO results in the HTL have been "NLO-improved" using the results of Refs. [110, 112]. In Ref. [123] approximate NNLO results including the effect of anomalous couplings were presented, see also Ref. [124] for the NLO case.

5.2.2 $gg \to HH$ in the Standard Model

The amplitude for the process $g(p_1,\mu) + g(p_2,\nu) \to h(p_3) + h(p_4)$ can be decomposed into form factors as

$$\begin{aligned} \mathcal{M}_{ab} &= \delta_{ab}\, \epsilon^\mu(p_1,n_1)\epsilon^\nu(p_2,n_2)\, \mathcal{M}_{\mu\nu} \\ \mathcal{M}^{\mu\nu} &= \frac{\alpha_s}{8\pi v^2} \left\{ F_1(\hat{s},\hat{t},m_h^2,m_t^2,D)\; T_1^{\mu\nu} + F_2(\hat{s},\hat{t},m_h^2,m_t^2,D)\; T_2^{\mu\nu} \right\} \,, \end{aligned} \tag{145}$$

where n_1, n_2 are arbitrary reference momenta for the two gluon polarization vectors $\epsilon^\mu, \epsilon^\nu$. Colour indices are denoted by a, b and

$$\hat{s} = (p_1+p_2)^2, \quad \hat{t} = (p_1-p_3)^2, \quad \hat{u} = (p_2-p_3)^2 \,. \tag{146}$$

The decomposition into tensors carrying the Lorentz structure is not unique. It is however convenient to define the form factors such that [102]

$$\begin{aligned} \mathcal{M}^{++} &= \mathcal{M}^{--} = -\frac{\alpha_s}{8\pi v^2}\, F_1 \\ \mathcal{M}^{+-} &= \mathcal{M}^{-+} = -\frac{\alpha_s}{8\pi v^2}\, F_2 \,, \end{aligned} \tag{147}$$

which is fulfilled with the following definitions

$$\begin{aligned} T_1^{\mu\nu} &= g^{\mu\nu} - \frac{p_1^\nu\, p_2^\mu}{p_1\cdot p_2} \,, \\ T_2^{\mu\nu} &= g^{\mu\nu} + \frac{1}{p_T^2\,(p_1\cdot p_2)} \left\{ m_h^2\, p_1^\nu\, p_2^\mu \right. \\ &\quad \left. -2\,(p_1\cdot p_3)\, p_3^\nu\, p_2^\mu - 2\,(p_2\cdot p_3)\, p_3^\mu\, p_1^\nu + 2\,(p_1\cdot p_2)\, p_3^\nu\, p_3^\mu \right\} \\ \text{where} \quad & p_T^2 = (\hat{u}\,\hat{t} - m_h^4)/\hat{s} \,,\; T_1\cdot T_2 = D-4 \,,\; T_1\cdot T_1 = T_2\cdot T_2 = D-2 \,. \end{aligned} \tag{148}$$

At leading order, we can further split F_1 into a "triangle" and a "box" contribution

$$F_1(\hat{s},\hat{t},m_h^2,m_t^2,D) = F_\triangle(\hat{s},\hat{t},m_h^2,m_t^2,D) + F_\square(\hat{s},\hat{t},m_h^2,m_t^2,D) \,. \tag{149}$$

The form factor F_2 only gets contributions from the box diagrams. As the LO form factor $F_\triangle$ only contains the triangle diagrams, which have no angular momentum dependence, it can be attributed entirely to an s-wave contribution. The form factors F_1 and F_2 can be attributed to the spin-0 and spin-2 states of the scattering amplitude, respectively.
At LO, the "triangle" form factor can be inferred from single Higgs production with subsequent decay of the virtual Higgs boson into two on-shell Higgs bosons. It therefore has the simple form

$$\begin{aligned} F_\triangle &= C_\triangle \bar{F}_\triangle \,,\; C_\triangle = \frac{\lambda_{hhh}}{\hat{s} - m_h^2} \,,\; \lambda_{hhh} = 3 m_h^2 \lambda \,, \\ \bar{F}_\triangle &= 4 m_q^2 \left\{ 2 + (4\, m_q^2 - \hat{s}) C_0 \right\} = 2 \hat{s}\, \tau_q \left[1 + (1 - \tau_q) f(\tau_q) \right] \,, \end{aligned} \tag{150}$$

where $\lambda = 1$ in the Standard Model, $\tau_q = 4\, m_q^2 / \hat{s}$ and

$$f(\tau_q) = \begin{cases} \arcsin^2 \dfrac{1}{\sqrt{\tau_q}} & \text{for } \tau_q \geq 1 \\ -\frac{1}{4} \left[\log \dfrac{1 + \sqrt{1 - \tau_q}}{1 - \sqrt{1 - \tau_q}} - i\pi \right]^2 & \text{for } \tau_q < 1 \end{cases} \,, \tag{151}$$

the same as given in Eq. (139).
The partonic leading order cross section for $gg \to hh$ can be written as

$$\hat{\sigma}^{\mathrm{LO}}(gg \to hh) = \frac{\alpha_s^2(\mu_R)}{2^{12} v^4 (2\pi)^3 \hat{s}^2} \int_{\hat{t}_-}^{\hat{t}_+} d\hat{t}\, \left\{ |F_1|^2 + |F_2|^2 \right\} . \tag{152}$$

The integration limits are derived from a momentum parametrisation in the centre-of-mass frame, leading to $\hat{t}_\pm = m_h^2 - \frac{\hat{s}}{2} (1 \mp \beta_h)$, where $\beta_h^2 = 1 - 4 \frac{m_h^2}{\hat{s}}$.

To obtain the hadronic cross section, we also have to integrate over the PDFs. Defining the luminosity function as

$$\frac{d\mathcal{L}_{ij}}{d\tau} = \sum_{ij} \int_\tau^1 \frac{dx}{x} f_i(x, \mu_F) f_j\left(\frac{\tau}{x}, \mu_F \right) , \tag{153}$$

the total cross section reads

$$\sigma^{\mathrm{LO}} = \int_{\tau_0}^1 d\tau\, \frac{d\mathcal{L}_{gg}}{d\tau}\, \hat{\sigma}^{\mathrm{LO}}(\hat{s} = \tau s) \,, \tag{154}$$

where s is the square of the hadronic centre of mass energy, $\tau_0 = 4m_h^2/s$, and μ_F is the factorisation scale.
In the $m_t \to \infty$ approximation the LO form factors are given by

$$\bar{F}_\triangle \;\to\; \frac{4}{3}\hat{s}\;,\; F_\square \to -\frac{4}{3}\hat{s}\;,\; F_2 \to 0\;, \tag{155}$$

which implies for the the effective ggH and $ggHH$ couplings

$$c_{ggh} = -c_{gghh} = \frac{\alpha_s}{4\pi}\,\frac{i}{3} + \mathcal{O}\left(\frac{m_h^2}{4m_t^2}\right)\;. \tag{156}$$

Note that the range of validity of the heavy top limit is

$$2m_h \le \sqrt{\hat{s}} \lesssim 2m_t\;, \tag{157}$$

which is a range of about 100 GeV only. Results comparing the full NLO calculation with the heavy top limit, both Born-improved and "basic", are shown in Fig. 44.

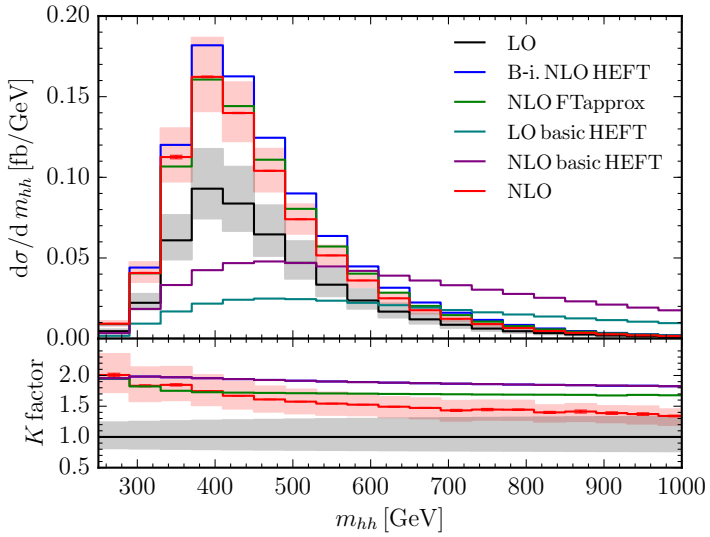

Figure 44: Full NLO results compared to approximations. What is called HEFT here is the heavy top limit. Figure from Ref. [107].

Combinations of the full NLO result with approximate NNLO results are shown in Fig. 45.

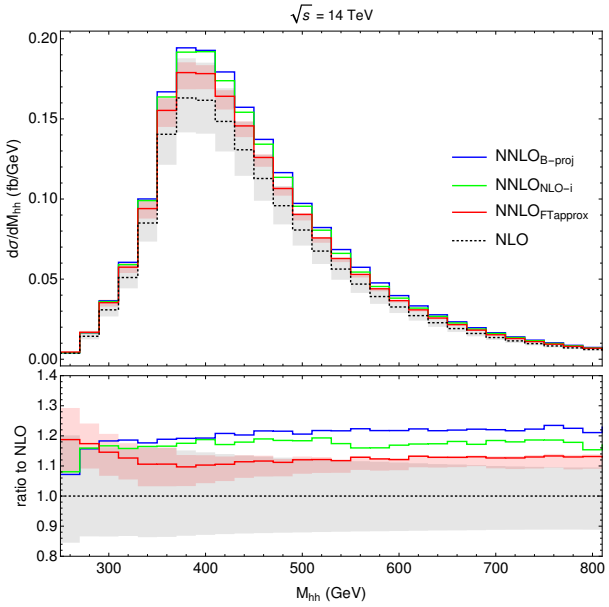

Figure 45: Higgs boson pair invariant mass distribution at NNLO for different approximations, together with the NLO prediction, at 14 TeV. The lower panels show the ratio with respect to the NLO prediction, and the filled areas indicate the NLO and $\text{NNLO}_{\text{FTapprox}}$ scale uncertainties. Figure from Ref. [119].

Fig. 46 shows the transverse momentum distribution of the Higgs boson pair for full NLO, Born-improved HTL and an example of anomalous couplings in the Higgs sector. One can see how important it is to know the SM prediction well enough in the tail of the distribution, in order to distinguish new physics effects. The blue curve corresponds to "benchmark point 4", which is the full NLO result including the anomalous couplings $c_{hhh} = 2.79, c_t = 0.61, c_{tt} = 1/3, c_{ggh} = -1/2, c_{gghh} = 1/6$ (see section 5.2.3), which is very similar to the SM prediction in the Born-improved $m_t \to \infty$ approximation (green).

5.2.3 Anomalous couplings

In the following we present a parametrisation of new physics effects in a non-linear EFT framework, sometimes also called Electroweak Chiral Lagrangian (EWChL) including a light Higgs boson [125, 126] or HEFT (Higgs Effective Field Theory), not to be confused with the heavy top limit, which is sometimes also called HEFT. It relies on counting the chiral dimension of the

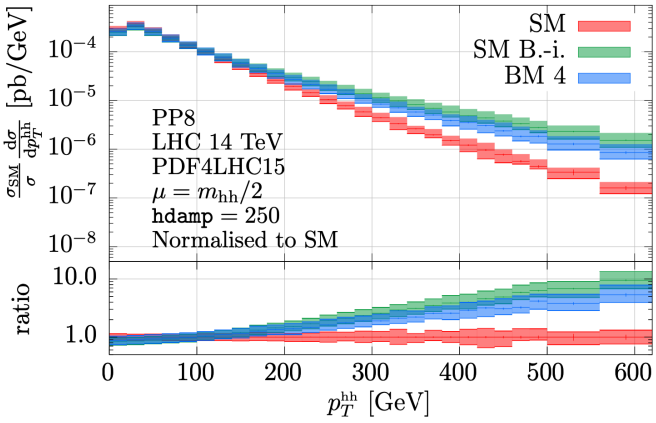

Figure 46: NLO results with full m_t-dependence versus Born-improved HTL compared to a result based on anomalous couplings (benchmark point 4). Figure from Ref. [113].

terms contributing to the Lagrangian [127], rather than counting the canonical dimension as in the Standard Model Effective Field Theory (SMEFT). As a consequence, the EWChL is also suitable to describe strong dynamics in the Higgs sector. Applying this framework to Higgs boson pair production in gluon fusion, keeping terms up to, and including, chiral dimension $d_\chi = 4$, we obtain the effective Lagrangian relevant to this process as

$$\mathcal{L} \supset -m_t \left(c_t \frac{h}{v} + c_{tt} \frac{h^2}{v^2} \right) \bar{t}\, t - c_{hhh} \frac{m_h^2}{2v} h^3 + \frac{\alpha_s}{8\pi} \left(c_{ggh} \frac{h}{v} + c_{gghh} \frac{h^2}{v^2} \right) G^a_{\mu\nu} G^{a,\mu\nu} \,. \tag{158}$$

In the EWChL framework there are a priori no relations between the couplings. In general, all couplings may have arbitrary values of $\mathcal{O}(1)$. The conventions are such that in the SM $c_t = c_{hhh} = 1$ and $c_{tt} = c_{ggh} = c_{gghh} = 0$. The EWChL coefficients can be related [124] to those in the SMEFT at Lagrangian level, however how to treat double insertions of operators and squared dimension-6 terms at cross section level is less straightforward when attempting to relate the two EFT frameworks. The diagrams at leading order in QCD and chiral dimension four are shown in Fig. 47.
We can describe the dependence of the NNLO cross section on the five anoma-

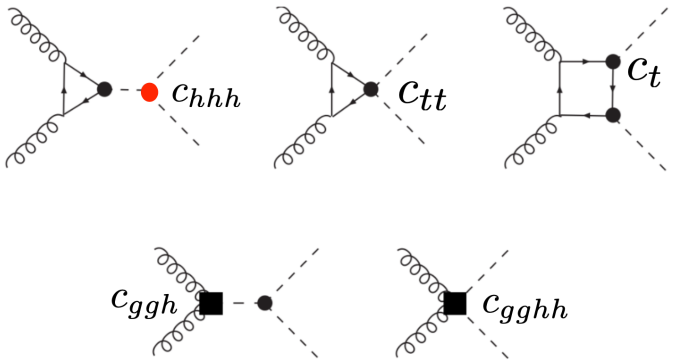

Figure 47: Higgs boson pair production in gluon fusion at leading order in QCD and at chiral dimension $d_\chi = 4$. The black dots indicate vertices from anomalous couplings present already at leading order in the chiral Lagrangian ($d_\chi = 2$), the black squares denote local operators contributing at ($d_\chi = 4$).

lous couplings in terms of 25 coefficients a_i [120]:

$$\begin{aligned}\sigma_{\rm BSM}/\sigma_{\rm SM} = {} & a_1\, c_t^4 + a_2\, c_{tt}^2 + a_3\, c_t^2 c_{hhh}^2 + a_4\, c_{ggh}^2 c_{hhh}^2 + a_5\, c_{gghh}^2 + a_6\, c_{tt} c_t^2 + a_7\, c_t^3 c_{hhh} \\ & + a_8\, c_{tt} c_t\, c_{hhh} + a_9\, c_{tt} c_{ggh} c_{hhh} + a_{10}\, c_{tt} c_{gghh} + a_{11}\, c_t^2 c_{ggh} c_{hhh} + a_{12}\, c_t^2 c_{gghh} \\ & + a_{13}\, c_t c_{hhh}^2 c_{ggh} + a_{14}\, c_t c_{hhh} c_{gghh} + a_{15}\, c_{ggh} c_{hhh} c_{gghh} + a_{16}\, c_t^3 c_{ggh} \\ & + a_{17}\, c_t c_{tt} c_{ggh} + a_{18}\, c_t c_{ggh}^2 c_{hhh} + a_{19}\, c_t c_{ggh} c_{gghh} + a_{20}\, c_t^2 c_{ggh}^2 \\ & + a_{21}\, c_{tt} c_{ggh}^2 + a_{22}\, c_{ggh}^3 c_{hhh} + a_{23}\, c_{ggh}^2 c_{gghh} + a_{24}\, c_{ggh}^4 + a_{25}\, c_{ggh}^3 c_t\,. \end{aligned} \tag{159}$$

While at LO only the first 15 coefficients contribute, at NLO 23 coupling combinations occur and at NNLO 25 combinations are possible.
In Fig. 48 we show the Higgs boson pair invariant mass distribution at NLO, where only the trilinear Higgs coupling is varied. It shows a characteristic dip in the distribution for c_{hhh} values 2.5 due to destructive interference of box-type and triangle-type constributions to the amplitude.
In Fig. 49 we show the approximate NNLO cross section as a function of each of the couplings present in the Lagrangian of Eq. (158). We vary each of the couplings independently while keeping the others at their SM value. The regions where the lines in Fig. 49 are solid correspond to the following

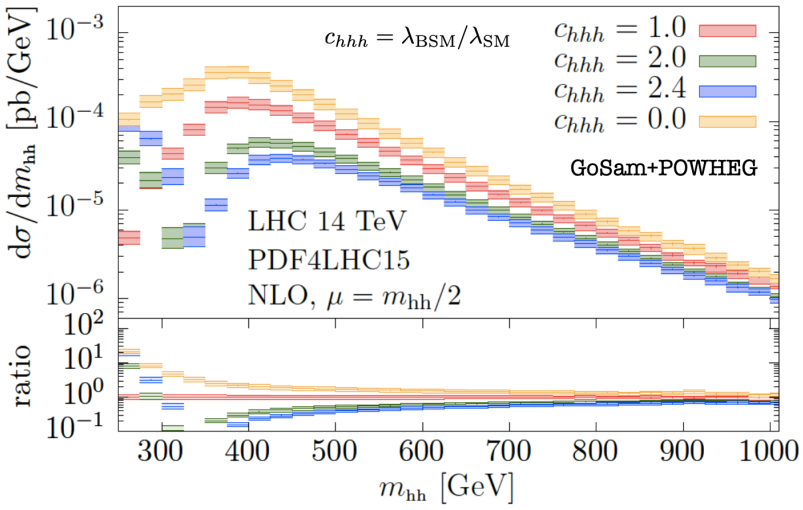

Figure 48: NLO results for the Higgs boson pair invariant mass distribution or different values of c_{hhh}. Figure from Ref. [112].

range in the EFT parameter space:

$$c_{hhh} \in [-5, 10],\ |c_t| \in [0.5, 1.5],\ c_{tt} \in [-1, 1.5],\ c_{ggh} \in [-0.2, 0.4],\ c_{gghh} \in [-1, 1].$$

The chosen range for each coefficient is motivated by current experimental constraints. We note that in the case of c_{gghh} the interval in Eq. (160) is chosen arbitrarily, since there are no experimental constraints on its value. The yellow horizontal line in Fig. 49 denotes the best experimental limit on the total di-Higgs production cross section of 4.1 times its SM value at 95% confidence level [70]. From this comparison we conclude that, with the only exception of c_{ggh}, all of the anomalous couplings can generate variations in the di-Higgs cross section which are larger than the current experimental limit. This indicates that, with the level of precision already achieved by the LHC, a simultaneous variation of all couplings is needed for a meaningful EFT analysis.
Fig. 50 (Fig. 51) shows the approximate NNLO (NNLO′) total cross section and K-factor, both normalised to the corresponding SM value, in the c_{hhh}–c_{ggh} (c_{hhh}–c_{tt}) plane. Here the K-factor is defined as the ratio between the NNLO′ and LO predictions. We set $c_t = 1$ and the remaining couplings to zero, except in the c_{hhh}–c_{ggh} case where we additionally set $c_{gghh} = c_{ggh}/2$

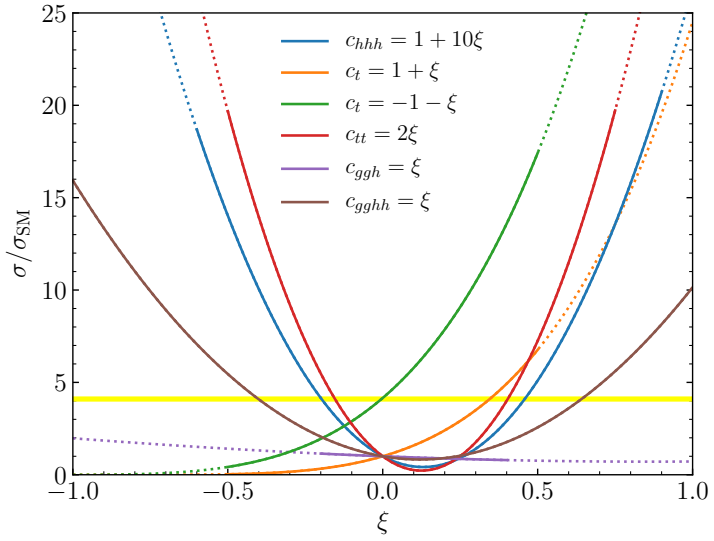

Figure 49: Total cross section, normalised to its SM value, as a function of each of the anomalous couplings. The horizontal line corresponds to the best current experimental limit [70].

in order to mimic the SMEFT situation, where the latter couplings are not independent of each other.
Comparing Figs. 50 and 51 (left), we observe that the cross section is more sensitive to variations of both c_{hhh} and c_{tt} than variations of c_{ggh} (within the range suggested by current constraints). It is also clear that the normalised K-factors, shown in Figs. 50 and 51 (right), only turn out to be rather flat under variations of the parameter c_{ggh}, which generates point-like (m_t-independent) effective interactions. In contrast, much stronger K-factor changes (up to 40%) are observed for modifications of c_{hhh} and c_{tt}, due to the effect of the full top quark mass dependence in the NLO corrections. Note that the K-factors shown here mostly have values below two because they are normalised to the SM K-factor.

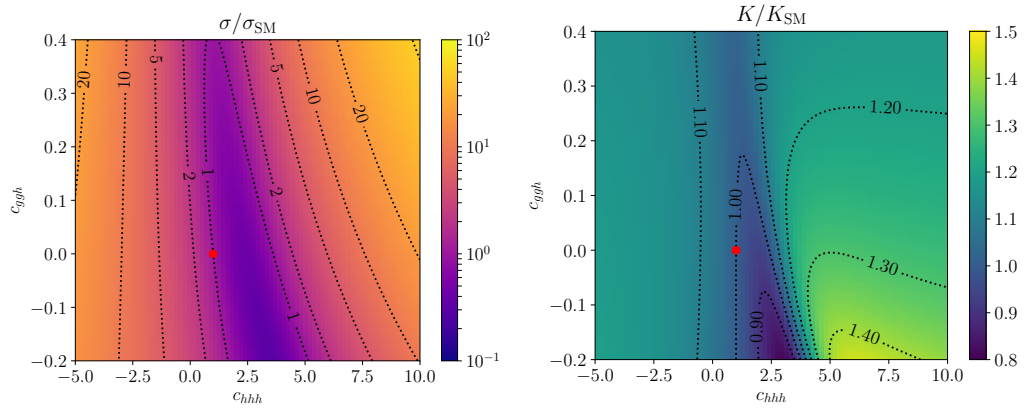

Figure 50: Ratio of (left) the total cross section to the SM cross section at NNLO′ and (right) the NNLO′/LO K-factor to the SM K-factor, in the $c_{hhh} - c_{ggh}$ plane. The red dot indicates the SM value for these couplings.

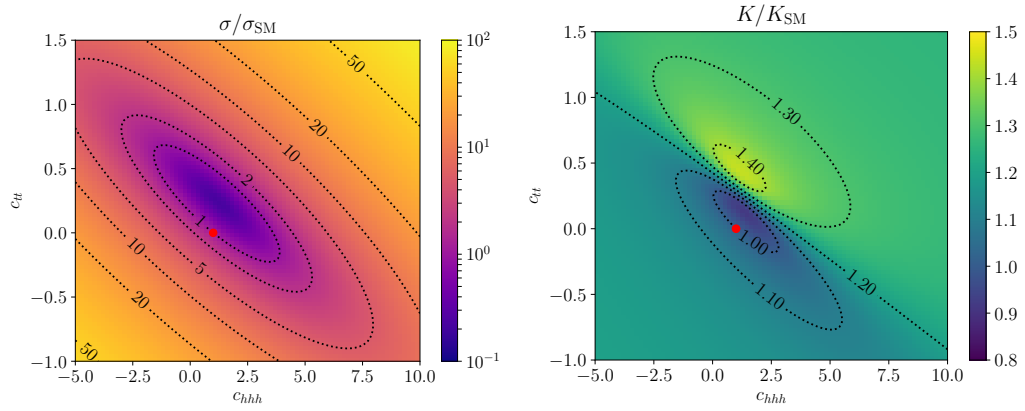

Figure 51: Same as Fig. 50 for the $c_{hhh} - c_{tt}$ plane.

5.3 Asymptotic expansions

We are considering Feynman integrals, at one loop or multi-loop. In cases where the kinematic invariants characterising the integral are not of the same order of magnitude, it can be beneficial to expand the integrand in a small parameter t, the ratio of appropriate kinematic invariants, for instance $t = s_{ij}/m^2$ in a large mass expansion. The individual terms of such an expansion then may be easier to evaluate. However, it is usually not possible to just Taylor expand the integrand in t. The integrand might not have a convergent Taylor series in the whole integration domain and we may need different Taylor expansions in different regions of the integration domain. Therefore a more careful strategy is required to perform valid expansions. This strategy goes under the name *expansion by regions*. The method of expansion by regions has been pioneered in Refs. [128–130], where it was formulated in terms of the momenta involved in a loop integral. Later it also has been formulated in Feynman parameter space, where it allows a geometric interpretation [131–134].

An example in momentum space

The various regions that can occur depend on the considered integral. In general there is a hard region where all components of the loop momentum are much bigger than the parameter we are expanding in. In addition, there can be various collinear regions, a soft region, an ultrasoft region, and other regions. For a discussion of these regions in momentum space we refer e.g. to Ref. [135].
To explain the basic principle, let us consider a simple example in momentum space, discussed in more detail in Ref. [136]. We consider the large-momentum expansion of the integral

$$I_2 = \mu^{2\epsilon} \int d\kappa \frac{1}{(k+p)^2(k^2-m^2)^2} \,, \tag{160}$$

depicted in Fig. 52.
We will expand the integrand in m^2/p^2 in the limit $|p^2| \gg m^2$. We can introduce a smallness parameter z, in terms of which a Taylor expansion is performed. For the hard region, where m^2 is small compared to $|k^2|$, we introduce $m^2 \to z\,m^2$, do a Taylor expansion in z and then set $z = 1$.

$$(h): \quad \frac{1}{(k+p)^2(k^2-m^2)^2} \to \frac{1}{(k+p)^2\,(k^2)^2} \left(1 + 2\frac{m^2}{k^2} + \dots\right). \tag{161}$$

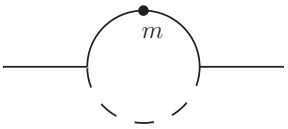

Figure 52: One-loop two-point function with the massive propagator squared.

This expansion is valid whenever $|k^2| > |m^2|$. However, since the integration domain also contains points that do not satisfy this condition, we need another region. This is the soft region, where we introduce z by $k^2 \to z\,k^2$, $m^2 \to z\,m^2$ and Taylor expand in z, after which we set $z = 1$.

$$(s): \quad \frac{1}{(k+p)^2(k^2-m^2)^2} \to \frac{1}{p^2\,(k^2-m^2)^2}\left(1 - \frac{k^2+2p\cdot k}{p^2} + \ldots\right). \tag{162}$$

The resulting expansion is valid whenever $k^2 + 2k\cdot p < p^2$. This means that this expansion covers the region where the hard region expansion, Eq. (161), does not converge. In the expansion by regions method one integrates both expansions over the whole integration domain. To compensate for this, one should subtract the extra contribution coming from extending the integration domain, but that contribution turns out to be a scaleless integral, which vanishes if properly regularised, in our example by dimensional regularisation. To see this, if we take the expansion in the hard region, expression Eq. (161), and expand it again in the soft region, we get

$$(hs): \frac{1}{(k+p)^2(k^2-m^2)^2} \to \frac{1}{p^2\,(k^2)^2}\left(1 - \frac{k^2+2p\cdot k}{p^2} + \ldots\right)\left(1 + 2\frac{m^2}{k^2} + \ldots\right). \tag{163}$$

Expanding the expression of the soft region, Eq. (70), again in the hard region leads to the same result. These are scaleless integrals to all orders in the expansion, and therefore we can ignore them.
Integrating the leading contributions in the soft and hard regions results in

$$I_2^{(h)} = \frac{1}{p^2}\left[-\frac{1}{\epsilon} + \ln\left(\frac{-p^2}{\mu^2}\right)\right] + \mathcal{O}(\epsilon, m^2/p^2)\,, \tag{164}$$

$$I_2^{(s)} = \frac{1}{p^2}\left[\frac{1}{\epsilon} - \ln\left(\frac{m^2}{\mu^2}\right)\right] + \mathcal{O}(\epsilon, m^2/p^2)\,, \tag{165}$$

such that

$$I_2 = I_2^{(h)} + I_2^{(s)} = \frac{1}{p^2} \ln\left(\frac{-p^2}{m^2}\right) + \mathcal{O}(\epsilon, m^2/p^2) \,. \tag{166}$$

Note that in both the soft and the hard region we encounter spurious poles that do not exist in the original integral. The pole in Eq. (164) is of infrared nature, while the pole in Eq. (165) is of UV nature, and Eq. (163) can be written as

$$I_2^{(h,s)} = \frac{1}{p^2}\left(\frac{1}{\epsilon_{UV}} - \frac{1}{\epsilon_{IR}}\right) \,. \tag{167}$$

Therefore, formally, the combinations $I_2^{(h)} - I_2^{(h,s)}$ and $I_2^{(s)} - I_2^{(h,s)}$ are separately IR and UV finite. In more general cases, the spurious poles are not always regulated by dimensional regularisation. Extra regulators must be introduced, which is most conveniently done by using so-called "analytic regulators" [135], where the propagators get extra powers α, and the α-dependence should cancel in the final result. An example for such a case is given by the high-energy expansion of a one-loop box diagram with a massive loop, analyzed in great detail in Ref. [137].
While a formal proof of expansion-by-regions to always reproduce the full result is still missing, or many complicated examples it has been shown in the literature that one can integrate each expansion over the whole integration domain to get the correct result.

References

[1] P. A. Baikov, K. G. Chetyrkin, J. H. Kühn and J. Rittinger, *Complete $\mathcal{O}(\alpha_s^4)$ QCD Corrections to Hadronic Z-Decays*, *Phys. Rev. Lett.* **108** (2012) 222003, [1201.5804].

[2] F. Herzog, B. Ruijl, T. Ueda, J. A. M. Vermaseren and A. Vogt, *On Higgs decays to hadrons and the R-ratio at N^4LO*, *JHEP* **08** (2017) 113, [1707.01044].

[3] T. van Ritbergen, J. A. M. Vermaseren and S. A. Larin, *The Four loop beta function in quantum chromodynamics*, *Phys. Lett.* **B400** (1997) 379–384, [hep-ph/9701390].

[4] P. A. Baikov, K. G. Chetyrkin and J. H. Kühn, *Five-Loop Running of the QCD coupling constant*, *Phys. Rev. Lett.* **118** (2017) 082002, [1606.08659].

[5] F. Herzog, B. Ruijl, T. Ueda, J. A. M. Vermaseren and A. Vogt, *The five-loop beta function of Yang-Mills theory with fermions*, *JHEP* **02** (2017) 090, [1701.01404].

[6] T. Luthe, A. Maier, P. Marquard and Y. Schröder, *The five-loop Beta function for a general gauge group and anomalous dimensions beyond Feynman gauge*, *JHEP* **10** (2017) 166, [1709.07718].

[7] K. G. Chetyrkin, G. Falcioni, F. Herzog and J. A. M. Vermaseren, *Five-loop renormalisation of QCD in covariant gauges*, *JHEP* **10** (2017) 179, [1709.08541].

[8] J. Davies, M. Steinhauser and D. Wellmann, *Completing the hadronic Higgs boson decay at order α_s^4*, *Nucl. Phys.* **B920** (2017) 20–31, [1703.02988].

[9] D. J. Gross and F. Wilczek, *Ultraviolet Behavior of Nonabelian Gauge Theories*, *Phys. Rev. Lett.* **30** (1973) 1343–1346.

[10] H. D. Politzer, *Reliable Perturbative Results for Strong Interactions?*, *Phys. Rev. Lett.* **30** (1973) 1346–1349.

[11] P. A. Baikov, K. G. Chetyrkin and J. H. Kühn, *Quark Mass and Field Anomalous Dimensions to $\mathcal{O}(\alpha_s^5)$*, *JHEP* **10** (2014) 076, [1402.6611].

[12] P. A. Baikov, K. G. Chetyrkin and J. H. Kühn, *Five-loop fermion anomalous dimension for a general gauge group from four-loop massless propagators*, *JHEP* **04** (2017) 119, [1702.01458].

[13] A. G. Grozin, P. Marquard, A. V. Smirnov, V. A. Smirnov and M. Steinhauser, *Matching the heavy-quark fields in QCD and HQET at four loops*, *Phys. Rev. D* **102** (2020) 054008, [2005.14047].

[14] F. Herren and A. E. Thomsen, *On Ambiguities and Divergences in Perturbative Renormalization Group Functions*, 2104.07037.

[15] A. Gehrmann-De Ridder, T. Gehrmann, E. W. N. Glover and G. Heinrich, *NNLO corrections to event shapes in e+ e- annihilation*, *JHEP* **12** (2007) 094, [0711.4711].

[16] E. W. N. Glover, *Progress in NNLO calculations for scattering processes*, *Nucl. Phys. B Proc. Suppl.* **116** (2003) 3–7, [hep-ph/0211412].

[17] J. Currie, E. W. N. Glover and J. Pires, *Next-to-Next-to Leading Order QCD Predictions for Single Jet Inclusive Production at the LHC*, *Phys. Rev. Lett.* **118** (2017) 072002, [1611.01460].

[18] M. Czakon, A. van Hameren, A. Mitov and R. Poncelet, *Single-jet inclusive rates with exact color at $\mathcal{O}$ (α_s^4)*, *JHEP* **10** (2019) 262, [1907.12911].

[19] B. Mistlberger, *Higgs boson production at hadron colliders at N^3LO in QCD*, *JHEP* **05** (2018) 028, [1802.00833].

[20] C. Anastasiou, C. Duhr, F. Dulat, F. Herzog and B. Mistlberger, *Higgs Boson Gluon-Fusion Production in QCD at Three Loops*, *Phys. Rev. Lett.* **114** (2015) 212001, [1503.06056].

[21] C. Duhr, F. Dulat, V. Hirschi and B. Mistlberger, *Higgs production in bottom quark fusion: matching the 4- and 5-flavour schemes to third order in the strong coupling*, *JHEP* **08** (2020) 017, [2004.04752].

[22] C. Duhr, F. Dulat and B. Mistlberger, *Charged current Drell-Yan production at N^3LO*, *JHEP* **11** (2020) 143, [2007.13313].

[23] J. Currie, A. Gehrmann-De Ridder, T. Gehrmann, E. W. N. Glover, A. Huss and J. a. Pires, *Infrared sensitivity of single jet inclusive production at hadron colliders*, *JHEP* **10** (2018) 155, [1807.03692].

[24] G. 't Hooft and M. J. G. Veltman, *Regularization and Renormalization of Gauge Fields*, *Nucl. Phys.* **B44** (1972) 189–213.

[25] C. G. Bollini and J. J. Giambiagi, *Dimensional Renormalization: The Number of Dimensions as a Regularizing Parameter*, *Nuovo Cim.* **B12** (1972) 20–26.

[26] P. Breitenlohner and D. Maison, *Dimensional Renormalization and the Action Principle*, *Commun. Math. Phys.* **52** (1977) 11–38.

[27] S. A. Larin, *The Renormalization of the axial anomaly in dimensional regularization*, *Phys. Lett.* **B303** (1993) 113–118, [hep-ph/9302240].

[28] F. Jegerlehner, *Facts of life with gamma(5)*, *Eur. Phys. J. C* **18** (2001) 673–679, [hep-th/0005255].

[29] J. Korner, D. Kreimer and K. Schilcher, *A Practicable gamma(5) scheme in dimensional regularization*, *Z. Phys. C* **54** (1992) 503–512.

[30] G. Passarino and M. J. G. Veltman, *One Loop Corrections for e+ e- Annihilation Into mu+ mu- in the Weinberg Model*, *Nucl. Phys.* **B160** (1979) 151–207.

[31] T. Hahn, *Feynman Diagram Calculations with FeynArts, FormCalc, and LoopTools*, *PoS* **ACAT2010** (2010) 078, [1006.2231].

[32] T. Hahn and M. Perez-Victoria, *Automatized one loop calculations in four-dimensions and D-dimensions*, *Comput. Phys. Commun.* **118** (1999) 153–165, [hep-ph/9807565].

[33] A. van Hameren, *OneLOop: For the evaluation of one-loop scalar functions*, *Comput. Phys. Commun.* **182** (2011) 2427–2438, [1007.4716].

[34] J. P. Guillet, G. Heinrich and J. F. von Soden-Fraunhofen, *Tools for NLO automation: extension of the golem95C integral library*, *Comput. Phys. Commun.* **185** (2014) 1828–1834, [1312.3887].

[35] G. Cullen, J. P. Guillet, G. Heinrich, T. Kleinschmidt, E. Pilon, T. Reiter et al., *Golem95C: A library for one-loop integrals with complex masses*, *Comput. Phys. Commun.* **182** (2011) 2276–2284, [1101.5595].

[36] T. Binoth, J. P. Guillet, G. Heinrich, E. Pilon and T. Reiter, *Golem95: A Numerical program to calculate one-loop tensor integrals with up to six external legs*, *Comput. Phys. Commun.* **180** (2009) 2317–2330, [0810.0992].

[37] A. Denner, S. Dittmaier and L. Hofer, *Collier: a fortran-based Complex One-Loop LIbrary in Extended Regularizations*, *Comput. Phys. Commun.* **212** (2017) 220–238, [1604.06792].

[38] H. H. Patel, *Package-X: A Mathematica package for the analytic calculation of one-loop integrals*, *Comput. Phys. Commun.* **197** (2015) 276–290, [1503.01469].

[39] S. Carrazza, R. K. Ellis and G. Zanderighi, *QCDLoop: a comprehensive framework for one-loop scalar integrals*, *Comput. Phys. Commun.* **209** (2016) 134–143, [1605.03181].

[40] R. K. Ellis and G. Zanderighi, *Scalar one-loop integrals for QCD*, *JHEP* **02** (2008) 002, [0712.1851].

[41] R. Ellis, Z. Kunszt, K. Melnikov and G. Zanderighi, *One-loop calculations in quantum field theory: from Feynman diagrams to unitarity cuts*, *Phys. Rept.* **518** (2012) 141–250, [1105.4319].

[42] T. Kinoshita, *Mass singularities of Feynman amplitudes*, *J. Math. Phys.* **3** (1962) 650–677.

[43] T. D. Lee and M. Nauenberg, *Degenerate Systems and Mass Singularities*, *Phys. Rev.* **133** (1964) B1549–B1562.

[44] S. Catani, T. Gleisberg, F. Krauss, G. Rodrigo and J.-C. Winter, *From loops to trees by-passing Feynman's theorem*, *JHEP* **09** (2008) 065, [0804.3170].

[45] W. J. Torres Bobadilla, *Lotty – The loop-tree duality automation*, 2103.09237.

[46] L. D. Landau, *On analytic properties of vertex parts in quantum field theory*, *Nucl. Phys.* **13** (1959) 181–192.

[47] R. J. Eden, P. V. Landshoff, D. I. Olive and J. C. Polkinghorne, *The Analytic S-Matrix*. Cambridge University Press, 1966.

[48] S. Catani and M. H. Seymour, *A General algorithm for calculating jet cross-sections in NLO QCD*, *Nucl. Phys.* **B485** (1997) 291–419, [hep-ph/9605323].

[49] S. Catani and M. Grazzini, *The soft gluon current at one loop order*, *Nucl. Phys.* **B591** (2000) 435–454, [hep-ph/0007142].

[50] Z. Trocsanyi, *QCD for collider experiments*, in *Proceedings, 2013 European School of High-Energy Physics (ESHEP 2013): Paradfurdo, Hungary, June 5-18, 2013*, pp. 65–116, 2015. 1608.02381. DOI.

[51] K. Long, *QCD at high-energy (experiments)*, hep-ex/0212008.

[52] S. Moch, B. Ruijl, T. Ueda, J. A. M. Vermaseren and A. Vogt, *Four-Loop Non-Singlet Splitting Functions in the Planar Limit and Beyond*, *JHEP* **10** (2017) 041, [1707.08315].

[53] B. Agarwal, A. von Manteuffel, E. Panzer and R. M. Schabinger, *Four-loop collinear anomalous dimensions in QCD and $\mathcal{N} = 4$ super Yang-Mills*, 2102.09725.

[54] R. N. Lee, A. von Manteuffel, R. M. Schabinger, A. V. Smirnov, V. A. Smirnov and M. Steinhauser, *Fermionic corrections to quark and gluon form factors in four-loop QCD*, 2105.11504.

[55] Y. L. Dokshitzer, *Calculation of the Structure Functions for Deep Inelastic Scattering and e+ e- Annihilation by Perturbation Theory in Quantum Chromodynamics.*, *Sov. Phys. JETP* **46** (1977) 641–653.

[56] V. N. Gribov and L. N. Lipatov, *Deep inelastic e p scattering in perturbation theory*, *Sov. J. Nucl. Phys.* **15** (1972) 438–450.

[57] G. Altarelli and G. Parisi, *Asymptotic Freedom in Parton Language*, *Nucl. Phys.* **B126** (1977) 298–318.

[58] ATLAS, CMS collaboration, G. Aad et al., *Measurements of the Higgs boson production and decay rates and constraints on its couplings from a combined ATLAS and CMS analysis of the LHC pp collision data at $\sqrt{s} = 7$ and 8 TeV*, *JHEP* **08** (2016) 045, [1606.02266].

[59] CMS collaboration, A. M. Sirunyan et al., *Observation of $\mathrm{t\bar{t}}H$ production*, *Phys. Rev. Lett.* **120** (2018) 231801, [1804.02610].

[60] ATLAS collaboration, M. Aaboud et al., *Observation of Higgs boson production in association with a top quark pair at the LHC with the ATLAS detector*, *Phys. Lett. B* **784** (2018) 173–191, [1806.00425].

[61] ATLAS collaboration, M. Aaboud et al., *Observation of $H \to b\bar{b}$ decays and VH production with the ATLAS detector*, *Phys. Lett. B* **786** (2018) 59–86, [1808.08238].

[62] CMS collaboration, A. M. Sirunyan et al., *Observation of Higgs boson decay to bottom quarks*, *Phys. Rev. Lett.* **121** (2018) 121801, [1808.08242].

[63] CMS collaboration, A. M. Sirunyan et al., *Observation of the Higgs boson decay to a pair of τ leptons with the CMS detector*, *Phys. Lett. B* **779** (2018) 283–316, [1708.00373].

[64] ATLAS collaboration, M. Aaboud et al., *Cross-section measurements of the Higgs boson decaying into a pair of τ-leptons in proton-proton collisions at $\sqrt{s} = 13$ TeV with the ATLAS detector*, *Phys. Rev. D* **99** (2019) 072001, [1811.08856].

[65] CMS collaboration, A. M. Sirunyan et al., *Evidence for Higgs boson decay to a pair of muons*, *JHEP* **01** (2021) 148, [2009.04363].

[66] ATLAS collaboration, G. Aad et al., *A search for the dimuon decay of the Standard Model Higgs boson with the ATLAS detector*, *Phys. Lett. B* **812** (2021) 135980, [2007.07830].

[67] CMS collaboration, A. M. Sirunyan et al., *Combination of searches for Higgs boson pair production in proton-proton collisions at $\sqrt{s} =$ 13 TeV*, *Phys. Rev. Lett.* **122** (2019) 121803, [1811.09689].

[68] ATLAS collaboration, G. Aad et al., *Combination of searches for Higgs boson pairs in pp collisions at $\sqrt{s} =$13 TeV with the ATLAS detector*, *Phys. Lett.* **B800** (2020) 135103, [1906.02025].

[69] CMS collaboration, A. M. Sirunyan et al., *Search for nonresonant Higgs boson pair production in final states with two bottom quarks and two photons in proton-proton collisions at $\sqrt{s} =$ 13 TeV*, *JHEP* **03** (2021) 257, [2011.12373].

[70] ATLAS collaboration, *Search for Higgs boson pair production in the two bottom quarks plus two photons final state in pp collisions at $\sqrt{s} = 13$ TeV with the ATLAS detector*, tech. rep., CERN, Geneva, Mar, 2021.

[71] C. Anastasiou, C. Duhr, F. Dulat, E. Furlan, T. Gehrmann, F. Herzog et al., *High precision determination of the gluon fusion Higgs boson cross-section at the LHC*, *JHEP* **05** (2016) 058, [1602.00695].

[72] G. Das, S. Moch and A. Vogt, *Approximate four-loop QCD corrections to the Higgs-boson production cross section*, *Phys. Lett. B* **807** (2020) 135546, [2004.00563].

[73] T. Ahmed, A. H. Ajjath, G. Das, P. Mukherjee, V. Ravindran and S. Tiwari, *Soft-virtual correction and threshold resummation for n-colorless particles to fourth order in QCD: Part I*, 2010.02979.

[74] J. Davies and F. Herren, *Higgs boson decay into photons at four loops*, 2104.12780.

[75] L. Cieri, X. Chen, T. Gehrmann, E. W. N. Glover and A. Huss, *Higgs boson production at the LHC using the q_T subtraction formalism at N^3LO QCD*, *JHEP* **02** (2019) 096, [1807.11501].

[76] F. Dulat, B. Mistlberger and A. Pelloni, *Precision predictions at N^3LO for the Higgs boson rapidity distribution at the LHC*, *Phys. Rev. D* **99** (2019) 034004, [1810.09462].

[77] M. Czakon, R. V. Harlander, J. Klappert and M. Niggetiedt, *Exact top-quark mass dependence in hadronic Higgs production*, 2105.04436.

[78] X. Chen, X. Chen, T. Gehrmann, E. W. N. Glover, A. Huss, B. Mistlberger et al., *Fully Differential Higgs Boson Production to Third Order in QCD*, 2102.07607.

[79] G. Billis, B. Dehnadi, M. A. Ebert, J. K. L. Michel and F. J. Tackmann, *The Higgs p_T Spectrum and Total Cross Section with Fiducial Cuts at $N^3LL'+N^3LO$*, 2102.08039.

[80] M. Spira, *Higgs Boson Production and Decay at Hadron Colliders*, *Prog. Part. Nucl. Phys.* **95** (2017) 98–159, [1612.07651].

[81] S. P. Jones, M. Kerner and G. Luisoni, *Next-to-Leading-Order QCD Corrections to Higgs Boson Plus Jet Production with Full Top-Quark Mass Dependence*, *Phys. Rev. Lett.* **120** (2018) 162001, [1802.00349].

[82] R. Boughezal, F. Caola, K. Melnikov, F. Petriello and M. Schulze, *Higgs boson production in association with a jet at next-to-next-to-leading order*, *Phys. Rev. Lett.* **115** (2015) 082003, [1504.07922].

[83] R. Boughezal, C. Focke, W. Giele, X. Liu and F. Petriello, *Higgs boson production in association with a jet at NNLO using jettiness subtraction*, *Phys. Lett.* **B748** (2015) 5–8, [1505.03893].

[84] F. Caola, K. Melnikov and M. Schulze, *Fiducial cross sections for Higgs boson production in association with a jet at next-to-next-to-leading order in QCD*, *Phys. Rev. D* **92** (2015) 074032, [1508.02684].

[85] X. Chen, J. Cruz-Martinez, T. Gehrmann, E. Glover and M. Jaquier, *NNLO QCD corrections to Higgs boson production at large transverse momentum*, *JHEP* **10** (2016) 066, [1607.08817].

[86] J. M. Campbell, R. K. Ellis and S. Seth, *H + 1 jet production revisited*, *JHEP* **10** (2019) 136, [1906.01020].

[87] K. Becker et al., *Precise predictions for boosted Higgs production*, 2005.07762.

[88] M. Schlaffer, M. Spannowsky, M. Takeuchi, A. Weiler and C. Wymant, *Boosted Higgs Shapes*, *Eur. Phys. J. C* **74** (2014) 3120, [1405.4295].

[89] S. Dawson, I. M. Lewis and M. Zeng, *Effective field theory for Higgs boson plus jet production*, *Phys. Rev. D* **90** (2014) 093007, [1409.6299].

[90] M. Grazzini, A. Ilnicka, M. Spira and M. Wiesemann, *Modeling BSM effects on the Higgs transverse-momentum spectrum in an EFT approach*, *JHEP* **03** (2017) 115, [1612.00283].

[91] S. Dawson, C. Englert and T. Plehn, *Higgs Physics: It ain't over till it's over*, *Phys. Rept.* **816** (2019) 1–85, [1808.01324].

[92] ATLAS collaboration, G. Aad et al., *CP Properties of Higgs Boson Interactions with Top Quarks in the $t\bar{t}H$ and tH Processes Using $H \to \gamma\gamma$ with the ATLAS Detector*, *Phys. Rev. Lett.* **125** (2020) 061802, [2004.04545].

[93] CMS collaboration, A. M. Sirunyan et al., *Measurements of $\mathrm{t\bar{t}}H$ Production and the CP Structure of the Yukawa Interaction between the Higgs Boson and Top Quark in the Diphoton Decay Channel*, *Phys. Rev. Lett.* **125** (2020) 061801, [2003.10866].

[94] F. Maltoni, E. Vryonidou and C. Zhang, *Higgs production in association with a top-antitop pair in the Standard Model Effective Field Theory at NLO in QCD*, *JHEP* **10** (2016) 123, [1607.05330].

[95] G. Heinrich, *Collider Physics at the Precision Frontier*, *Phys. Rept.* **922** (2021) 1–69, [2009.00516].

[96] H. E. Logan, *TASI 2013 lectures on Higgs physics within and beyond the Standard Model*, 1406.1786.

[97] LHC Higgs Cross Section Working Group collaboration, D. de Florian et al., *Handbook of LHC Higgs Cross Sections: 4. Deciphering the Nature of the Higgs Sector*, 1610.07922.

[98] M. Cepeda et al., *Report from Working Group 2: Higgs Physics at the HL-LHC and HE-LHC*, *CERN Yellow Rep. Monogr.* **7** (2019) 221–584, [1902.00134].

[99] M. L. Mangano, G. Ortona and M. Selvaggi, *Measuring the Higgs self-coupling via Higgs-pair production at a 100 TeV p-p collider*, *Eur. Phys. J. C* **80** (2020) 1030, [2004.03505].

[100] M. McCullough, *An Indirect Model-Dependent Probe of the Higgs Self-Coupling*, *Phys. Rev. D* **90** (2014) 015001, [1312.3322].

[101] ATLAS collaboration, *Constraints on the Higgs boson self-coupling from the combination of single-Higgs and double-Higgs production analyses performed with the ATLAS experiment*, .

[102] E. W. N. Glover and J. J. van der Bij, *Higgs Boson Pair Production via Gluon Fusion*, *Nucl. Phys.* **B309** (1988) 282.

[103] T. Plehn, M. Spira and P. M. Zerwas, *Pair production of neutral Higgs particles in gluon-gluon collisions*, *Nucl. Phys.* **B479** (1996) 46–64, [hep-ph/9603205].

[104] S. Dawson, S. Dittmaier and M. Spira, *Neutral Higgs boson pair production at hadron colliders: QCD corrections*, *Phys. Rev.* **D58** (1998) 115012, [hep-ph/9805244].

[105] F. Maltoni, E. Vryonidou and M. Zaro, *Top-quark mass effects in double and triple Higgs production in gluon-gluon fusion at NLO*, *JHEP* **11** (2014) 079, [1408.6542].

[106] S. Borowka, N. Greiner, G. Heinrich, S. P. Jones, M. Kerner, J. Schlenk et al., *Higgs Boson Pair Production in Gluon Fusion at Next-to-Leading Order with Full Top-Quark Mass Dependence*, *Phys. Rev. Lett.* **117** (2016) 012001, [1604.06447].

[107] S. Borowka, N. Greiner, G. Heinrich, S. P. Jones, M. Kerner, J. Schlenk et al., *Full top quark mass dependence in Higgs boson pair production at NLO*, *JHEP* **10** (2016) 107, [1608.04798].

[108] J. Baglio, F. Campanario, S. Glaus, M. Mühlleitner, M. Spira and J. Streicher, *Gluon fusion into Higgs pairs at NLO QCD and the top mass scheme*, *Eur. Phys. J.* **C79** (2019) 459, [1811.05692].

[109] J. Baglio, F. Campanario, S. Glaus, M. Mühlleitner, J. Ronca, M. Spira et al., *Higgs-Pair Production via Gluon Fusion at Hadron Colliders: NLO QCD Corrections*, *JHEP* **04** (2020) 181, [2003.03227].

[110] G. Heinrich, S. P. Jones, M. Kerner, G. Luisoni and E. Vryonidou, *NLO predictions for Higgs boson pair production with full top quark mass dependence matched to parton showers*, *JHEP* **08** (2017) 088, [1703.09252].

[111] S. Jones and S. Kuttimalai, *Parton Shower and NLO-Matching uncertainties in Higgs Boson Pair Production*, *JHEP* **02** (2018) 176, [1711.03319].

[112] G. Heinrich, S. P. Jones, M. Kerner, G. Luisoni and L. Scyboz, *Probing the trilinear Higgs boson coupling in di-Higgs production at NLO QCD including parton shower effects*, *JHEP* **06** (2019) 066, [1903.08137].

[113] G. Heinrich, S. P. Jones, M. Kerner and L. Scyboz, *A non-linear EFT description of $gg \to HH$ at NLO interfaced to POWHEG*, *JHEP* **10** (2020) 021, [2006.16877].

[114] D. de Florian and J. Mazzitelli, *Two-loop virtual corrections to Higgs pair production*, *Phys. Lett.* **B724** (2013) 306–309, [1305.5206].

[115] D. de Florian and J. Mazzitelli, *Higgs Boson Pair Production at Next-to-Next-to-Leading Order in QCD*, *Phys. Rev. Lett.* **111** (2013) 201801, [1309.6594].

[116] J. Grigo, K. Melnikov and M. Steinhauser, *Virtual corrections to Higgs boson pair production in the large top quark mass limit*, *Nucl. Phys.* **B888** (2014) 17–29, [1408.2422].

[117] J. Grigo, J. Hoff and M. Steinhauser, *Higgs boson pair production: top quark mass effects at NLO and NNLO*, *Nucl. Phys. B* **900** (2015) 412–430, [1508.00909].

[118] D. de Florian, M. Grazzini, C. Hanga, S. Kallweit, J. M. Lindert, P. Maierhöfer et al., *Differential Higgs Boson Pair Production at Next-to-Next-to-Leading Order in QCD*, *JHEP* **09** (2016) 151, [1606.09519].

[119] M. Grazzini, G. Heinrich, S. Jones, S. Kallweit, M. Kerner, J. M. Lindert et al., *Higgs boson pair production at NNLO with top quark mass effects*, *JHEP* **05** (2018) 059, [1803.02463].

[120] D. de Florian, I. Fabre, G. Heinrich, J. Mazzitelli and L. Scyboz, *Anomalous couplings in Higgs boson pair production at approximate NNLO QCD*, 2106.14050.

[121] L.-B. Chen, H. T. Li, H.-S. Shao and J. Wang, *Higgs boson pair production via gluon fusion at N^3LO in QCD*, *Phys. Lett. B* **803** (2020) 135292, [1909.06808].

[122] L.-B. Chen, H. T. Li, H.-S. Shao and J. Wang, *The gluon-fusion production of Higgs boson pair: N^3LO QCD corrections and top-quark mass effects*, *JHEP* **03** (2020) 072, [1912.13001].

[123] D. de Florian, I. Fabre and J. Mazzitelli, *Higgs boson pair production at NNLO in QCD including dimension 6 operators*, *JHEP* **10** (2017) 215, [1704.05700].

[124] R. Gröber, M. Mühlleitner, M. Spira and J. Streicher, *NLO QCD Corrections to Higgs Pair Production including Dimension-6 Operators*, *JHEP* **09** (2015) 092, [1504.06577].

[125] R. Alonso, M. B. Gavela, L. Merlo, S. Rigolin and J. Yepes, *The Effective Chiral Lagrangian for a Light Dynamical "Higgs Particle"*, *Phys. Lett.* **B722** (2013) 330–335, [1212.3305].

[126] G. Buchalla, O. Catà and C. Krause, *Complete Electroweak Chiral Lagrangian with a Light Higgs at NLO*, *Nucl. Phys. B* **880** (2014) 552–573, [1307.5017].

[127] G. Buchalla, O. Cata and C. Krause, *On the Power Counting in Effective Field Theories*, *Phys. Lett.* **B731** (2014) 80–86, [1312.5624].

[128] V. Smirnov, *Renormalization and asymptotic expansions*, vol. 14. 1991.

[129] M. Beneke and V. A. Smirnov, *Asymptotic expansion of Feynman integrals near threshold*, *Nucl. Phys. B* **522** (1998) 321–344, [hep-ph/9711391].

[130] V. A. Smirnov and E. R. Rakhmetov, *The Strategy of regions for asymptotic expansion of two loop vertex Feynman diagrams*, *Theor. Math. Phys.* **120** (1999) 870–875, [hep-ph/9812529].

[131] V. A. Smirnov, *Problems of the strategy of regions*, *Phys. Lett. B* **465** (1999) 226–234, [hep-ph/9907471].

[132] A. Pak and A. Smirnov, *Geometric approach to asymptotic expansion of Feynman integrals*, *Eur. Phys. J. C* **71** (2011) 1626, [1011.4863].

[133] B. Ananthanarayan, A. Pal, S. Ramanan and R. Sarkar, *Unveiling Regions in multi-scale Feynman Integrals using Singularities and Power Geometry*, *Eur. Phys. J. C* **79** (2019) 57, [1810.06270].

[134] B. Ananthanarayan, A. B. Das and R. Sarkar, *Asymptotic Analysis of Feynman Diagrams and their Maximal Cuts*, 2003.02451.

[135] T. Becher, A. Broggio and A. Ferroglia, *Introduction to Soft-Collinear Effective Theory*, vol. 896. Springer, 2015, 10.1007/978-3-319-14848-9.

[136] B. Jantzen, *Foundation and generalization of the expansion by regions*, *JHEP* **12** (2011) 076, [1111.2589].

[137] G. Mishima, *High-Energy Expansion of Two-Loop Massive Four-Point Diagrams*, *JHEP* **02** (2019) 080, [1812.04373].